CHAPTER 5: RESULTS AND DISCUSSION

5.1 Preformulation Studies

Preformulation studies are vital for evaluating and confirming the physicochemical properties as well as the identity and purity of the raw material to be used in formulation development, especially the active pharmaceutical ingredient. Preformulation studies of Resveratrol were carried out to confirm its identity and purity as well as to establish the most suitable analytical technique for determining its concentration in various formulations. The studies helped in selecting the appropriate formulation ingredients, solvent system process variables, etc to develop a novel, patient compliant, high quality, and safe formulation.

5.1.1 Identification of Resveratrol

Resveratrol was recognized by evaluating its organoleptic properties, ultraviolet spectroscopy, IR spectroscopy, and melting point.

5.1.1.1 Physical appearance

The physical appearance of Resveratrol was observed and noted visually. It was found to be an off-white and odorless powder which is comparable to reference standards.

5.1.1.2 UV spectroscopy for determining λ_{max}

Resveratrol was dissolved in methanol to prepare a solution of a concentration equivalent of 10 µg/mL. This solution was then scanned spectrophotometrically using a UV visible spectrophotometer in a range of 200-400 nm for determining its λ_{max} and confirming its identity and purity. The UV spectrum of Resveratol is presented in Figure 5.1 showing λ_{max} of Resveratrol in methanol was found to be 306 nm (USP 2016). The reported λ_{max} is 306 nm. The results ensured the identification and purity of Resveratrol.

5.1.1.3 Fourier Transform Infra-Red spectroscopy

FTIR spectroscopy studies were done using the FTIR spectrophotometer. The obtained spectrum was compared with the reference spectrum. Corresponding peaks for the functional groups were observed confirming the identity of the gift sample of Resveratrol

obtained. Spectrum showing corresponding functional groups (USP 2016) are represented in Figure 5.2 and Table 5.1.

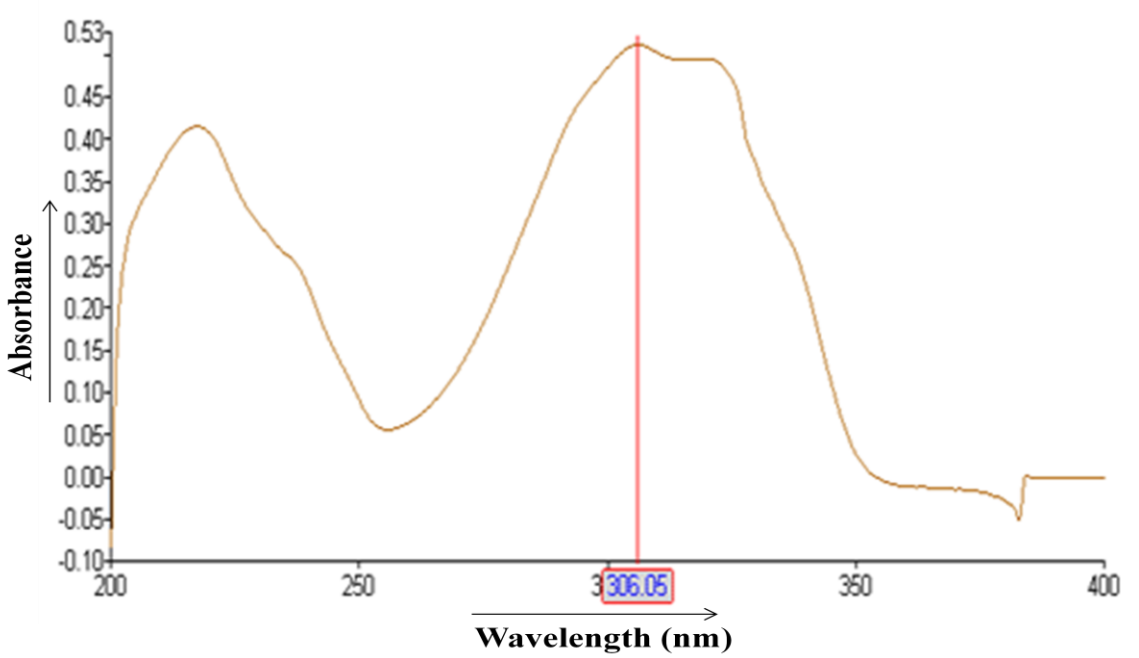

Figure 5.1: UV spectrum of Resveratrol in methanol

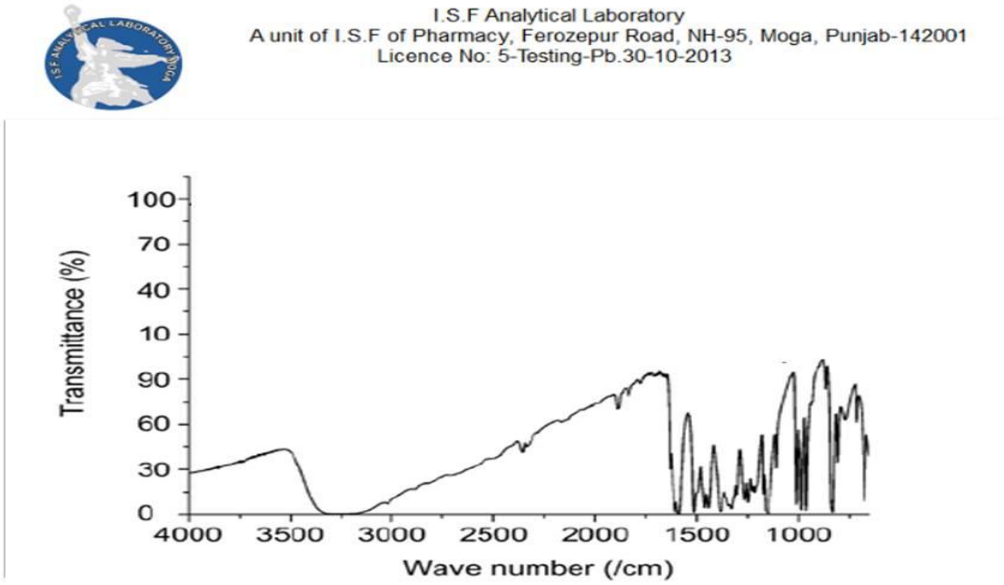

Figure 5.2: FTIR spectrum of Resveratrol

All the characteristic peaks of Resveratrol were found to be comparable with the reference spectrum (Agarwal et al. 2014).

Table 5.1: Explanation of spectrum obtained during Fourier Transform Infra-Red spectroscopy

Observed Wavenumber (cm^{-1})	Reference Wavenumber (cm^{-1})	Type of Vibration	Functional group
965	1000-650	Bending	olefinic band
1605	1667-1640	Stretching	trans olefinic band
3281	3400-2400	Stretching (Broad band)	O-H
1215	1300-1000	Stretching	C–O
1585	1600-1585	Aromatic double-bond stretching	C–C

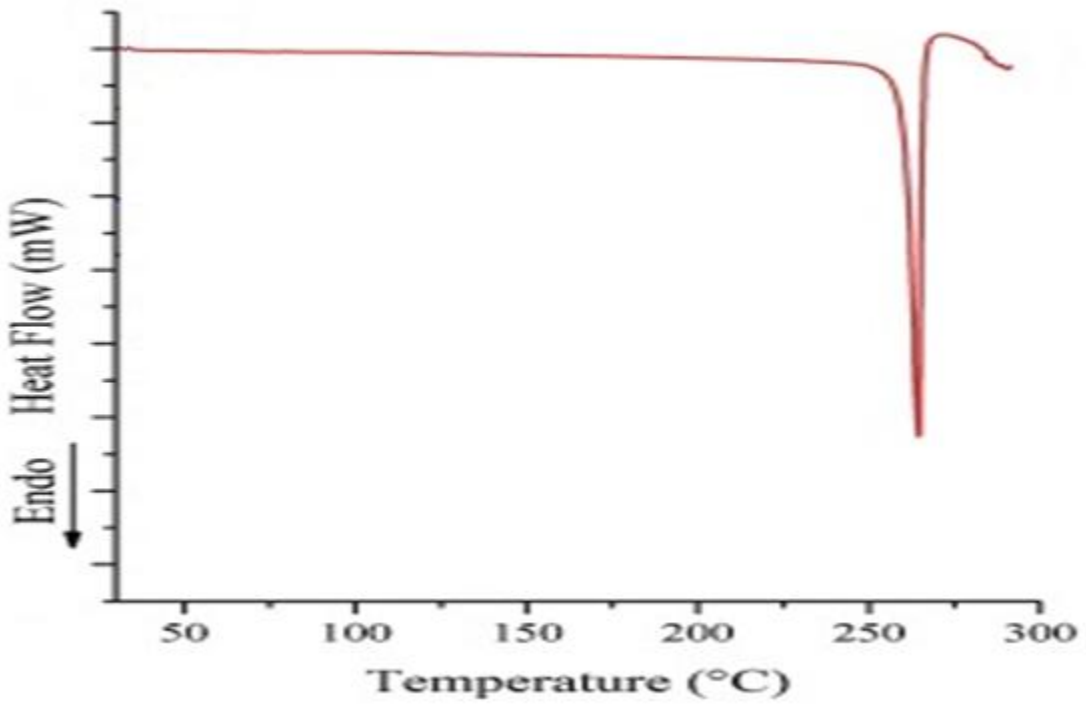

Figure 5.3: DSC thermogram of Resveratrol

5.1.1.4 Determination of melting point

The capillary method and DSC were employed for the determination of the melting point of Resveratrol. The melting point of Resveratrol was found to be 262-265 ºC by the capillary method. The reported range is 261-263 ˚C. DSC thermogram has also shown in Figure 5.3 the endothermic peak at 265 ºC. This study also confirmed the purity of Resveratrol.

5.1.2 Development of the analytical methods

5.1.2.1 UV-visible spectroscopy studies

The standard plot of Resveratrol was developed in methanol at observed λ_{max} i.e. 306 nm. The observed absorbance at each dilution is given in Table 5.2. Linear regression was applied to get the equation and coefficient of correlation. The linearity of the curve was confirmed as the value of the regression coefficient of correlation was found to be 0.999. The calibration plot is shown in Figure 5.4.

Table 5.2: Calibration curve of Resveratrol in methanol at 306 nm using UV spectrophotometric method

Concentration (µg/mL)	Absorbance
1	0.1672
2	0.2728
3	0.4026
4	0.506
5	0.6226
6	0.7359
7	0.8481
8	0.9537

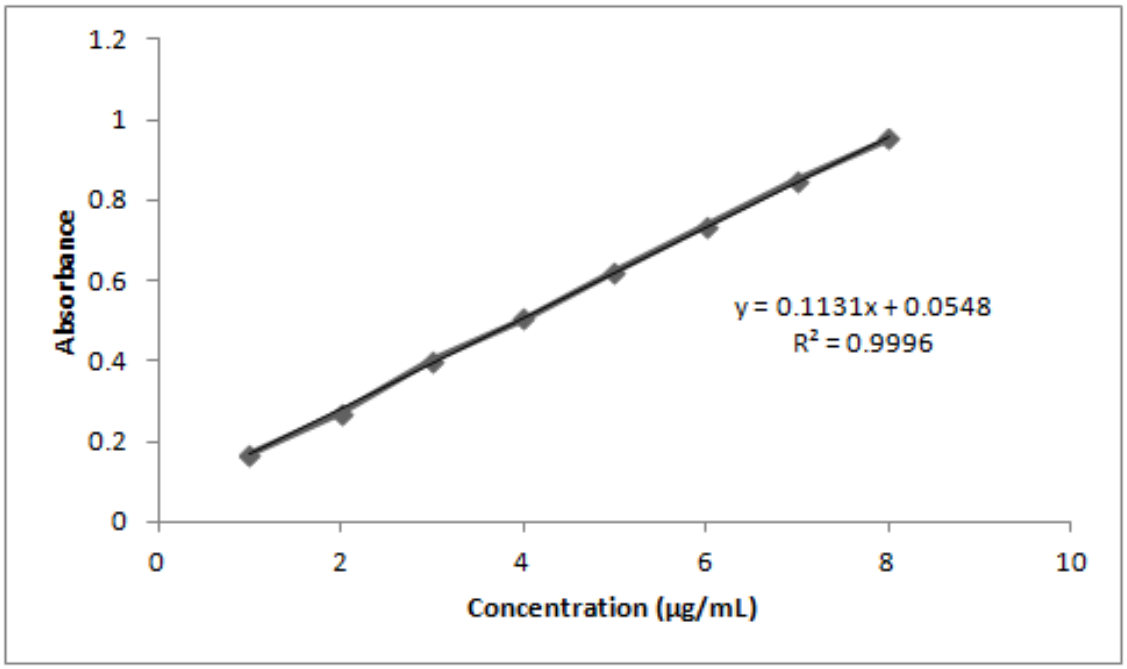

Figure 5.4: Calibration plot of Resveratrol in methanol at 306 nm using UV spectrophotometric method

Similarly, the standard plot of Resveratrol was plotted in a mixture of PBS pH 7.4 and ethanol (7:3 v/v) at observed λ_{max} i.e. 306 nm.. The observed absorbance at each dilution is given in Table 5.3. Linear regression was applied to get the equation and coefficient of correlation. The linearity of the curve was confirmed as the value of the regression coefficient of correlation was found to be 0.999. The calibration curve is shown in Figure 5.5.

5.1.2.2 HPLC method for Resveratrol determination

Analytical method development and its validation are the two key elements in the process of product development. The performance of any pharmaceutical product is assessed with respect to set standards of quality with the help of a validated analytical method. Therefore, it is obligatory to develop a reliable technique for the accurate evaluation of drugs during various stages of product development and stability studies.

Table 5.3: Calibration curve of Resveratrol in a mixture of PBS pH 7.4 and ethanol (7:3 v/v) at 306 nm using UV spectrophotometric method

Concentration (µg/mL)	Absorbance
1	0.142
2	0.223
3	0.291
4	0.362
5	0.442
6	0.532
6	0.603
8	0.687
9	0.762
10	0.839

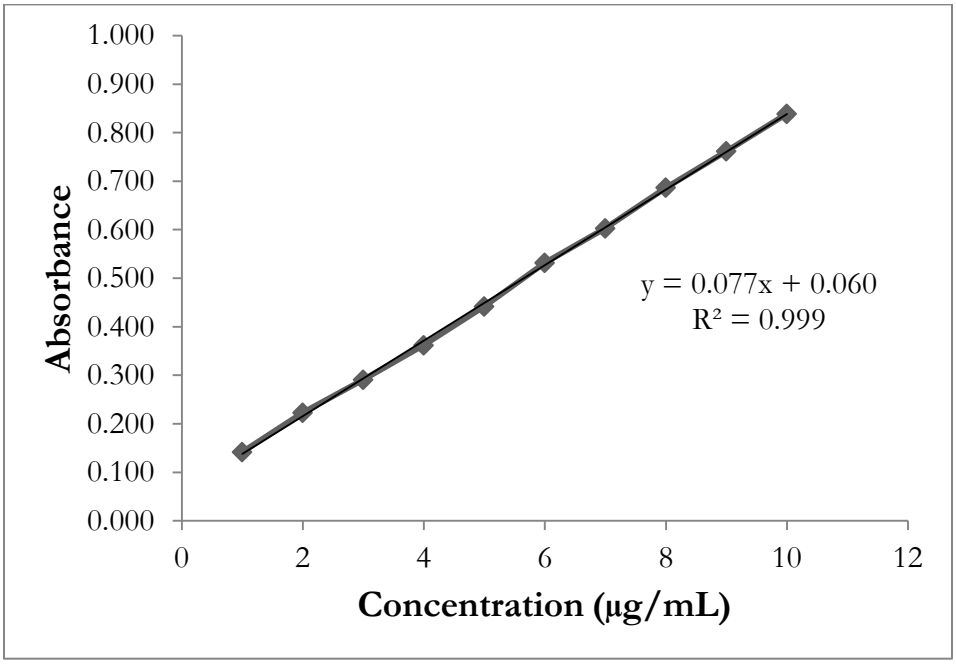

Figure 5.5: Calibration curve of Resveratrol in a mixture of PBS pH 7.4 and ethanol (7:3 v/v) at 306 nm using UV spectrophotometric method

The HPLC chromatogram of Resveratrol was obtained in the mobile phase of methanol, water, and acetic acid (69:30:1, v/v/v) as shown in Figure 5.6. The retention time was observed to be 3.5 min.

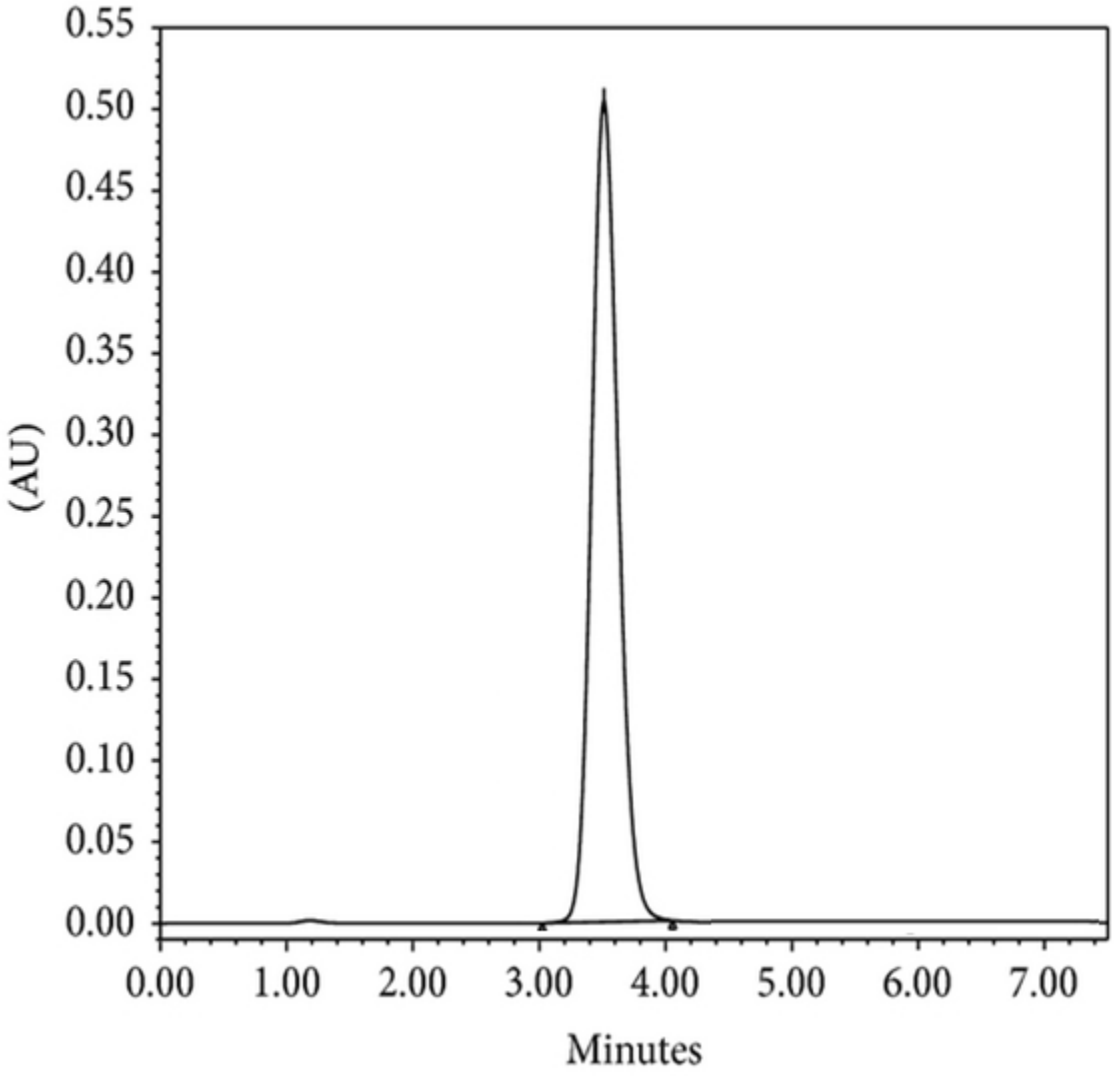

Figure 5.6: HPLC chromatogram of Resveratrol

The standard curve of Resveratrol was prepared by plotting a curve as peak area *vs* concentration of Resveratrol solution in the methanol (306 nm) using varied concentrations of 5-60 µg/mL. The plot showed good linearity in the working concentration range. The correlation coefficient value and the linear equation obtained revealed the linearity in the developed method. The obtained data are presented in Table 5.4 and Figure 5.7.

Table 5.4: Calibration curve of Resveratrol using HPLC method

Concentration (µg/mL)	Peak Area
5	27779
10	117129
15	194782
20	306301
25	384836
30	474072
40	652544
50	833356
60	997788

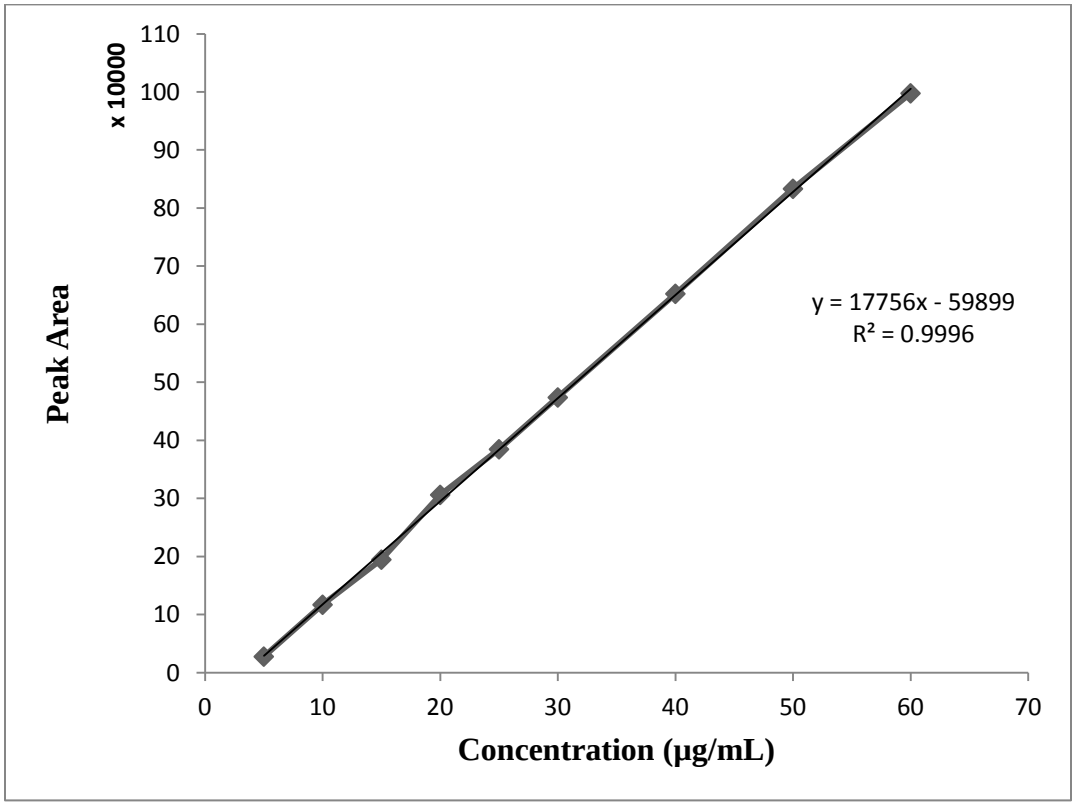

Figure 5.7: Calibration curve of Resveratrol using HPLC method

5.1.3 Determination of partition coefficient

The extent of lipophilicity of Resveratrol was evaluated in this study. The experiment was conducted thrice and the observed value of the partition coefficient is 3.58 ± 0.64, while the reported value is 3.1 (Herbig & Evers 2013). The results revealed the lipophilic characteristics of Resveratrol.

5.1.4 Solubility determination

Determination of drug solubility is a fundamental part of the pre-formulation studies. It is important in the selection of appropriate medium for varied studies including, i.e., hydration, entrapment, permeation and stability. Solubility studies, therefore, were conducted in different solvent systems to find out a suitable medium for various studies during the development of drug-loaded carrier systems.

Table 5.5 represents the saturated solubility of Resveratrol in different mediums. The solubility of Resveratrol in water was found to be negligible and another aqueous solvent. The addition of ethanol in the permeation medium could help maintain sink conditions.

Table 5.5: Saturated solubility of Resveratrol in different mediums

Solvent	Solubility (mg/mL)
Water	0.032 ± 0.007
Ethanol	68.5 ± 2.43
Methanol	70.3 ± 3.21
DMSO	65.7 ± 1.65
PBS pH 7.2	0.1 ± 0.09
Ethanol (40%)	44.5 ± 3.54
Chloroform	36.4 ± 1.90

5.2 Formulation development

Two types of nanocarriers were developed for the successful topical delivery of Resveratrol. The first one is polymer-based polymeric micelles and the second is a lipid-based delivery system i.e. vitamin-E oil-based nanoemulsion. Both of these systems were then incorporated into the carbomer based hydrogels.

5.2.1 Formulation of Resveratrol loaded polymeric micelles: QbD based optimization

Resveratrol loaded Polymeric Micellar formulation was formulated constituted of a mixture of two block copolymers i.e. Pluronic P123 and Pluronic F127.

QbD supported optimization was done by employing the Design of Experiment (DoE) with a holistic perception of product and processes optimization was employed to formulate Resveratrol loaded polymeric micelles (Singh et al. 2011). QbD is "A systematic approach of development that begins with predefined objectives and emphasizes product and process understanding and process control, based on sound science and quality risk management as described in ICH Q8(R2) International Conference on Harmonisation of Technical Requirements for Registration of Pharmaceuticals for Human Use 2009" (Saydam & Takka 2018).

The basic elements and tools of QbD approach such as identifying Quality Target Product Profile (QTPP), Critical Quality Attributes (CQAs), Critical Material Attributes (CMAs), and Critical Process Parameters (CPPs) were employed along with the application of DoE to establish the relationship between CQAs and CMAs.

5.2.1.1 Defining QTPP and Identifying CQAs for applying QbD approach

As per the ICH guidelines, Table 5.6 is given which depicts defined QTPP and related characteristics for the development of Resveratrol loaded polymeric micelles with better skin retention, permeation, and pharmacodynamic properties. Similarly identified CQAs accountable to fulfill defined QTPP are represented in Table 5.7 along with its pertinent explanation. Particle size, micellar incorporation efficiency, and skin retention potential of micelles were chosen as CQAs.

Table 5.6: QTPP elements for the production of Resveratrol loaded polymeric micelles

QTPP Elements	Target	Justification(s)
Dosage form/delivery systems	Micelles based gel	Helps in enhanced permeation of bioactive in the dermal region and will control the skin retention
Route of administration	Topical	Local topical application to enhance the availability of bioactive at target site i.e. skin and avoid systemic exposure
Dosage type	Controlled release	Controlled release leading to enhanced therapeutic effects
Appearance	Transparent gel	Elegance and aesthetic appeal
Skin permeation	Higher flux and skin retention	Required for achieving higher bioactive levels in the skin for enhanced benefits
Stability (Physical & chemical)	At least 6 months at various storage temperatures	To maintain the therapeutic potential of the bioactive during the storage period
Container closure system	Collapsible opaque tube suitable for the product	To ensure target shelf-life and to facilitate administration

Table 5.7: Identified CQAs accountable to fulfill defined QTPP

CQA	Target	Justification(s)
Globule size	In range (100 – 200 nm)	It was considered highly critical due to its importance in permeation and retention of the bioactive in the dermal layer. Smaller size facilities movement inside the layers of skin, but beyond a level it leads to systemic absorption.
Micellar incorporation efficiency (MIE)	Highest	Higher incorporation efficiency required to reduce the quantity of formulation to be applied and pharmaceutical properties of the formulation
The extent of Resveratrol deposition in the dermal layer of skin (Skin deposition, SD)	High	High skin retention is required for better therapeutic benefits because the target site is located in the dermis region of the skin. Therefore it was also selected as highly critical.

5.2.1.2 Risk assessment analysis

Ishikawa fishbone diagram as shown in Figure 5.8 was created for the risk assessment during formulation. It was done to layout the influential formulation and process variables/ parameters affecting selected CQAs. Failure mode and effect analysis (FMEA) was executed to screen out the crucial parameters affecting the quality, safety, and efficacy of the drug product. RPN scores (based on severity, occurrence, and delectability) were assigned to each material and process attributes as shown in Table 5.8. The attributes associated with high RPN value (301-500) were screened to further optimize at different levels using DoE based approach. However, the attributes having medium or low risk were fixed at optimum values during the formulation of all batches.

These were found to be the concentration of Pluronic P123 and the amount of Resveratrol to be used as they showed RPN scores above 300.

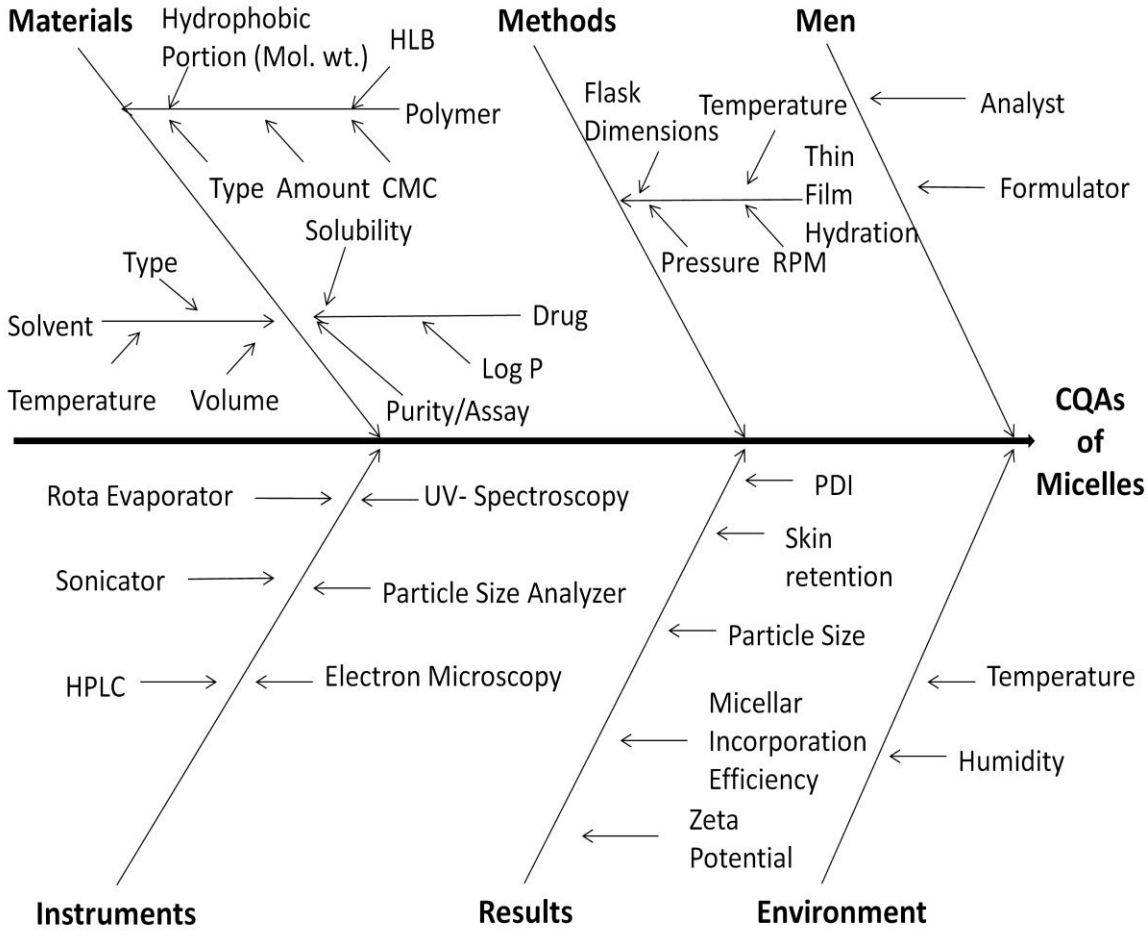

Figure 5.8: "Ishikawa Fish-bone diagram" for the development of polymeric micelles

5.2.1.3 DoE (Central Composite Design) based optimization of Resveratrol loaded polymeric micelles

Mixed pluronic based polymeric micellar dispersion was successfully developed using a thin-film hydration method. Micelles based on the single polymer are known to face several drawbacks such as large particle size, less stable, low drug-carrying capacity, high CMC, etc, (Ebrahim Attia et al. 2011) while mixed micelles show synergistic properties. Widely used amphiphilic triblock copolymers are Pluronics which are made of hydrophilic polyethylene oxide (PEO) and hydrophobic polypropylene oxide (PPO) blocks (PEO–PPO–PEO).

Table 5.8: FMEA for Risk assessment for Resveratrol loaded polymeric micelles

S. No.	Materials and Process variables	S	O	D	RPN	Impact on CQAs
1	Drug properties like solubility, log P	4	3	3	36	MIE
2	Amount of drug	8	8	6	384	PS, MIE, SD
3	Type of polymer	6	6	4	144	PS, MIE, SD
4	Amount of polymer	6	5	4	120	PS
5	Molecular weight of hydrophobic portion of polymer	5	6	7	252	MIE, SD
6	HLB of polymer	5	7	7	245	PS, MIE, SD
7	Ratio of hydrophilic and hydrophobic polymer in mixed micelles	8	8	7	448	PS, MIE, SD
8	Method of preparation	3	5	5	75	PS
9	Type of aqueous phase	6	5	4	120	PS
10	Volume of aqueous phase (ml)	4	6	2	48	MIE
11	Temperature of aqueous phase	5	4	5	100	MIE
12	Rotation speed (rpm)	6	6	4	144	PS, MIE
13	Rotation Time (min)	5	6	6	180	PS
14	Flask geometry and size	5	6	4	120	PS
15	Sonication speed and time	6	7	7	294	PS

Risk Ranking: Low risk (0-100), Medium risk (101-300), High risk (301-500)

Particle size (PS), Micellar Incorporation Efficiency (MIE), Skin deposition (SD)

Pluronic F127 (PEO_{100}–PPO_{69}–PEO_{100}) is known to have a high HLB value (approximate 22) and a monomer unit ratio of 100/69/100. Owing to the higher proportionate of PEO and long hydrophilic chains, it is quite more hydrophilic with a higher CMC value and yields kinetically stable micelles produced by steric hindrance. While Pluronic P123 (PEO_{20}–PPO_{65}–PEO_{20}) have less HLB value (approximate 7-9) yield more thermodynamically stable micelles because of more tight hydrophobic interactions of PPO chains. Thus, mixed pluronic micelles were developed (Abd-Elsalam et al. 2018). Optimization of the ratio of P123 and F127 to get desired CQAs was done using DoE.

Response surface methodology using Face Centered Central Composite Design (FCCCD) was employed for the optimization of Resveratrol loaded micelles. Two variables i.e. the percentage of Pluronic P123 in the mixture of two Pluronics (P123 and F127) (X1) and the amount of Resveratrol (X2) were varied at three different levels i.e. low, medium, and high represented by coded levels (-1, 0 and +1) as shown in Table 5.9.

Table 5.9: CQAs and CMAs used in a full factorial design with coded and actual values of CMAs

CMAs	**Coded and Actual Levels**		
	Low (-1)	Medium (0)	High (+1)
Ratio of P123, % (X1)	10	50	90
Amount of Resveratrol, mg (X2)	50	75	100
CQAs	**Target**		
Micellar Incorporation efficiency (MIE, %) (Y1)	Maximum		
Particle size (PS, nm) (Y2)	In range (100-200 nm)		
Extent of Skin deposition (SD, %) (Y3)	Maximum		

Thirteen batches in triplicate were developed and analyzed for selected CQAs. The responses of the experimental runs are given in Table 5.10. The ranges of responses for all batches were 51.72 to 96.73 % micellar incorporation efficiency (Y1), 24.16 to 204.47 nm particle size (Y2), and 18.64 to 48.12 % of skin deposition (Y3).

Table 5.10: Response values of experimental runs for development of micelles

Batch No	Variable levels in coded form		Response Variables		
	X1	X2	MIE (%) (Y1)	Particle size (nm) (Y2)	Skin deposition (SD) %
PM 1	-1	-1	77.71 ± 6.56	24.16 ± 1.56	18.64 ± 1.25
PM 2	-1	0	68.16 ± 5.08	60.7 ± 1.02	31.41 ± 2.51
PM 3	-1	+1	51.72 ± 4.52	79.34 ± 3.55	33.91 ± 3.52
PM 4	0	-1	83.64 ± 6.89	110.13 ± 4.26	41.72 ± 3.72
PM 5	0	0	77.32 ± 5.85	114.93 ± 4.22	43.97 ± 4.69
PM 6	0	+1	65.43 ± 5.95	139.36 ± 6.66	44.31 ± 2.70
PM 7	+1	-1	96.73 ± 8.22	182.41 ± 6.21	47.43 ± 4.83
PM 8	+1	0	92.10 ± 6.02	191.63 ± 6.98	48.12 ± 4.91
PM 9	+1	+1	83.33 ± 4.77	204.47 ± 7.09	30.46 ± 2.61
PM 10*	0	0	78.19 ± 7.64	117.21 ± 4.89	43.61 ± 4.16
PM 11*	0	0	76.23 ± 5.78	115.23 ± 4.55	45.42 ± 4.32
PM 12*	0	0	73.24 ± 2.45	118.21 ± 3.29	44.12 ± 4.21
PM 13*	0	0	74.33 ± 5.32	117.98 ± 6.12	43.34 ± 2.18

[All values are expressed as mean ± S.D., (n = 3)]

**Formulated in quintuplicate as 4 additional center points per block All other parameters were kept constant*

5.2.1.4 Model generation for optimization in polymeric micelles

The obtained results were analyzed using Design-Expert software. The software suggested the best-fitted model which was analyzed and validated by applying ANOVA. All CQAs were found to follow the quadratic model. The value of $p < 0.05$ indicated statistical significance, while the lack of fit was found to be insignificant in all cases. Additionally, adjusted R^2 and predicted R^2 values for all responses were in reasonable agreement, indicating that the data were described adequately by the mathematical model. The polynomial equations for each CQA were generated by the software which portrayed the main and interaction terms of CMAs on each CQA. Design summary, build information, and values of R^2, SD, and % CV are calculated via software as suggested by literature (Imam et al. 2017) presented in Table 5.11.

Table 5.11: Outline and build information on the applied design of polymeric micelles

File Version	**12.0.5.0**						
Study Type	Response Surface		**Subtype**			Randomized	
Design Type	Central composite		**Runs**			13	
Design Model	Quadratic		**Blocks**			No Blocks	
Response	**Analysis**	**R^2**	**Adjusted R^2**	**Predicted R^2**	**Std. Dev.**	**%CV**	**Model**
R1 (MIE)	Polynomial	0.9987	0.9973	0.9891	0.6474	0.8353	Quadratic
R2 (PS)	Polynomial	0.9945	0.9890	0.9551	5.83	4.79	Quadratic
R3 (SD)	Polynomial	0.9561	0.9122	0.8618	2.69	6.94	Quadratic

5.2.1.5 Model analysis and diagnostic for optimization in polymeric micelles

A normal plot of residuals plotted amid normal % probability *vs* externally studentized residuals is shown in Figure 5.9 (i-iii). In all the responses normal distribution of points was observed. It indicated that the transformation of data in this was not required. All other responses presented fair analysis.

Residuals *vs* Predicted plot is shown in Figure 5.10 (i-iii) for testing the constant variance assumption. Consequently, a fair analysis of the model is suggested.

Residuals *vs* run plot is shown in Figure 5.11 (i-iii) for analyzing hidden variables that may manipulate the response. In all responses arbitrarily scattering of almost all points amid specified range was observed through the steady array. Thus the fair analysis of hidden variables is confirmed by the plot and the order of runs also suggested fair randomization.

Box-Cox Plot for selecting power transformation is shown in Figure 5.12 (i-iii) plotted between *Ln* residual and lambda value. Based on the calculated value of λ power transformation is suggested by the software. In the case of Y1 and Y3, the value of λ was 1, thus none transformation is suggested. While in the case of the Y1 value of λ was 2.42, thus power transformation is suggested.

Predicted *vs* Actual Plot is shown in Figure 5.13 (i-iii), it is plotted to detect the difficulty to predict values using the model. In all responses, all points were very lying very near to the diagonal line. Thus it can be concluded that the analysis is valid and it could help in steering the selected design.

The plot of leverage versus Runs is shown in Figure 5.14 (i-iii). The fit of the suggested model is determined using this. All the points were found to lie between the recommended range of leverage i.e. 0 to 1. Thus the significance of the model was confirmed by these diagnostic plots. The value of 1 for lambda indicates that no transformation was required.

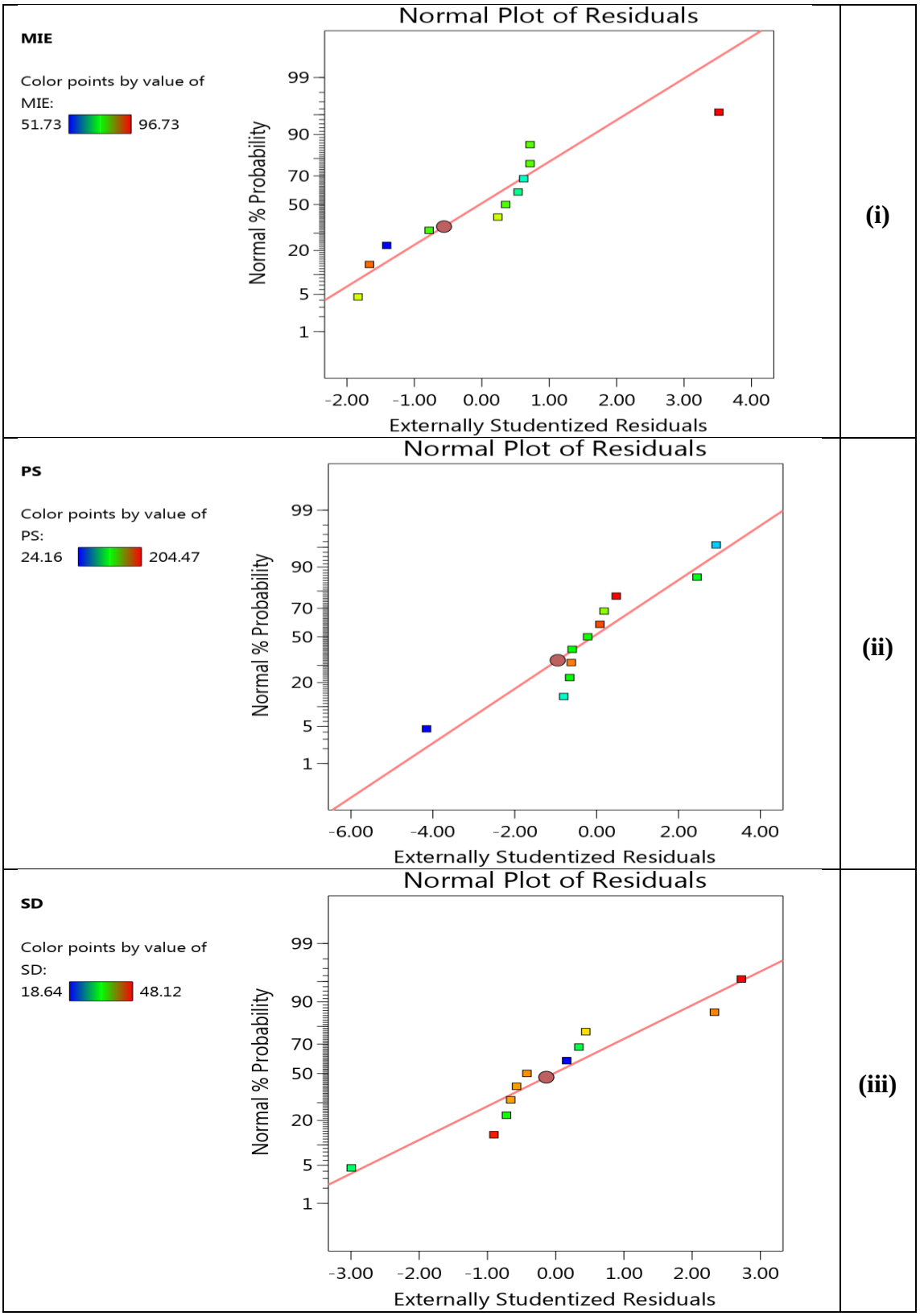

Figure 5.9: Normal plot of Residuals for Resveratrol loaded polymeric micelles, (i) Micellar incorporation efficiency (ii) Particle size, and (iii) Skin deposition

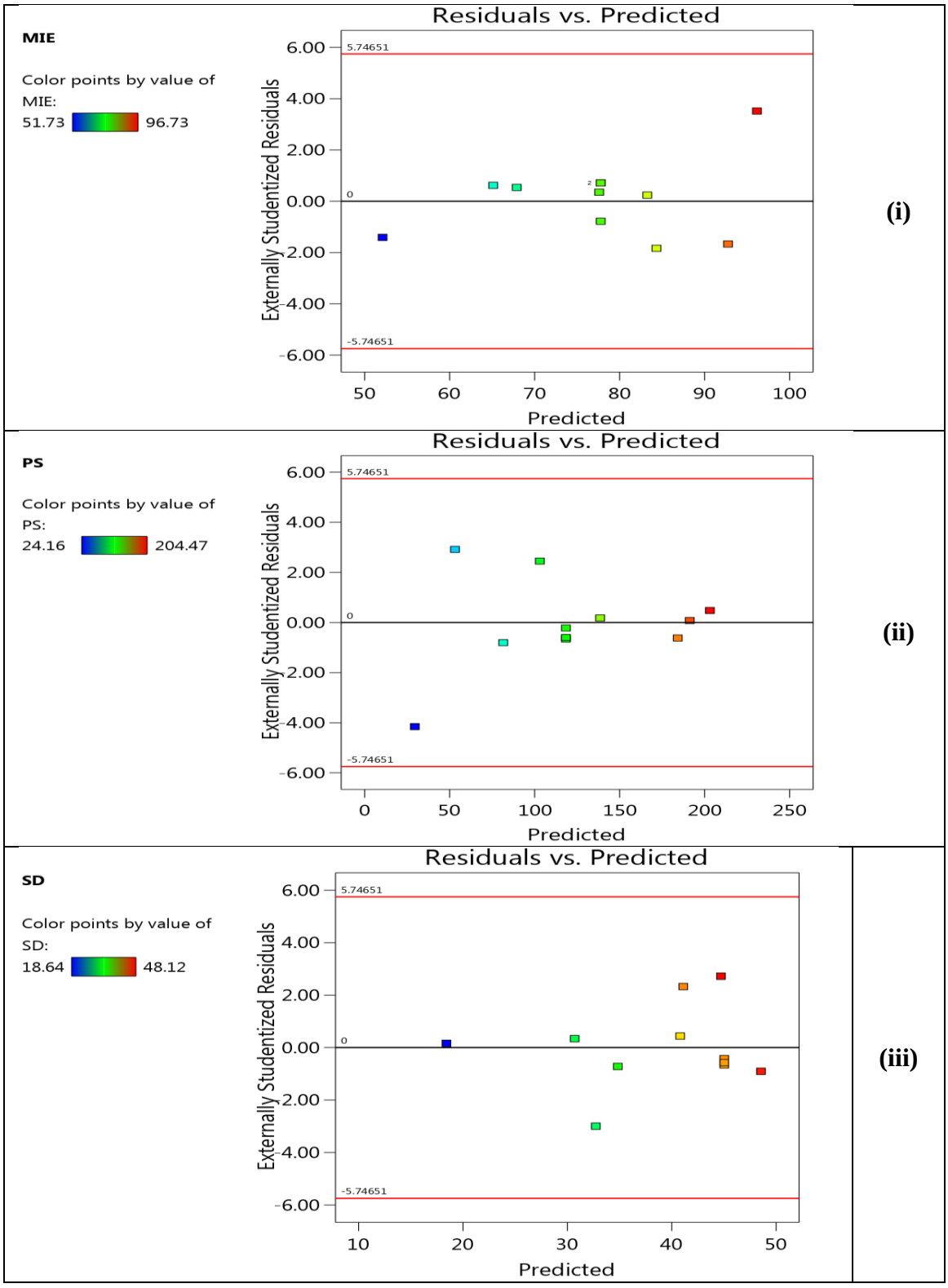

Figure 5.10: Residuals *vs* Predicted plot for Resveratrol loaded polymeric micelles, (i) Micellar incorporation efficiency (ii) Particle size, and (iii) Skin deposition

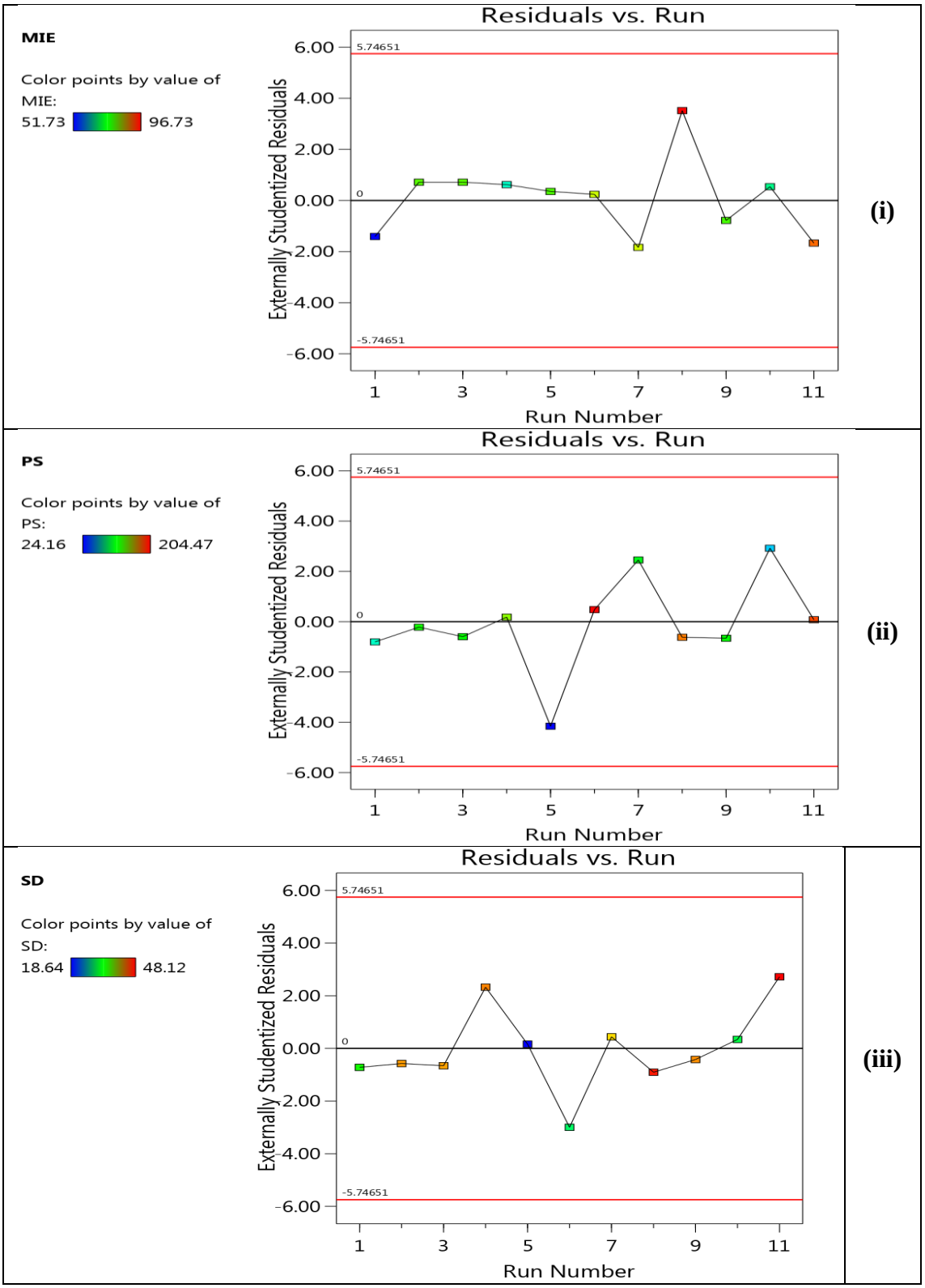

Figure 5.11: Residuals *vs* run plot for Resveratrol loaded polymeric micelles, (i) Micellar incorporation efficiency (ii) Particle size, and (iii) Skin deposition

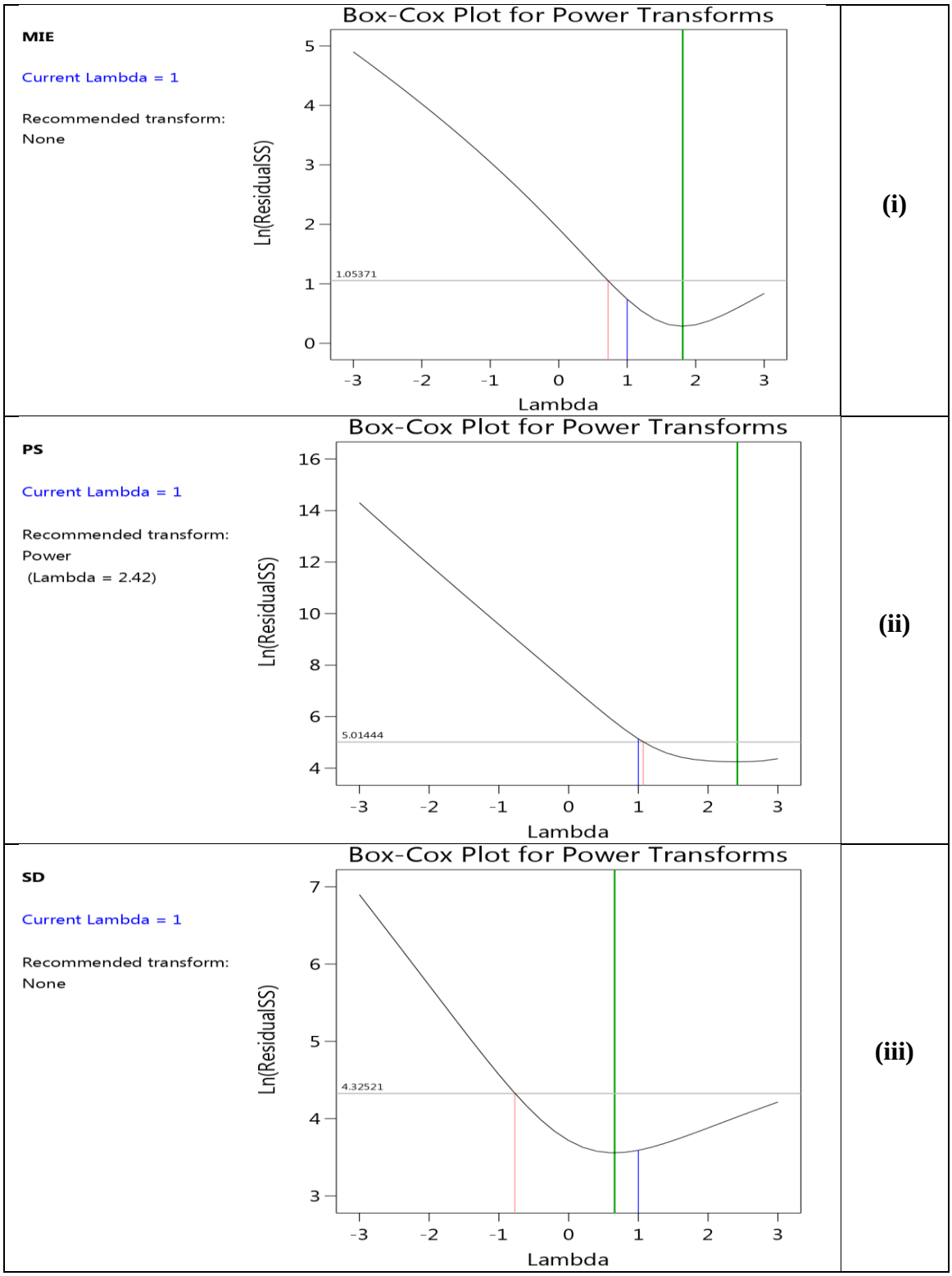

Figure 5.12: Box-Cox Plot for power transform for Resveratrol loaded polymeric micelles, (i) Micellar incorporation efficiency (ii) Particle size, and (iii) Skin deposition

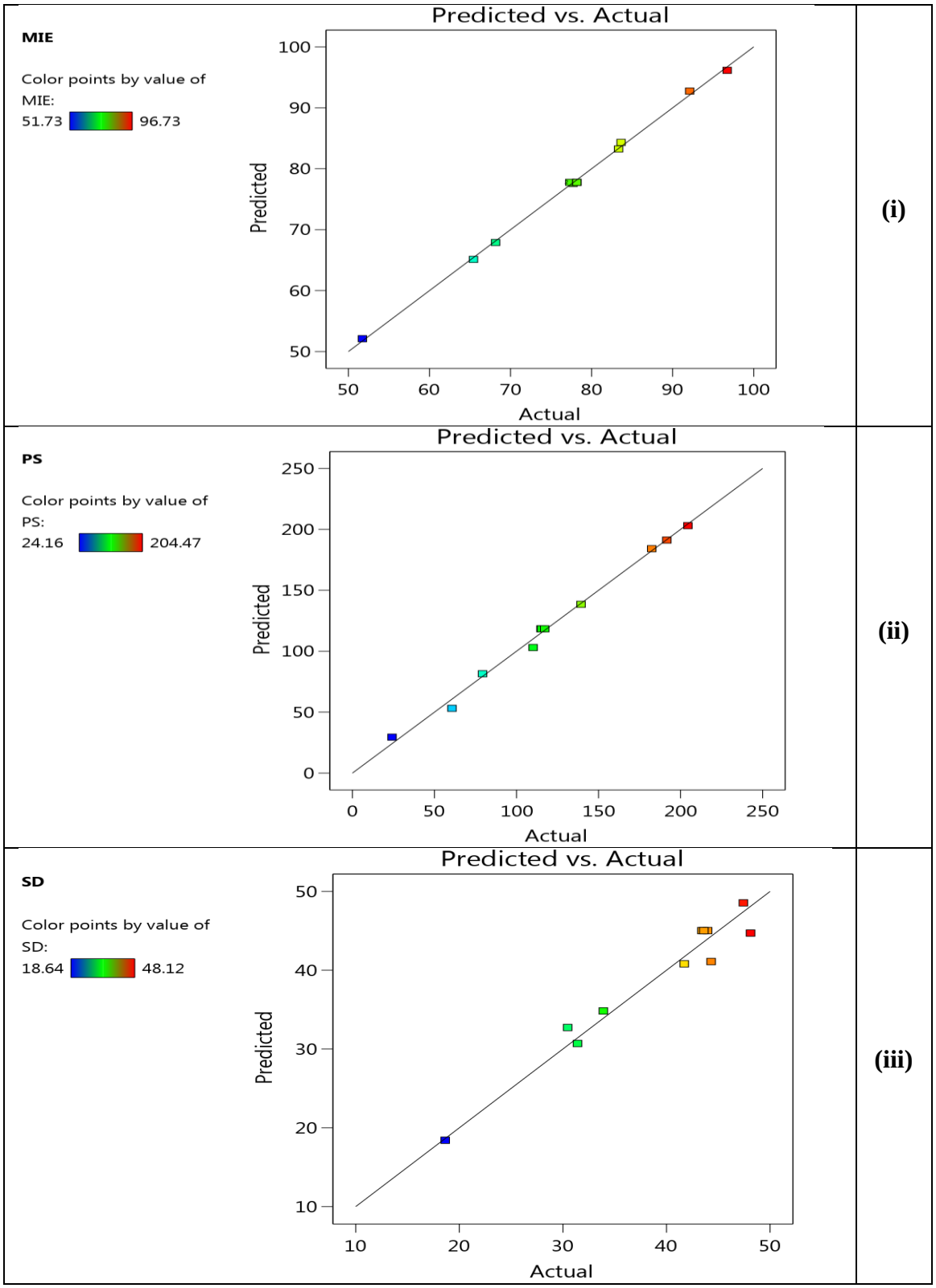

Figure 5.13: Predicted *vs* Actual Plot for Resveratrol loaded polymeric micelles, (i) Micellar incorporation efficiency (ii) Particle size, and (iii) Skin deposition

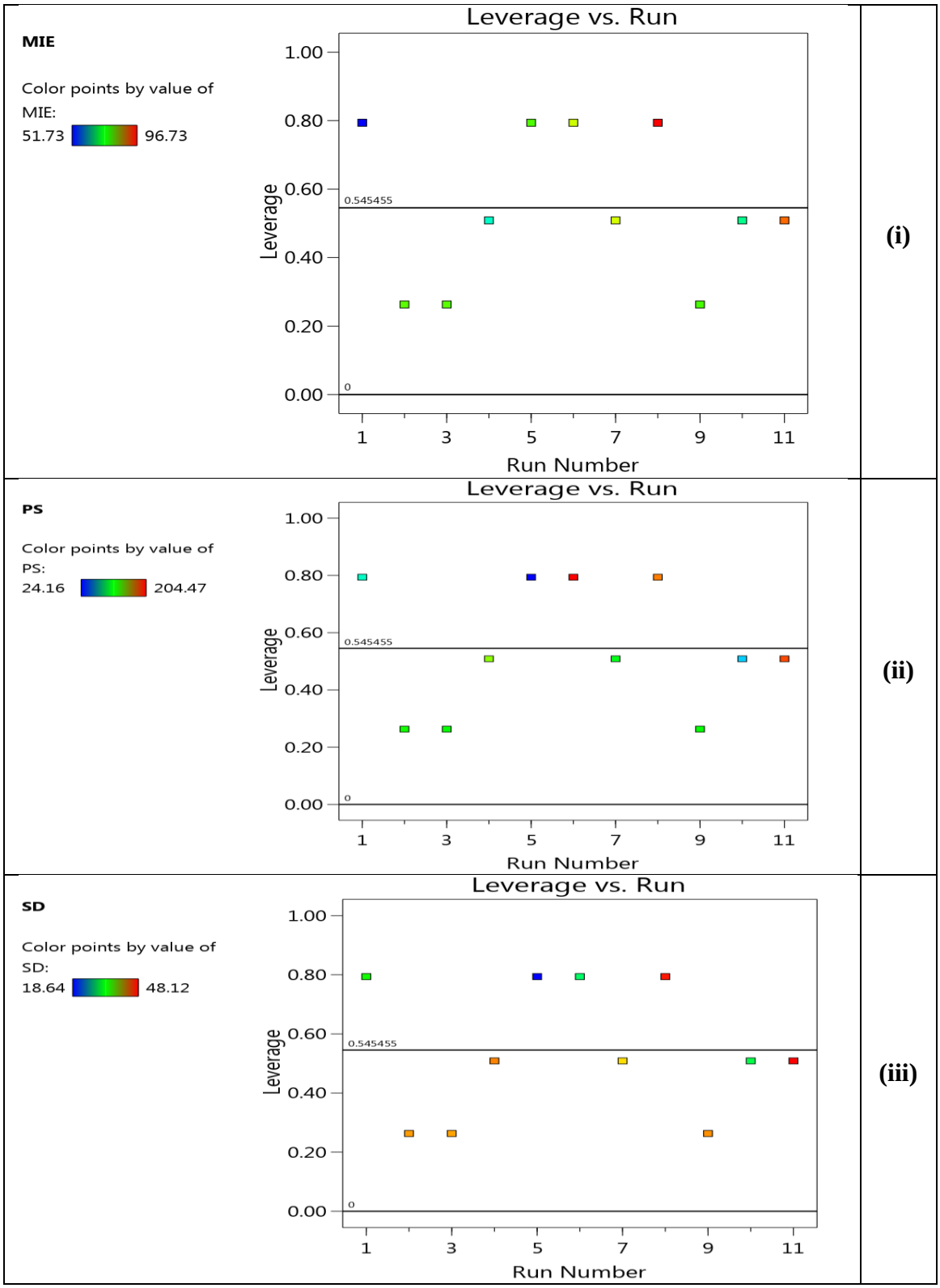

Figure 5.14: Leverage versus Runs Plot for Resveratrol loaded polymeric micelles, (i) Micellar incorporation efficiency (ii) Particle size, and (iii) Skin deposition

5.2.1.6 Response analysis through polynomial equations for polymeric micelles

5.2.1.6.1 Effect of CMAs on the MIE of polymeric micelles (Y1)

MIE is one of the highly critical attributes as the therapeutic response could be greatly influenced by it, as well as higher drug loading results in a reduction in dosing frequency. The following polynomial equation (equation 5.1) is generated by the software to study the interaction effect of X1 and X2 on YI.

$$MIE\ (Y1) = +77.77 + 12.43\ X1 - 9.60\ X2 + 3.14\ X1X2 + 2.55\ X1^2 \qquad \text{- eqn. 5.1}$$

According to the model and equation and perturbation curve, 2D contour plot, and 3D plots represented in Figure 5.15-5.17, it was ratified that the concentration of Pluronic P123 and the amount of resveratrol has a significant effect on MIE ($p < 0.0001$). The higher the proportion of P123 as compared to F127, the higher is the encapsulation of Resveratrol.

This is attributed to the relatively higher lipophilicity of P123 as compared to F127, as discussed earlier. Better entrapment of lipophilic molecule like Resveratrol is thus expected with a higher content of P123 due to its better capacity of solubilization of lipophilic moiety as compared to F127 (Wei et al. 2009; Fares et al. 2018). The obtained results are in agreement with the finding of other researchers

Results shown in Table 5.10 revealed that at lower levels of the amount of Resveratrol added during the formulation of micelles, higher MIE was achieved, while it decreased with increasing its level from low to higher at a constant level of X1. It might be due to precipitation of Resveratrol owing to saturation of the inner core of the micelles at higher levels of Resveratrol added. So it can be concluded that higher content of Pluronic P123 with a lower amount of Resveratrol yields in higher MIE (Fares et al. 2018). The results are very much substantiated by Figure 5.15 also.

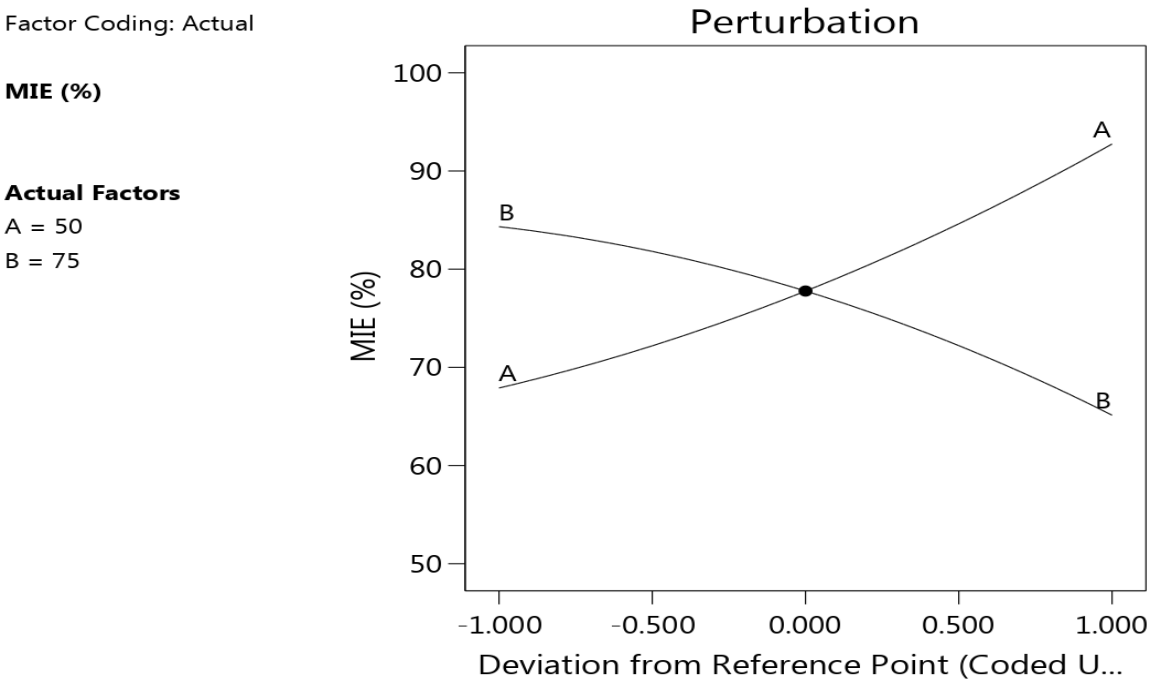

Figure 5.15: Perturbation curve for Micellar incorporation efficiency of polymeric micelles

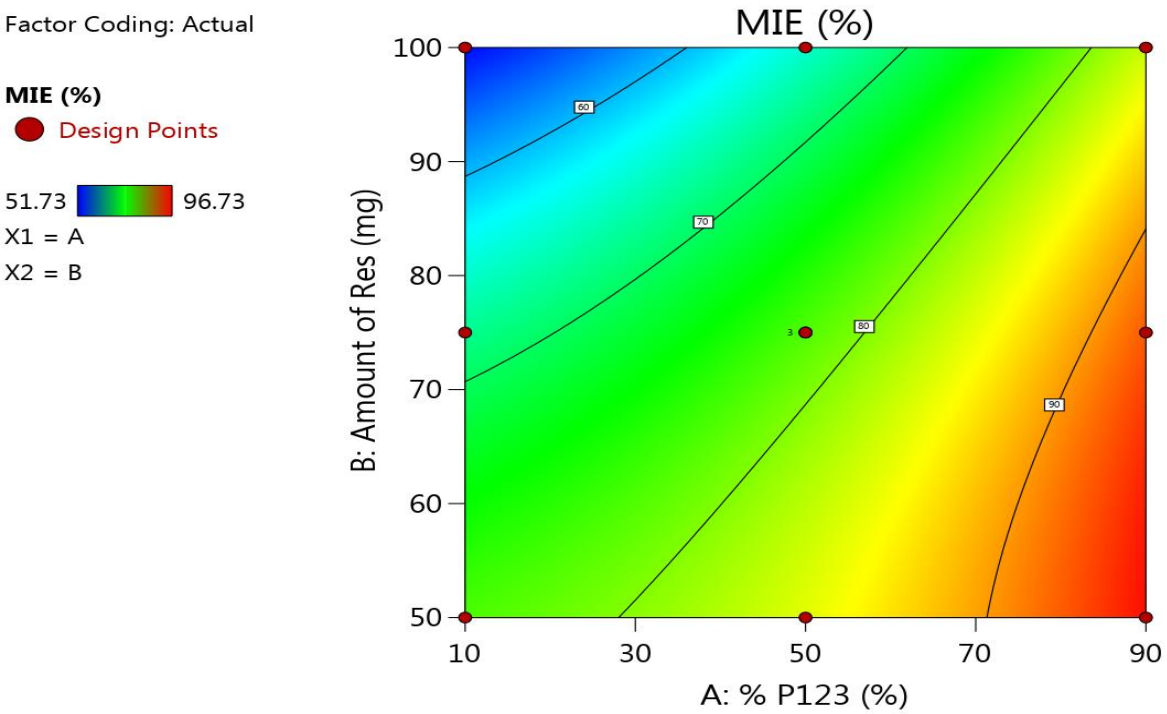

Figure 5.16: 2D contour plot for Micellar incorporation efficiency of polymeric micelles

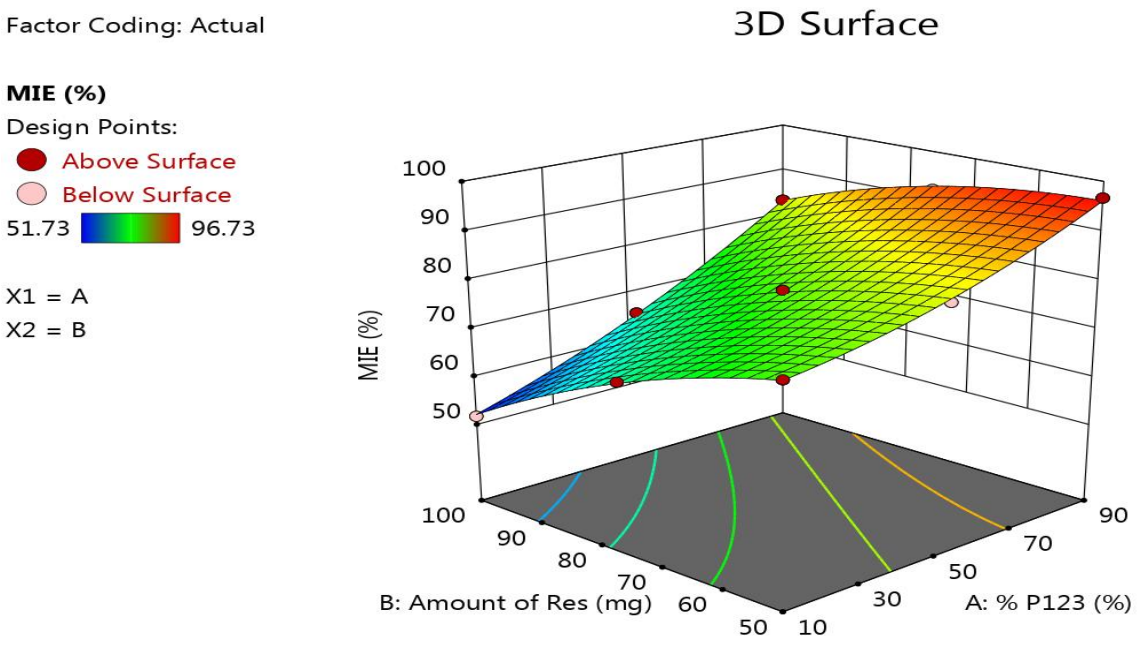

Figure 5.17: 3D Response surface morphology for Micellar incorporation efficiency of polymeric micelles

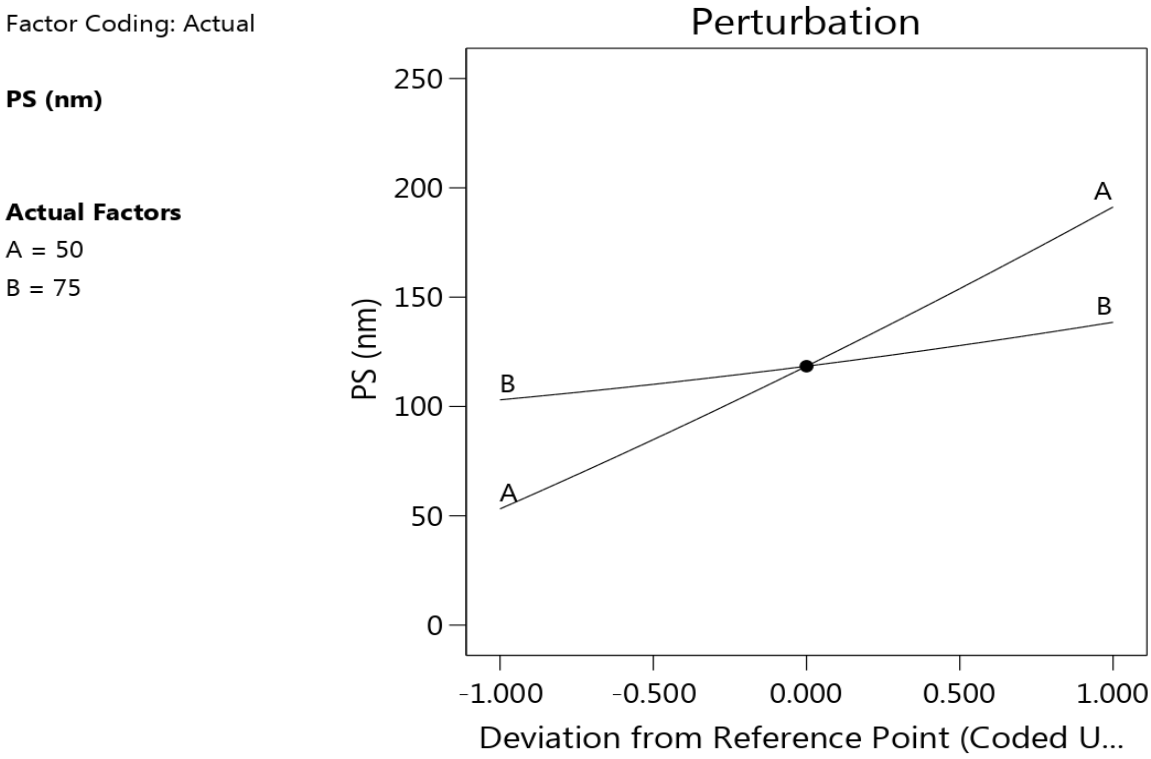

Figure 5.18: Perturbation curve for particle size of polymeric micelles

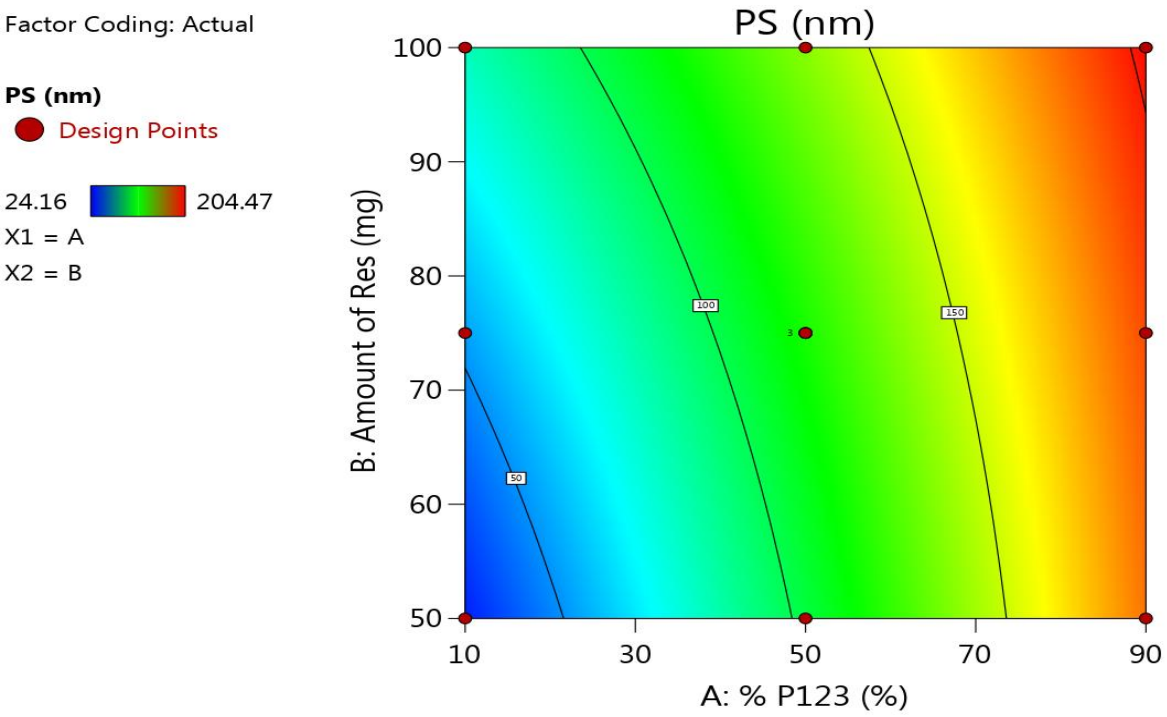

Figure 5.19: 2D contour plot for particle size of polymeric micelles

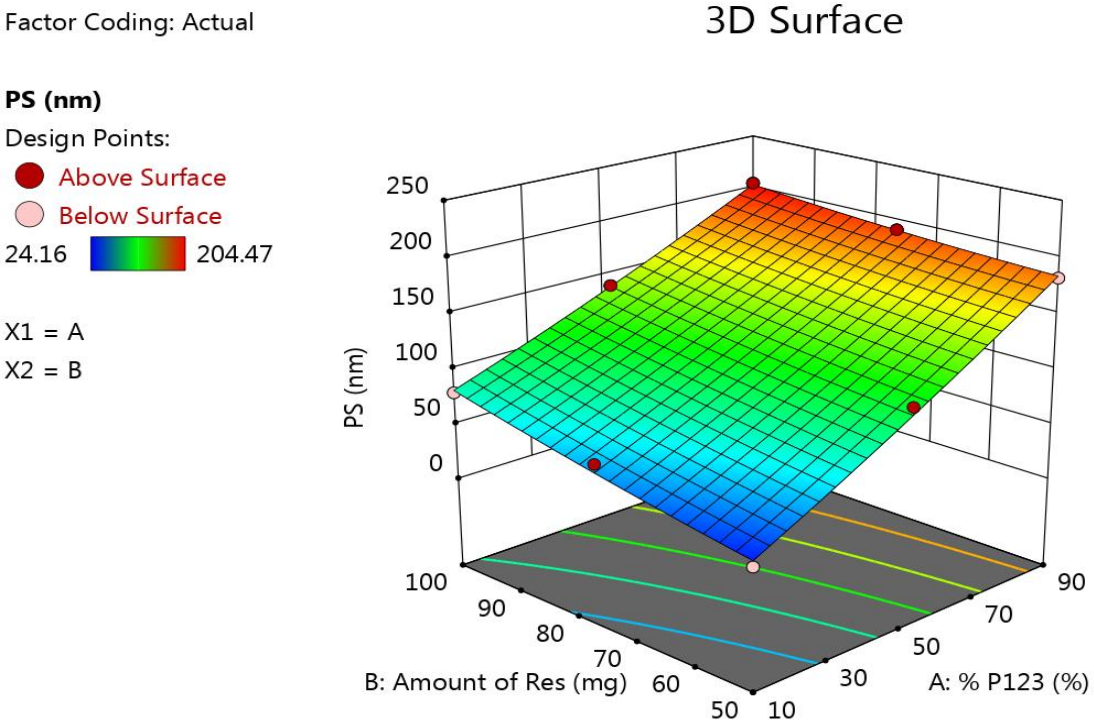

Figure 5.20: 3D Response surface morphology for particle size of polymeric micelles

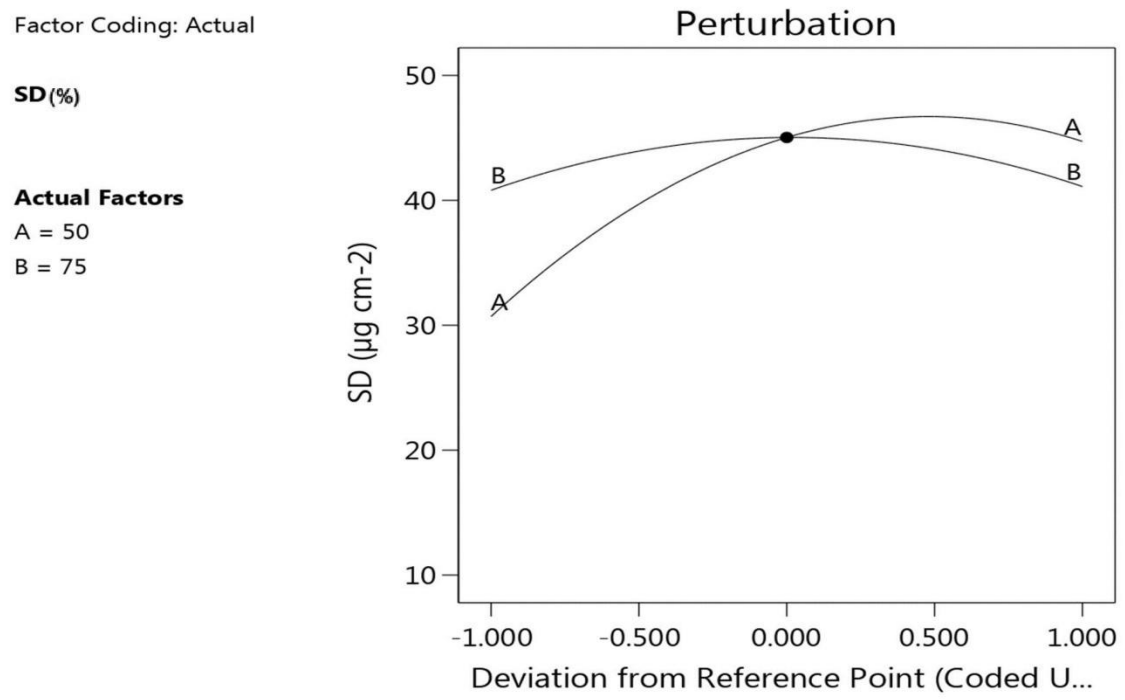

Figure 5.21: Perturbation curve for skin deposition of polymeric micelles

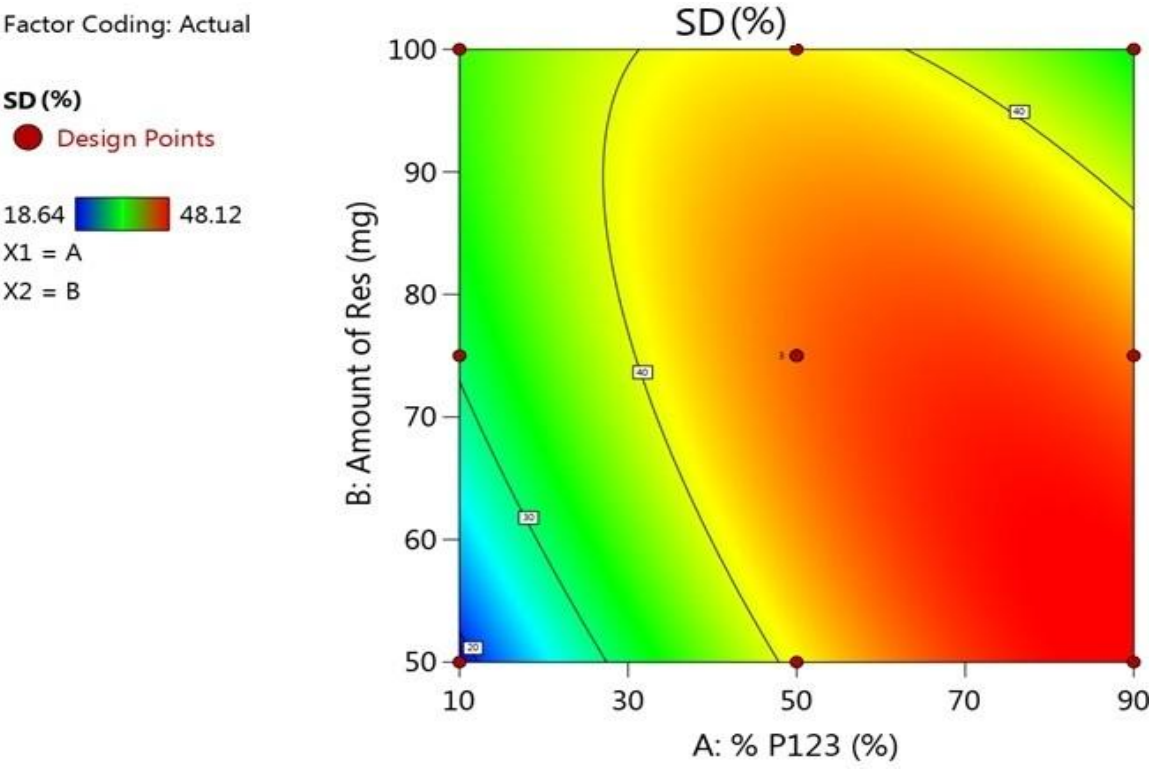

Figure 5.22: 2D contour plot for skin deposition of polymeric micelles

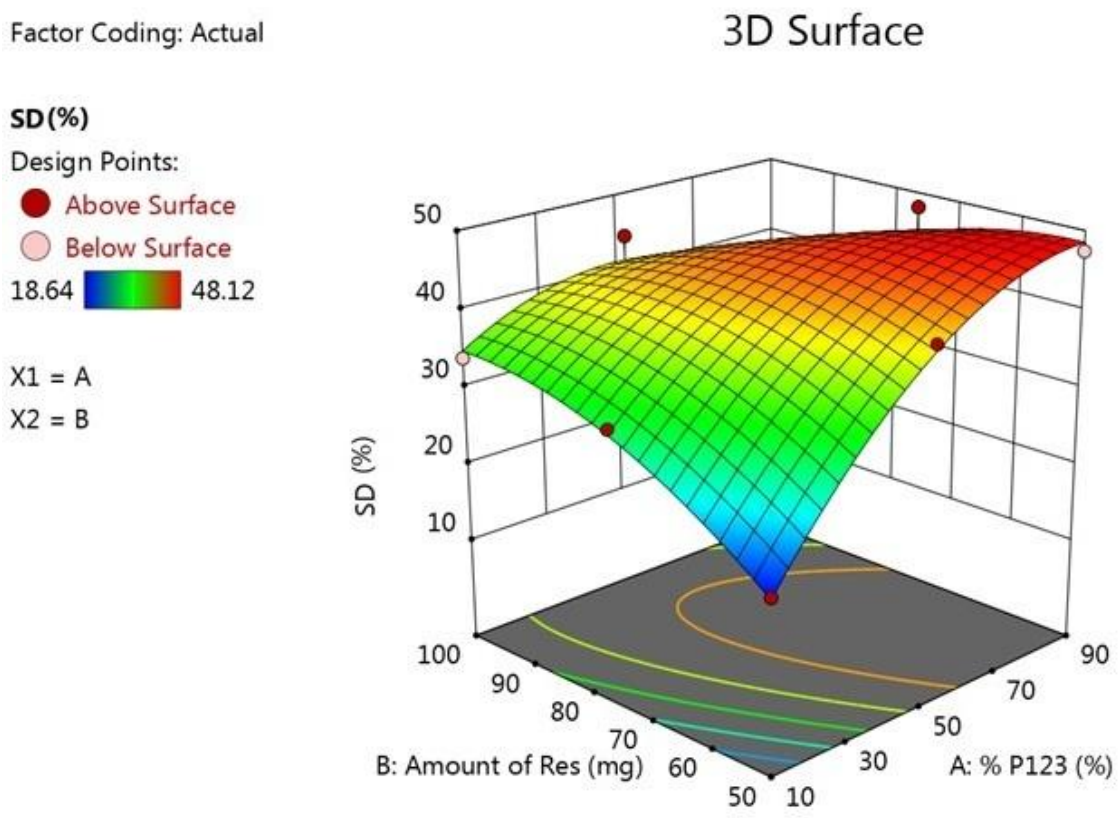

Figure 5.23: 3D Response surface morphology for skin deposition of polymeric micelles

5.2.1.6.2 Effect of CMAs on particle size (Y2)

The particle size of the micellar formulation is one of the critical variables affecting skin permeation. Smaller particle size assists the bioactive to pass through the small pores of the skin leading to more enhanced skin permeation. But for better dermatological benefits, the particle size should be in an optimum range, as the very smaller particle size of the carrier may lead to more systemic absorption of cargos entrapped with lesser skin retention. At the same time, higher particle size will resist the movement of the carrier through the stratum corneum barrier. Thus to get the optimum particle size it was selected as one of the prerequisite CQA. The following polynomial equation (equation 5.2) is generated by the software to study the interaction effect of X1 and X2 on Y2.

$$PS = +118.43 + 69.05\,X1 + 17.75\,X2 - 8.28\,X12 + 3.78\,X1^2 + 2.36\,X2^2 \quad \text{-eqn. 5.2}$$

According to the model and equation and perturbation curve, 2D contour plot and 3D plots represented in Figure 5.18-5.20 and Table 5.10 illustrates that increasing the levels of both CMAs has increased in particle size of micelles.

The analysis of particle size confirmed that the positive relationship with both the selected CMAs. Nonetheless, a strong influencing factor for particle size the concentration of Pluronic P123 as it is supported by equation 5.2 depicting a strong positive coefficient.

Increasing concentration of P123 in a mixture of P123 and F127 pluronic indicates a lesser proportion of F127 which generally kinetically stabilizes the micelles by steric hindrance results in the formation of larger mixed micelles. Increasing the Resveratrol amount relative to the amount of pluronic used, an increase in particle size was observed because at this high level higher entrapment of lipophilic Resveratrol takes place and thus leads to enlargement of the hydrophobic core region of the polymeric micelles (Fares et al. 2018). In addition to it, another reason can be attributed to the adsorption of Resveratrol on the outer shell of the micelles. The obtained results are concordant with the previously reported results (Kulthe et al. 2011)

5.2.1.6.3 Effect of CMAs on skin deposition potential (Y3)

Skin deposition of bioactive is also selected as one of the very crucial CQAs especially in the case of topical drug delivery where the target site is the dermal layer of skin as in the case of psoriasis treatment. The bioactive that reaches systemic circulation represents transdermal delivery, while higher retention of Resveratrol indicates local topical skin delivery which is the most critical for achieving enhanced therapeutic and dermatological benefits of loaded bio cargos.

The optimization process indicated that both CMAs have a significant quadratic effect on skin deposition as revealed by equation 5.3 and Figure 5.21.

$$SD = +45.04 + 7.01\,X1 + 0.1483\,X2 - 8.06\,X12 - 7.32\,X1^2 - 4.07\,X2^2 \quad \text{- eqn. 5.3}$$

The skin deposition of Resveratrol, at the lowest levels of both CMAs, was found to be less, however, it increased at intermediate levels, and then either the increment has declined or it reduced at higher levels of CMAs.

These results are well correlated with the particle size model, as skin deposition is largely affected by particle size. Very less particle size (less than 100 nm), might result in more permeation of Resveratrol in the systemic circulation, which means lesser skin retention, However larger size of colloidal particles may not even permeate through the tough skin barrier, which also resulted in poor skin retention. The Perturbation curve, 2D Contour plot and 3D response surface plot as depicted in Figure 5.21-5.23 ratified the above results.

5.2.1.7 Search for optimum formulation based on desirability approach and checkpoint analysis

Constraints were set for desired responses i.e. MIE (Y1) to be maximum, particle size (Y2) to be in range (100 nm < Y2 < 200nm), and skin deposition (Y3) also to be maximum. Both numerical and graphical optimization was carried out using the desirability approach and post prediction checkpoint analysis was done to get the final optimized micellar formulation. The solution having the highest desirability suggested by the software was selected among 21 solutions.

The optimized level of P123 concentration was found to be 0.584 i.e. 73.5 %. The optimum value lies in between intermediate level (0 i.e. 50 %) and high level (+1 i.e. 90%) tested. The optimum level of the Resveratrol amount to be used was found to be -0.940 i.e. 51.5 mg. This value is very near to the minimum level tested (i.e. -1) with a Desirability value of 0.916. The desirability and overlay plot are represented in Figure 5.24 and 5.25 respectively. At suggested levels of CMAs, the responses (CQAs) were obtained according to desired target values. The predicted and observed responses were compared and the percentage prediction error was within specified limits as shown in Table 5.12. The observed MIE was 93.45 ± 2.34 %, particle size was 142.67 ± 6.98 nm with skin deposition of 51.63 ± 1.97 %. The predicted and observed responses were compared and the percentage prediction error was within specified limits as shown in Table 5.13. It represented a high degree of predictive ability and validated the generated design for the evaluation and optimization of polymeric micelles.

Table 5.12: Target constraints set for CMAs and CQAs during numerical optimization of polymeric micelles

Name	Target	Lower Limit	Upper Limit
Concentration of P123 (X1)	Within level	-1	1
Amount of Resveratrol (X2)	Within level	-1	1
Micellar Incorporation efficiency (%) (Y1)	Maximize	51.73	96.73
Particle size (nm) (Y2)	In range	100	200
Skin deposition SD (%) (Y3)	maximal	18.64	48.12

Table 5.13: Solution obtained after Post analysis point prediction using Desirability approach suggested by Design-Expert Software with the predicted values of CQAs along with observed values and percentage prediction error

Batch No	CMAs		CQAs		
			MIE (%)	**Particle size (nm)**	**Skin deposition (%)**
	X_1	X_2	**Predicted values**		
			90.503	150	47.32
			Observed values		
PM 14	**73.4 %**	**51.5 mg**	93.45 ± 2.34	142.67 ± 6.98	51.63 ± 1.97
Percentage prediction error (%)			3.26	4.89	9.1

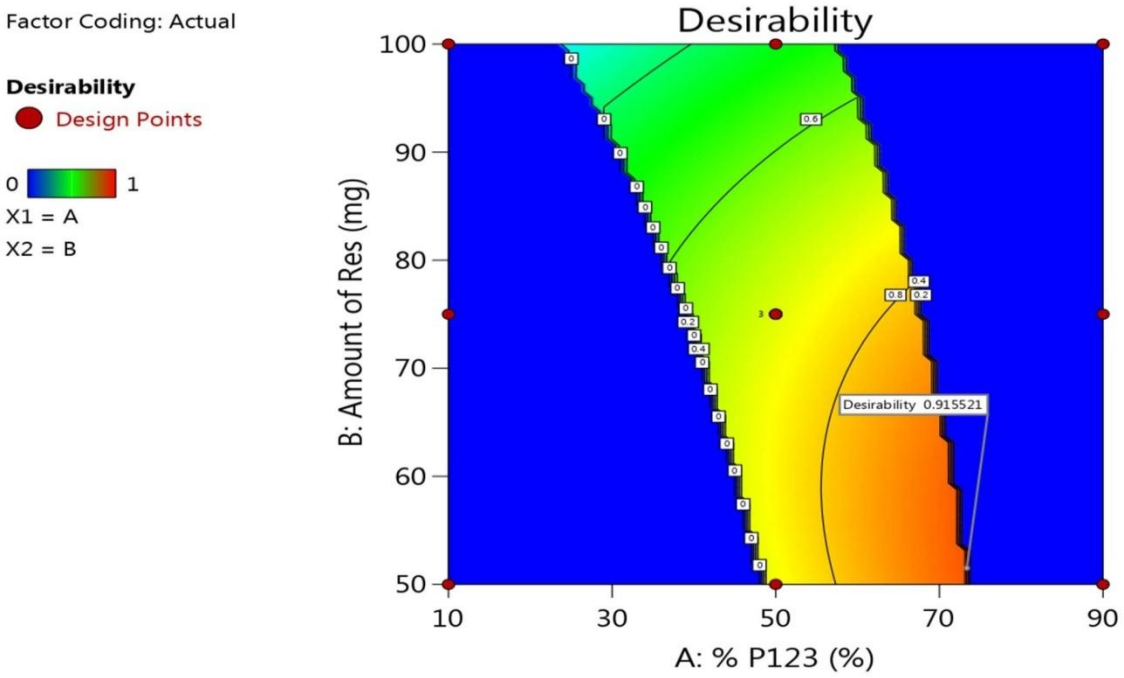

Figure 5.24: Desirability plot for the numerically optimized polymeric micellar formulation

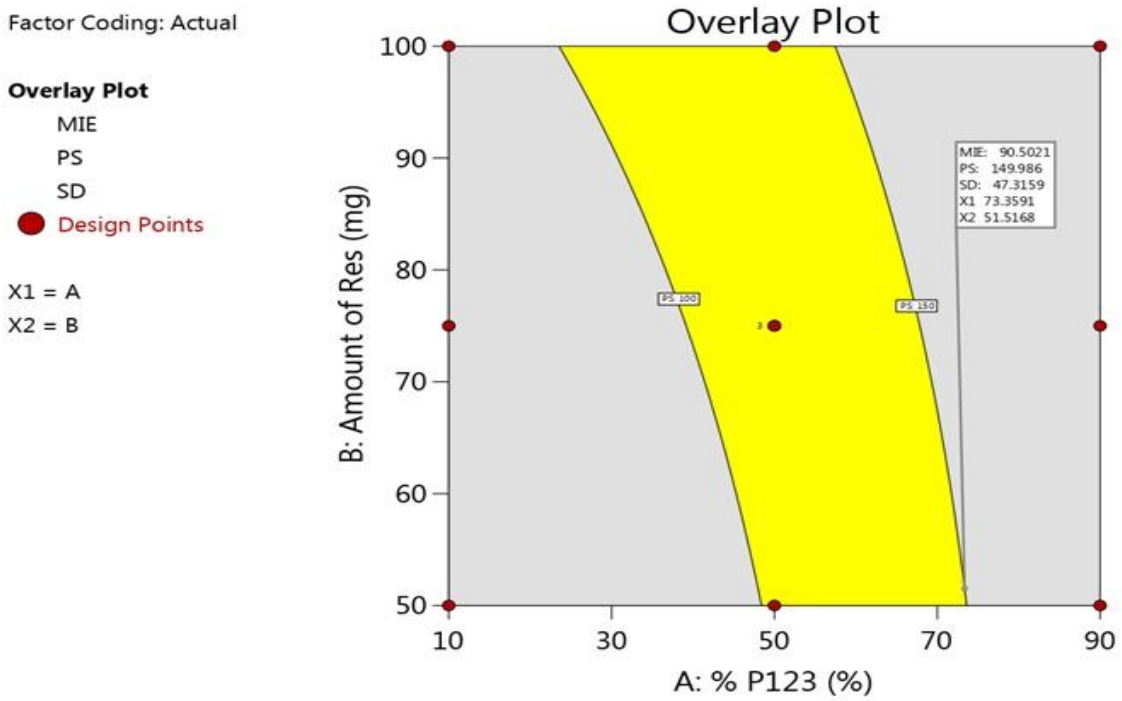

Figure 5.25: Overlay plot showing predicted results during graphical optimization of polymeric micelles formulation

5.2.1.8 Characterization of developed polymeric Micellar (PM) formulation

5.2.1.8.1 Size, polydispersity index, and zeta potential

The mean particle size and PDI of prepared micelles were found to be 142.67 ± 6.98 nm and 0.165 ± 0.096 respectively. The zeta potential of polymeric micelles found to be -33.65 ± 2.45 mV. Lesser values of PDI indicated homogeneity if colloidal carriers as well as predicted the stability of these during storage. All the parameters were also found to be optimum for topical skin delivery and indicate stable colloidal carriers. Particle size, PDI, and zeta potential reports are given in Figure 5.26-5.27 respectively.

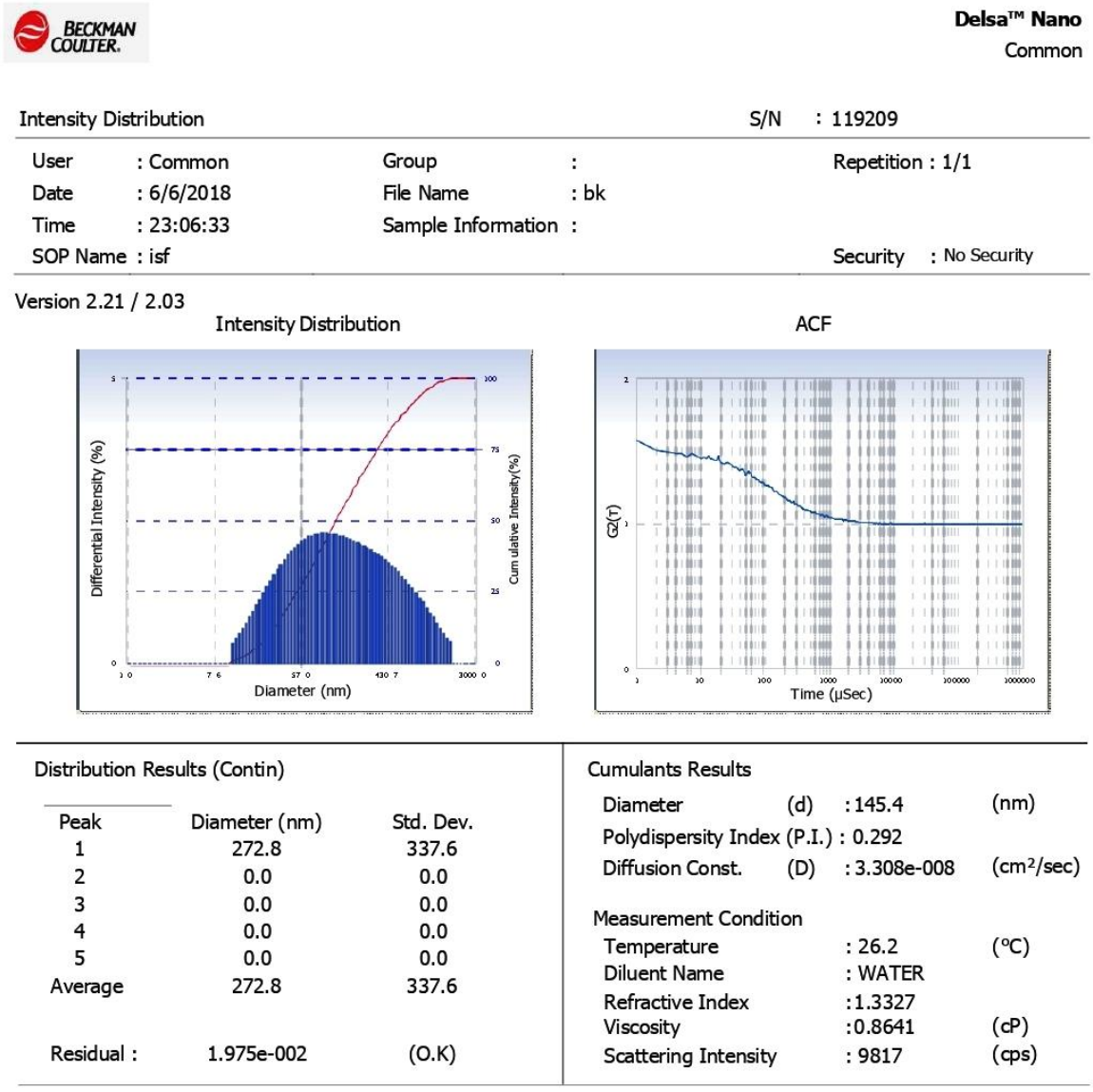

Figure 5.26: Size and PDI report of polymeric micelles

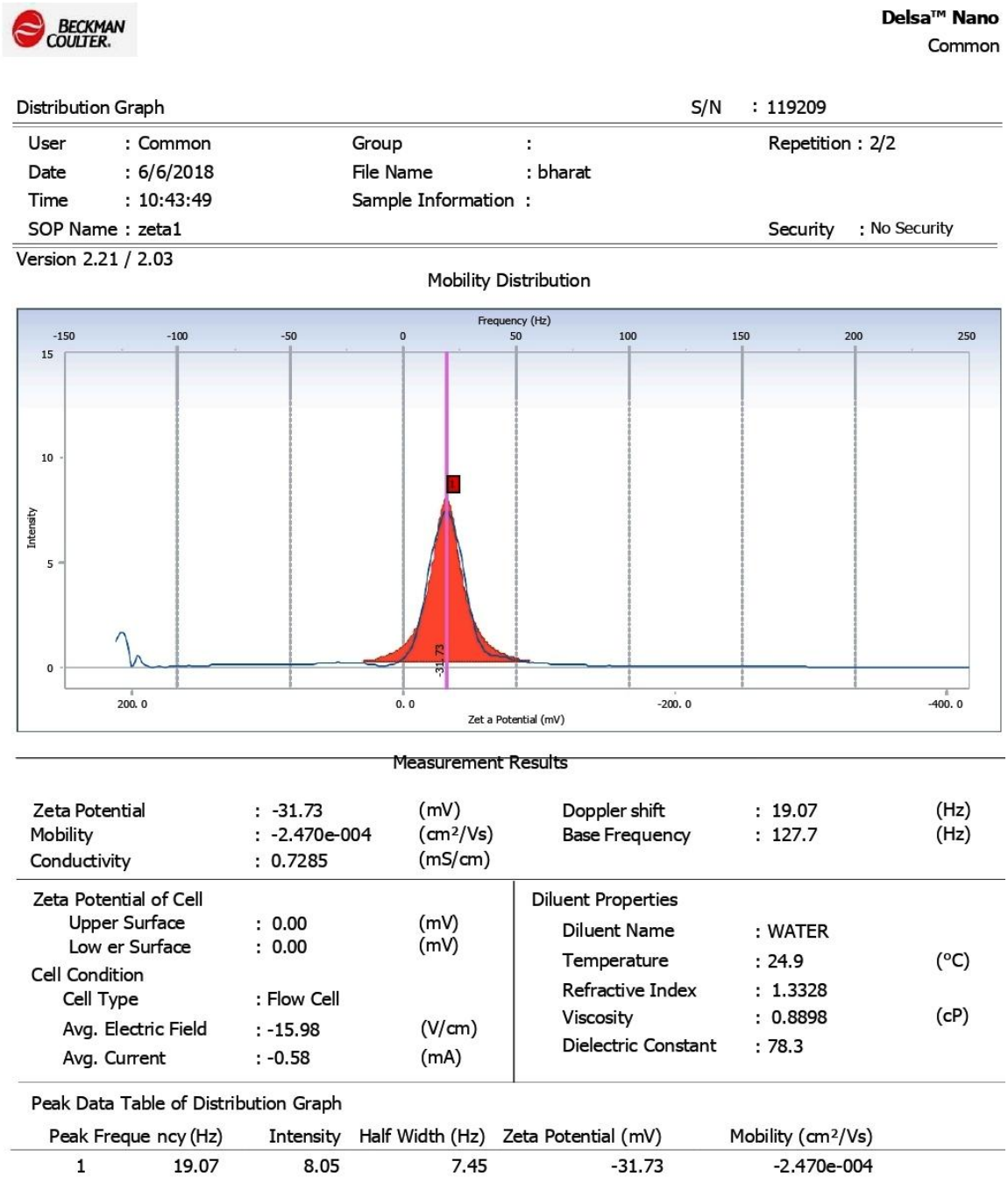

BECKMAN COULTER

Delsa™ Nano
Common

Distribution Graph S/N : 119209

User	: Common	Group	:	Repetition	: 2/2
Date	: 6/6/2018	File Name	: bharat		
Time	: 10:43:49	Sample Information	:		
SOP Name	: zeta1			Security	: No Security

Version 2.21 / 2.03

Mobility Distribution

Measurement Results

Zeta Potential	: -31.73	(mV)	Doppler shift	: 19.07	(Hz)
Mobility	: -2.470e-004	(cm²/Vs)	Base Frequency	: 127.7	(Hz)
Conductivity	: 0.7285	(mS/cm)			

Zeta Potential of Cell			Diluent Properties		
Upper Surface	: 0.00	(mV)	Diluent Name	: WATER	
Low er Surface	: 0.00	(mV)	Temperature	: 24.9	(°C)
Cell Condition			Refractive Index	: 1.3328	
Cell Type	: Flow Cell		Viscosity	: 0.8898	(cP)
Avg. Electric Field	: -15.98	(V/cm)	Dielectric Constant	: 78.3	
Avg. Current	: -0.58	(mA)			

Peak Data Table of Distribution Graph

Peak	Freque ncy (Hz)	Intensity	Half Width (Hz)	Zeta Potential (mV)	Mobility (cm²/Vs)
1	19.07	8.05	7.45	-31.73	-2.470e-004

Figure 5.27: Zeta potential report of polymeric micelles

5.2.1.8.2 Morphological evaluation

Morphological evaluation by TEM as shown in Figure 5.28 revealed that polymeric micelles obtained were spherical particles with a well-identified structure, uniform size, and distribution in the aqueous medium.

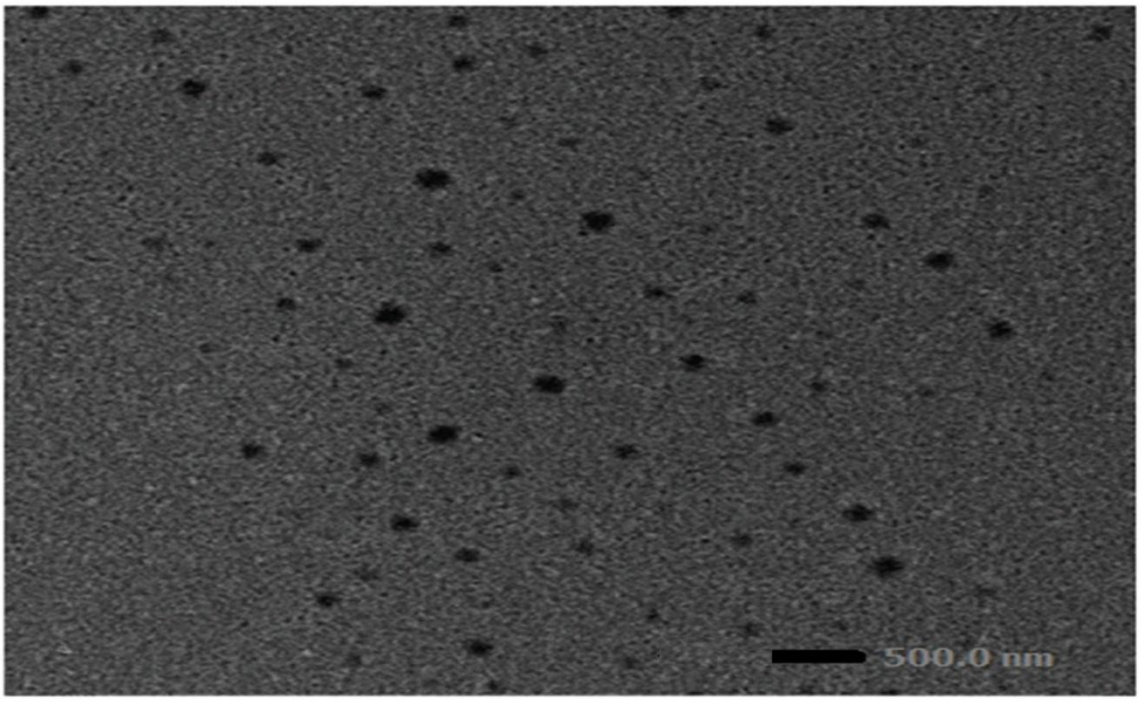

Figure 5.28: Transmission electron microscopic image of polymeric micelles

5.2.1.8.3 Encapsulation efficiency

Micellar encapsulation efficiency was found to be 93.45 ± 2.34 %, thus, the carrier has shown that it has high carrying capacity especially for a highly lipophilic molecule like Resveratrol. This property makes polymeric micelles suitable for topical skin drug/bioactive delivery for superior dermatological benefits.

5.2.1.9 Formulation and characterization of the corresponding hydrogel

To improve the skin applicability properties of the formulated colloidal formulation, it was converted into the carbomer-based hydrogel i.e. micellar hydrogel (PMG). Carbomer was selected due to its ideal characteristics (i.e. gelling property at a lower concentration and ease of preparation) and its wide use in a topical formulation. Conventional hydrogel (CG) was formulated to be used as a control for comparative purposes. Each gel was formulated to have 1% w/w Resveratrol. All the developed gels were colorless, translucent, and free from any gritty particles.

The size and PDI of colloidal carrier incorporated in the gel were observed to be statistically similar to the size and PDI of colloid in the form of dispersion, indicating the structural stability of micelles in the gel. The manufacturing process of the gel was well tolerated by the dispersion as it has not shown any signs of disruption.

5.3.1 Formulation of Resveratrol loaded vitamin E based nanoemulsion

5.3.1.1 Preliminary screening studies: Solubility studies of resveratrol in several excipients

Oil is one of the foremost excipients in the formulation of nanoemulsion as it plays an important role in solubilizing lipophilic drugs and bioactive like resveratrol. The drug would get precipitated if the selection of oil is not done considerably. In the present work, the maximum solubility of resveratrol was observed in ethyl oleate among all tested oils i.e. 130.20 ± 6.60 mg/mL as shown in Table 5.14. While in a mixture of ethyl oleate and vitamin E, solubility was found to be 106.43 ± 5.43 mg/mL. Here, vitamin E is used preferably as it can be used as an apt solvent for resveratrol as well as it has potent synergistic antioxidant benefits. Vitamin E is reported to have a beneficial effect on the psoriatic skin. Also, it forms a protective barrier on the skin (Chen et al. 2017). A wide range of surfactants and cosurfactants can be used in the formulation of nanoemulsion. The selection of combinations should be done very deliberately so that interfacial tension could be reduced maximally with the formation of a stable emulsion of the desired size range, as well as, minimal skin irritancy; thus, the preference is given to non-ionic surfactants. Generally used surfactants consist of tween® (polysorbates), cremophor®, lecithin, etc. The surfactant was also screened based on solubility and miscibility. It was observed that resveratrol has shown the highest solubility in the tween 80 i.e. 45.76 ± 2.56 mg/mL. Tween 80 is reported to be non-irritant and non-toxic in several reports thus broadly used in the manufacturing of emulsions. It is also listed in US Pharmacopeia-National Formulary; European Pharmacopeia (Patel et al. 2016) and categorized as essential nonirritant. Moreover, it has low critical micelle concentrations, with a high HLB value which is a prerequisite property to form an o/w nanoemulsion (Kalam et al. 2016).

Surfactant alone is unable to remove the transient negative interfacial tension, thus to aid its activity, a co-surfactant is required to be used as another important imperative excipient in the formulation of nanoemulsion (Pangeni et al. 2014). Co-surfactants enhance the flexibility of the interface, which results in increased flexibility of the hydrocarbon tail leading to superior dispersion of the oil into this area and helps in obtaining nanoemulsion systems at low surfactant concentration (Salem et al. 2019). Various co-surfactants such as transcutol P, PEG 400, and propylene glycol were screened. The maximum solubility of resveratrol among all co-surfactants screened was found to be in transcutol P. It was also observed that transcutol P along with tween 80 has a maximum solubilization capacity for the selected combination of oil also. Thus, a mixture of ethyl oleate and vitamin E (1:1) as oil, tween 80 as a surfactant, and transcutol P as co-surfactant were selected as major excipients to be used in the formulation of resveratrol loaded nanoemulsion.

Table 5.14: Solubility of resveratrol in different excipients (oil, surfactant, and co-surfactant)

Excipient	**Solvent**	**Solubility (mg/mL)**
Oil	Castor oil	18.76 ± 2.98
	Olive oil	23.13 ± 1.87
	Coconut oil	31.42 ± 2.76
	Ethyl Oleate	130.20 ± 6.60
	Vitamin E	40.50 ± 2.22
	Combination (EO +Vit. E)	106.43 ± 5.43
Surfactant	Tween 20	24.54 ± 3.62
	Tween 80	45.76 ± 2.56
Co-Surfactant	Propylene glycol	98.54 ± 17.12
	PEG 400	122.32 ± 12.10
	Transcutol P	235.52 ± 14.56

5.3.1.2 Construction of pseudo ternary phase diagram

Optimization of the ratio of surfactant:co-surfactant i.e. (Smix) was carried out by plotting pseudo ternary phase diagrams as presented in Figure 5.29. In the phase diagrams, Smix was the first component, oil was second and a variable amount of water was used as the third component. The simple aqueous titration method was adopted to construct the pseudo-ternary phase diagrams. The phase diagram at Smix ratio 3:1 has shown the highest area of emulsification and thus it was selected for further optimization.

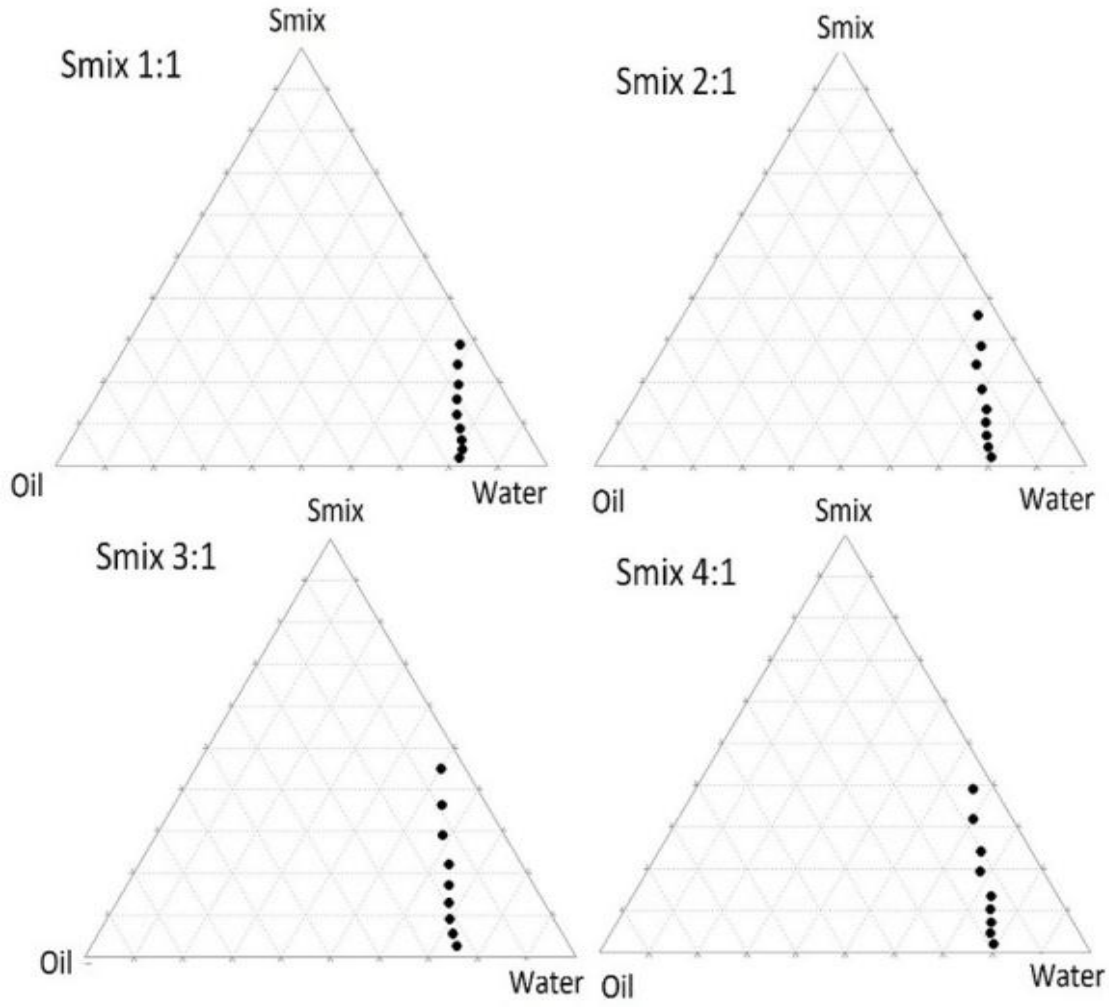

Figure 5.29: Pseudo-ternary phase diagram showing o/w nanoemulsion region for *S*mix (Tween 80:Transcutol P) ratio a 1:1, b 2:1, c 3:1, d 4:1. Maximum emulsification was obtained with *S*mix of 3:1 ratio

5.3.1.3 Formulation and optimization of Resveratrol loaded vitamin E based nanoemulsion using 3^2 factorial design

High energy emulsification (high-pressure homogenizer) is a widely used and accepted method for the preparation of nanoemulsions, which involves the use of mechanical energy (disruptive force) that disrupts the phases and leads to the formation of small droplets. The main advantages of this technique include the simple and easy production of nanoemulsions. Thus, in the present study, a high-pressure homogenization method was employed to formulate nanoemulsion.

The optimization process involved full factorial design by varying CMAs at different levels for evaluating their multivariate influence on CQAs as shown in Table 5.15 and response values of experimental runs as shown in Table 5.16. The ranges of responses for all batches were 143 to 340 nm (globule size), 3.25 to 4.92 % (% Cumulative resveratrol permeation), 2.04 to 10.16 µg hr^{-1} cm^{-2} (permeation flux) and 157 to 976 µg cm^{-2} (skin deposition).

Table 5.15: Variables (CQAs and CMAs) used for employing Factorial Design with coded and actual values for developing nanoemulsion

CMAs	**Coded and Actual Levels**		
	Low (-1)	**Medium (0)**	**High (+1)**
Concentration of Oil (X1)	5 %	10 %	15 %
Concentration of Smix (X2)	2.5 %	5 %	7.5 %
CQAs	**Target**		
Globule size (Y1)	Minimum		
Percent Cumulative Permeation (Y2)	Maximum		
Permeation flux J (µg hr^{-1} cm^{-2}) (Y3)	Enhanced but in range		
Skin deposition SD (µg cm^{-2}) (Y4)	Maximum		

Table 5.16: Response values of experimental runs for development of nanoemulsion

Batch No	Variable levels in coded form		Response Variables			
	X_1	X_2	Globule size (nm)	% Cumulative resveratrol permeation (Q_5)	Permeation flux (J) (µg hr^{-1} cm^{-2})	Skin deposition (SD) (µg cm^{-2})
NE 1	-1	-1	143 ± 10.3	4.23 ± 0.4	5.13 ± 0.2	480 ± 23.2
NE 2	0	-1	167 ± 12.5	4.76 ± 0.6	7.44 ± 0.6	656 ± 15.4
NE 3	+1	-1	198 ± 8.4	4.92 ± 0.3	10.16 ± 0.7	976 ± 13.5
NE 4	-1	0	196 ± 15.8	4.09 ± 0.3	3.42 ± 0.1	269 ± 16.3
NE 5	0	0	208 ± 21.4	4.34 ± 0.2	5.39 ± 0.2	483 ± 11.3
NE 6	+1	0	265 ± 16.3	4.60 ± 0.1	8.76 ± 0.4	798 ± 21.5
NE 7	-1	+1	252 ± 21.9	3.25 ± 0.5	2.04 ± 0.6	157 ± 16.6
NE 8	0	+1	297 ± 14.7	3.97 ± 0.1	3.47 ± 0.7	309 ± 17.7
NE 9	+1	+1	340 ± 16.7	4.17 ± 0.6	7.63 ± 0.3	578 ± 20.6
NE 10	0	0	211 ± 13.09	4.12 ± 0.1	5.35 ± 0.1	477 ± 9.3
NE 11	0	0	199 ± 10.76	4.32 ± 0.2	5.31 ± 0.1	485 ± 8.1
NE 12	0	0	232 ± 12.54	4.54 ± 0.2	5.43 ± 0.3	482 ± 8.3
NE 13	0	0	218 ± 7.89	4.37 ± 0.3	5.40 ± 0.2	475 ± 9.0

All other process variables were constant.[Values are expressed as mean ± S.D., (n = 3)]

5.3.1.4 Model generation for optimization in nanoemulsion

Each response was fitted to a second-order quadratic model and the best-fitted model was determined. Model significance was identified and confirmed by ANOVA, lack-of-fit test, and multiple correlation coefficients (R^2) tests. Statistical significance was observed with all suggested models as a value of $p < 0.0001$ in all cases. Values of "lack of fit" were found to be insignificant as $p > 0.005$. The r^2 values for these models were found to be greater than 0.998, and indicating the commendable fit of the derived polynomials to the obtained response values. The design summary is represented in Table 5.17.

Table 5.17: Design summary and build information for optimization of nanoemulsion

File Version	**11.0.5.0**						
Study Type	Response Surface		**Subtype**			Randomized	
Design Type	3 Level Factorial		**Runs**			13	
Design Model	Quadratic		**Blocks**			No Blocks	
Response	**Analysis**	**Std. Dev.**	**R^2**	**Adjusted R^2**	**Predicted R^2**	**%CV**	**Model**
Y1	Polynomial	6.76	0.9905	0.9837	0.9345	3.03	Quadratic
Y2	Polynomial	0.1267	0.9185	0.9022	0.8028	2.96	Linear
Y3	Polynomial	0.2546	0.9925	0.9871	0.9237	4.41	Quadratic
Y4	Polynomial	16.33	0.9966	0.9942	0.9666	3.20	Quadratic

Main and interaction effects are evaluated and the polynomial equations. These polynomials portrayed significant information corresponding to coefficient values and mathematical sign against each coefficient indicated the extent type of effect/ interaction.

A synergistic or positive correlation between variables is established if the coefficient carries a positive sign while an antagonistic or negative correlation is found to be established with a negative sign.

ANOVA was applied to the obtained results using software that indicated the validity of the data. All the studied CMAs were found to significantly influence the selected CQAs. There were a good correlation and concurrency between the R^2 values (observed and predicted) of every response. It was followed by the application of ANOVA to ascertain the statistical significance ($p < 0.05$) and the degree of the main effects of each variable and their interactions.

The equation showing the quadratic effect of studied variables on globule size is shown in equation 5.4 to 5.7.

$$\text{Globule Size (Y1)} = +210.93 + 35.33\,A + 63.50\,B + 8.25\,AB + 12.24\,A^2 + 13.74\,B^2 \quad \text{-eqn. 5.4}$$

$$\%\ Q5\ (Y2) = +4.28385 + 0.353333\,A - 0.420000\,B \quad \text{-eqn. 5.5}$$

$$\text{Permeation flux (Y3)} = +5.38 + 2.66\,A - 1.60\,B + 0.1400\,AB + 0.7410\,A^2 + 0.1060\,B^2 \quad \text{-eqn. 5.6}$$

$$SD\ (Y4) = =+480.97 + 241.00A - 178.00B - 18.75\,AB + 57.62\,A^2 + 6.62\,B^2 \quad \text{-eqn. 5.7}$$

5.3.1.5 Model analysis and diagnostic for optimization in nanoemulsion

A normal plot of residuals plotted amid normal % probability *vs* internally studentized residuals is shown in Figure 5.30 (i-iv). In all the responses normal distribution of points was observed except. It indicated that the transformation of data in this was required. All other responses presented fair analysis.

Residuals *vs* Predicted plot is shown in Figure 5.31 (i-iv) for testing the constant variance assumption. Consequently, a fair analysis of the model is suggested.

Residuals *vs* run plot is shown in Figure 5.32 (i-iv) for analyzing hidden variables that may manipulate the response. In all responses arbitrarily scattering of almost all points amid specified range was observed through the steady array. Thus the fair analysis of hidden variables is confirmed by the plot and the order of runs also suggested fair randomization.

Box-Cox Plot for selecting power transformation is shown in Figure 5.33 (i-iv) plotted between Ln residual and lambda value. Based on the calculated value of λ power transformation is suggested by the software. In the case of Y1, Y2, and Y3, the value of λ was 1, thus none transformation is suggested. While in the case of the Y4 value of λ was 0.5, thus the square root model transformation is suggested.

Predicted *vs* Actual Plot is shown in Figure 5.34 (i-iv), it is plotted to detect the difficulty to predict values using the model. In all responses, all points were very lying very near to the diagonal line. Thus it can be concluded that the analysis is valid and it could help in steering the selected design.

The plot of leverage versus Runs is shown in Figure 5.35 (i-iv). The fit of the suggested model is determined using this. All the points were found to lie between the recommended range of leverage i.e. 0 to 1. Thus the significance of the model was confirmed by these diagnostic plots.

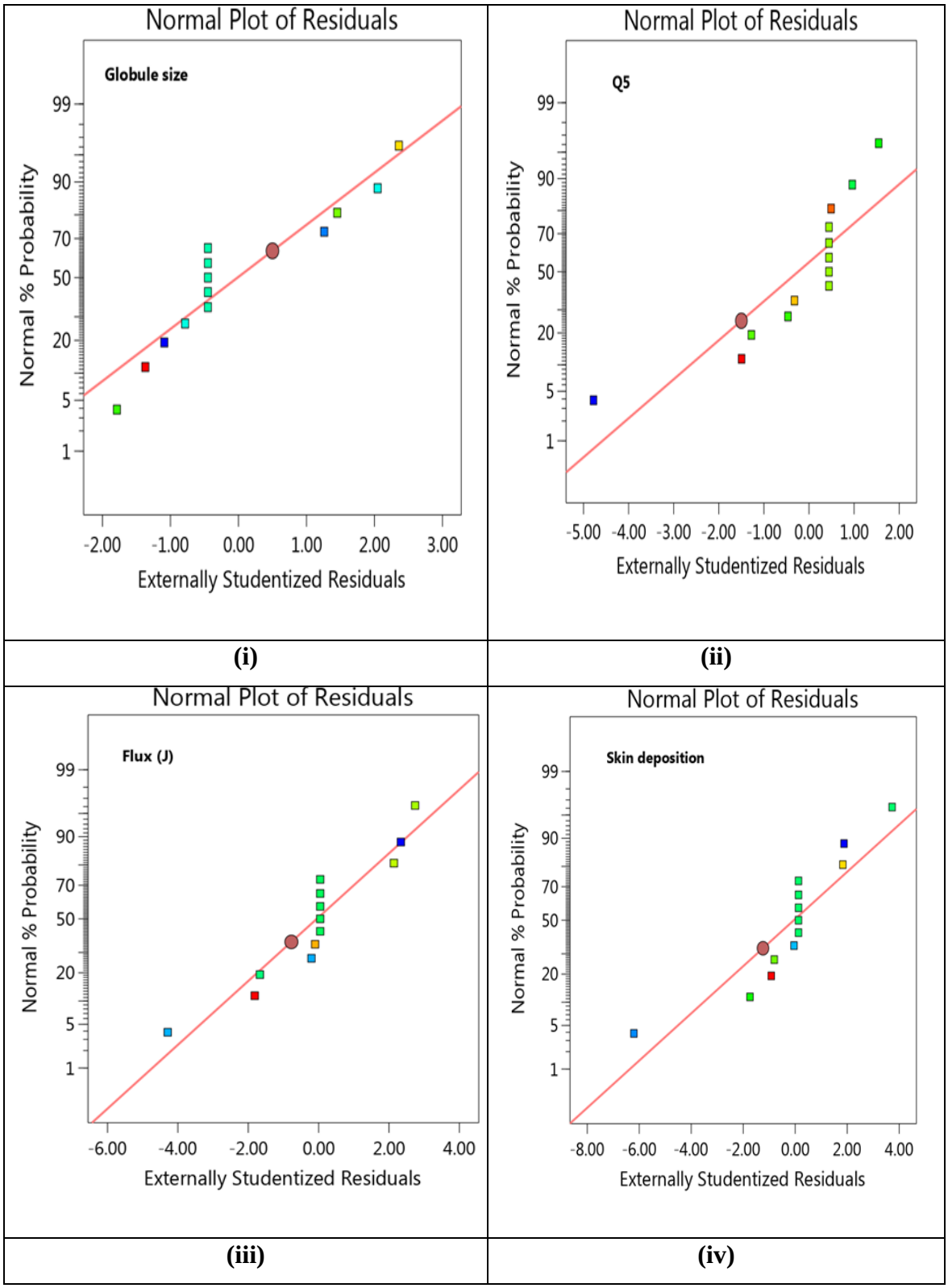

Figure 5.30: Graph showing residuals for Resveratrol loaded nanoemulsion, (i) Globule size (ii) Q5 (iii) Flux and, (iv) Skin deposition

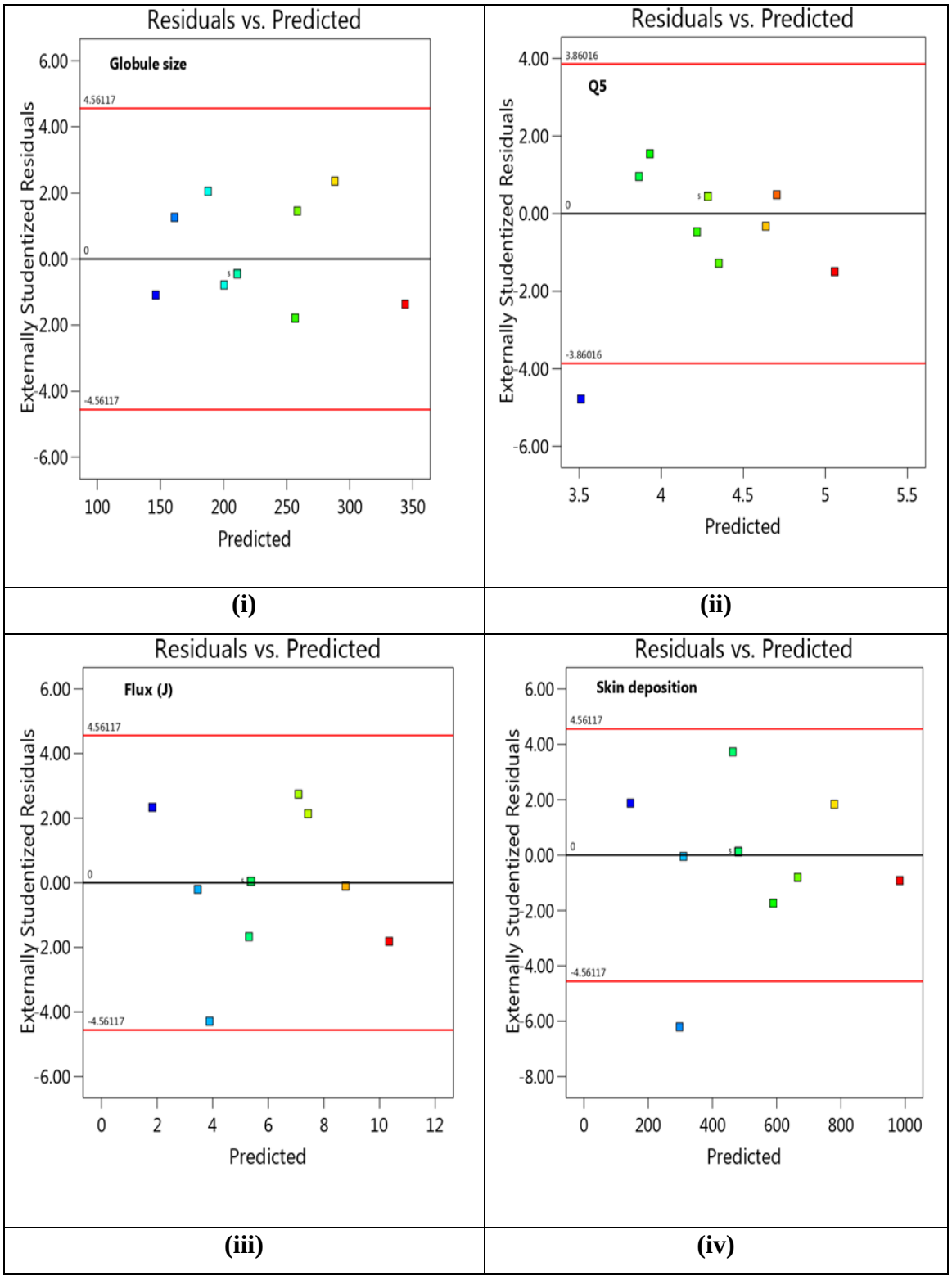

Figure 5.31: Graph between Residuals and Predicted plot related to Resveratrol containing nanoemulsion, (i) Globule size (ii) Q5 (iii) Flux and, (iv) Skin deposition

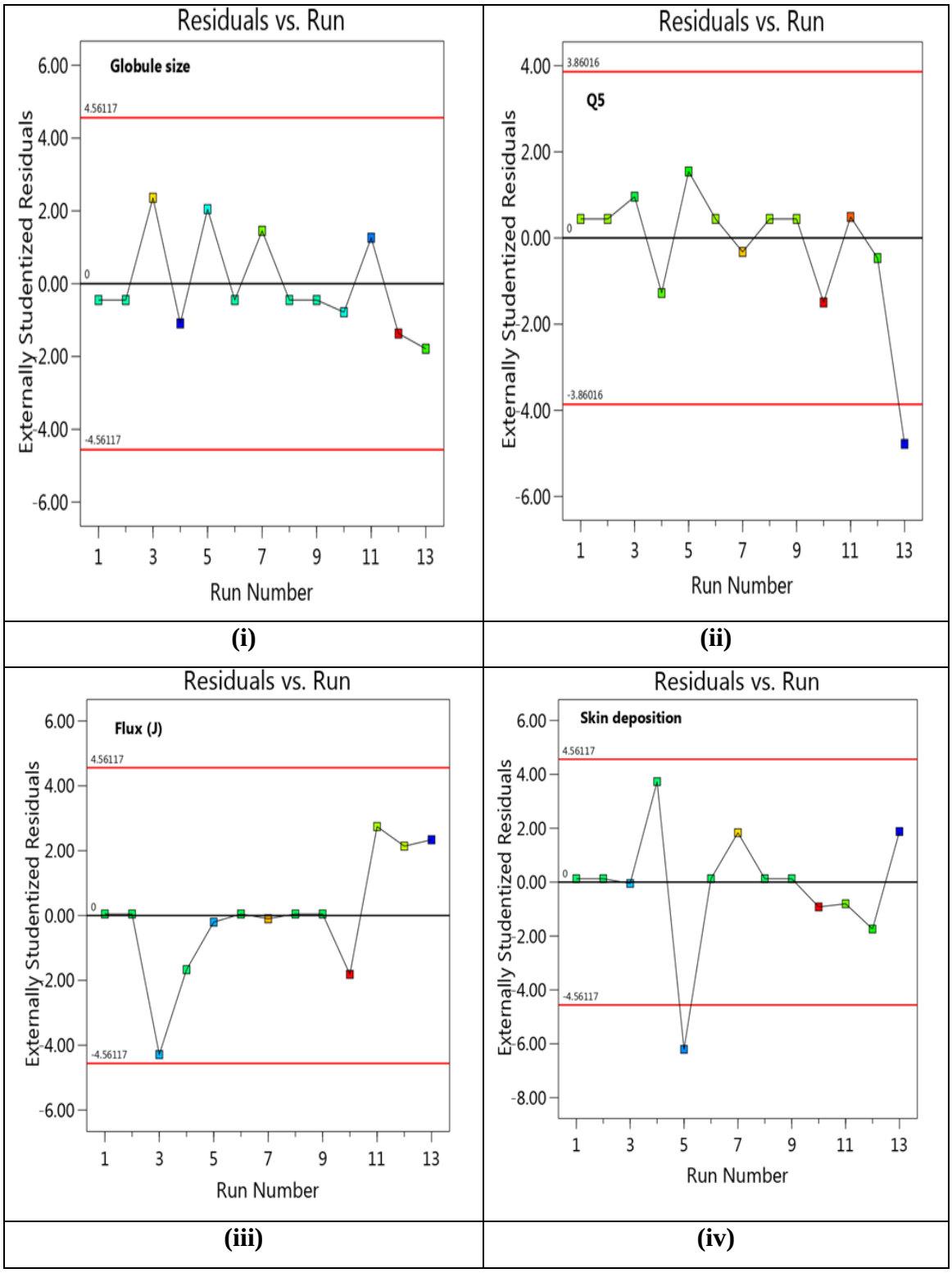

Figure 5.32: Graph between Residuals and run plot related to Resveratrol containing nanoemulsion, (i) Globule size (ii) Q5 (iii) Flux and, (iv) Skin deposition

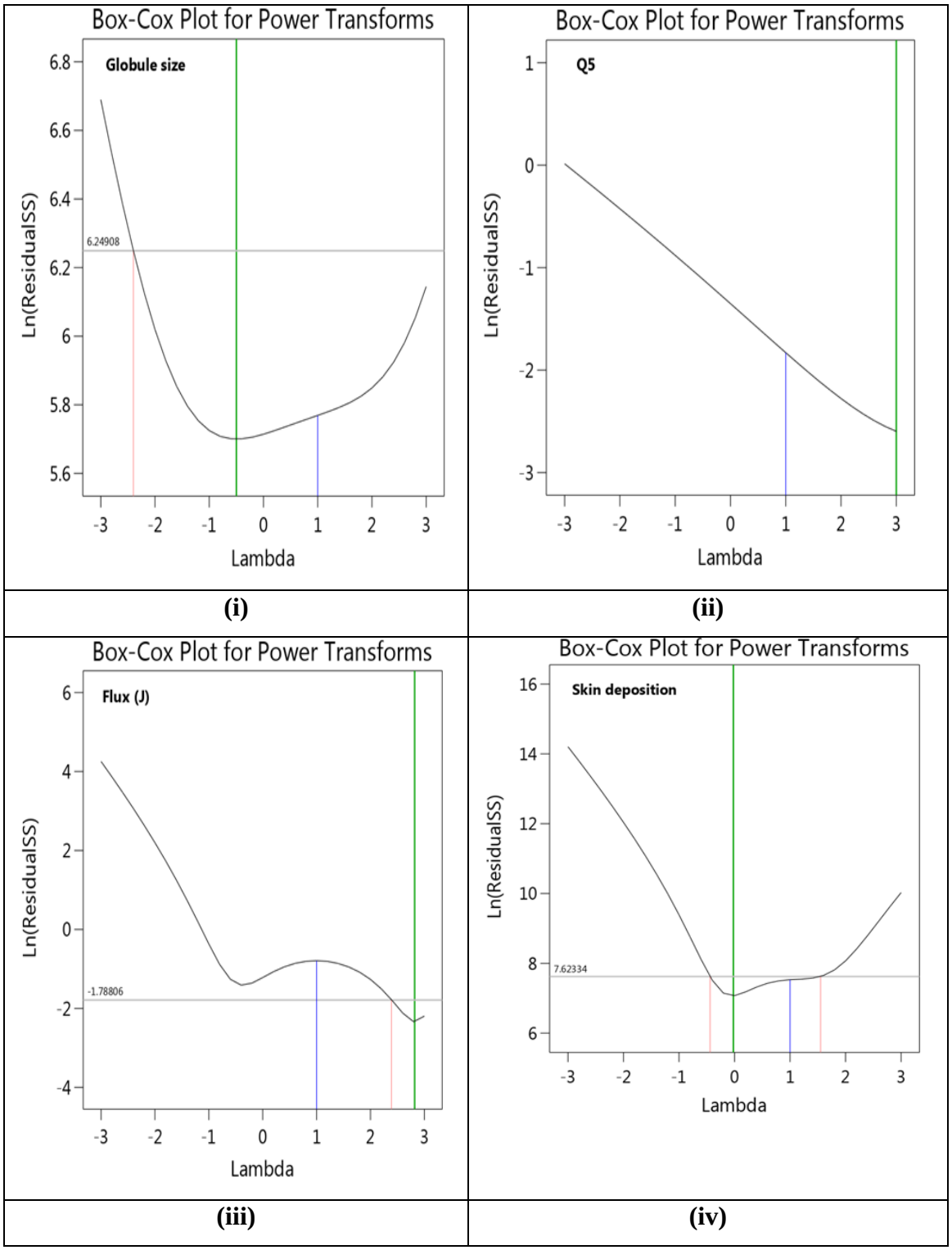

Figure 5.33: Box-Cox curve for power transform for Resveratrol containing nanoemulsion, (i) Globule size (ii) Q5 (iii) Flux and (iv) Skin deposition

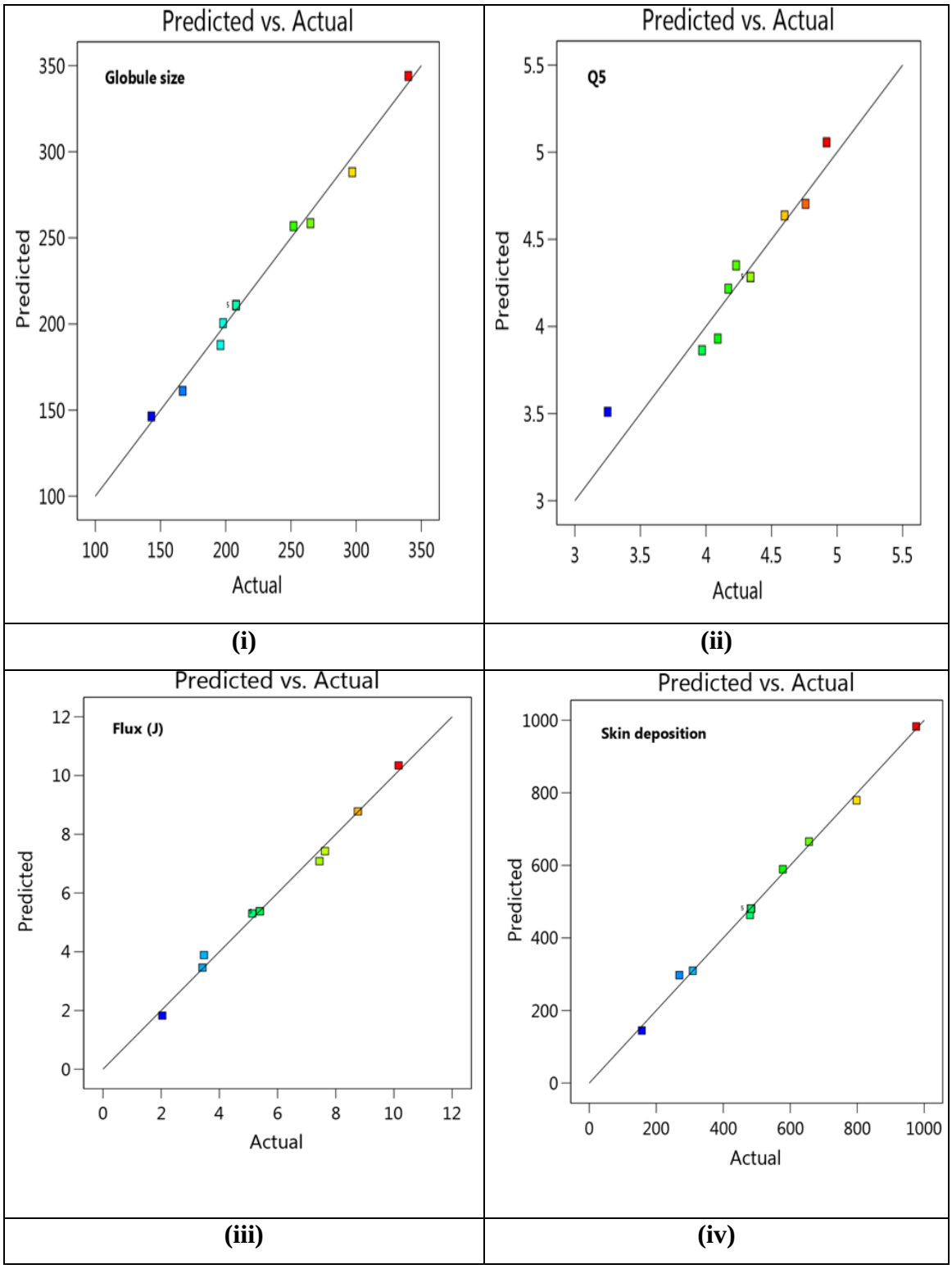

Figure 5.34: Predicted *vs* Actual Plot for Resveratrol containing nanoemulsion, (i) Globule size (ii) Q5 (iii) Flux and, (iv) skin deposition

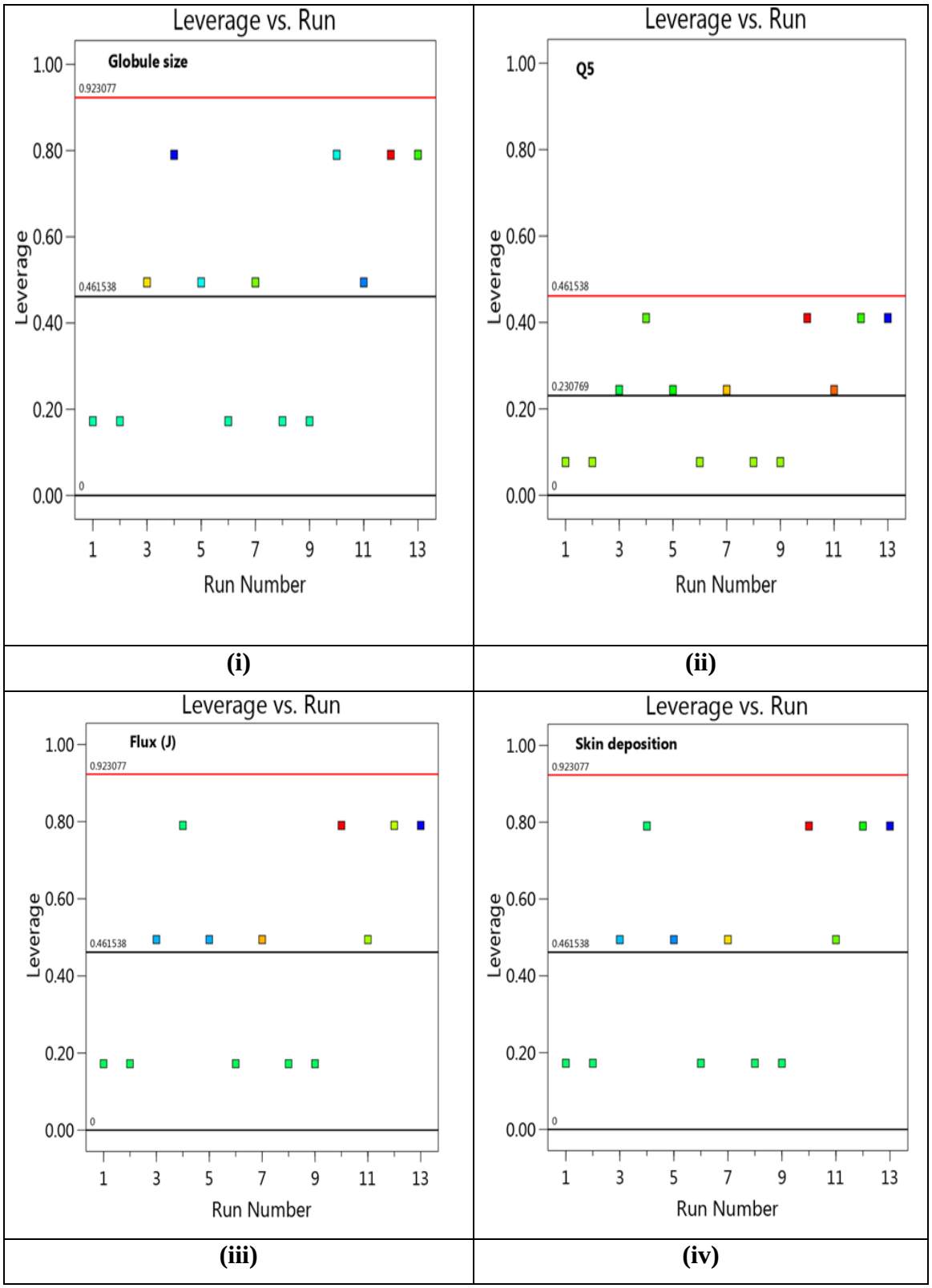

Figure 5.35: Leverage versus Runs Plot for Resveratrol containing nanoemulsion, (i) Globule size (ii) Q5 (iii) Flux and, (iv) skin deposition

5.3.1.6 Response surface methodology through polynomial equations for nanoemulsion

To evaluate the effect of examined variables on globule size, polynomial equations, perturbation curve, 2D contour plot, and 3D response surface plots as shown in Figure 5.36-5.47 were correlated and main effects along with interaction effect were determined.

From the graphs and polynomial equation, it can be ratified that both the variables have a significant positive effect on the globule size of nanoemulsion. Thus, the lowest level of oil, as well as Smix, resulted in minimum globule size.

However, the impact of the concentration of Smix on globule size was more as compared to the concentration of oil. Globule size increases significantly when more oil is incorporated due to the enlargement of the oil droplet of the emulsion. These results also match with the previous research showing similar results.

Results indicated that both the variables have a linear effect on the percentage of cumulative drug permeation. On increasing oil concentration, percent permeation was found to be increased while it was decreased upon increasing the concentration of Smix.

Permeation flux is also affected positively by increasing oil concentration, while a negative effect was observed by increasing the Smix ratio. Similar to it, skin deposition is also highly affected by the concentration of Smix in a negative manner.

However, increasing oil concentration resulted in higher skin deposition. Both variables have a significant quadratic effect on the skin deposition of bioactive. From the above main and interaction effects of independent variables on individual quality attributes, it could be ratified that Smix content should be minimal while the in to get the minimum globule size of nanoemulsion and maximum skin deposition with required flux.

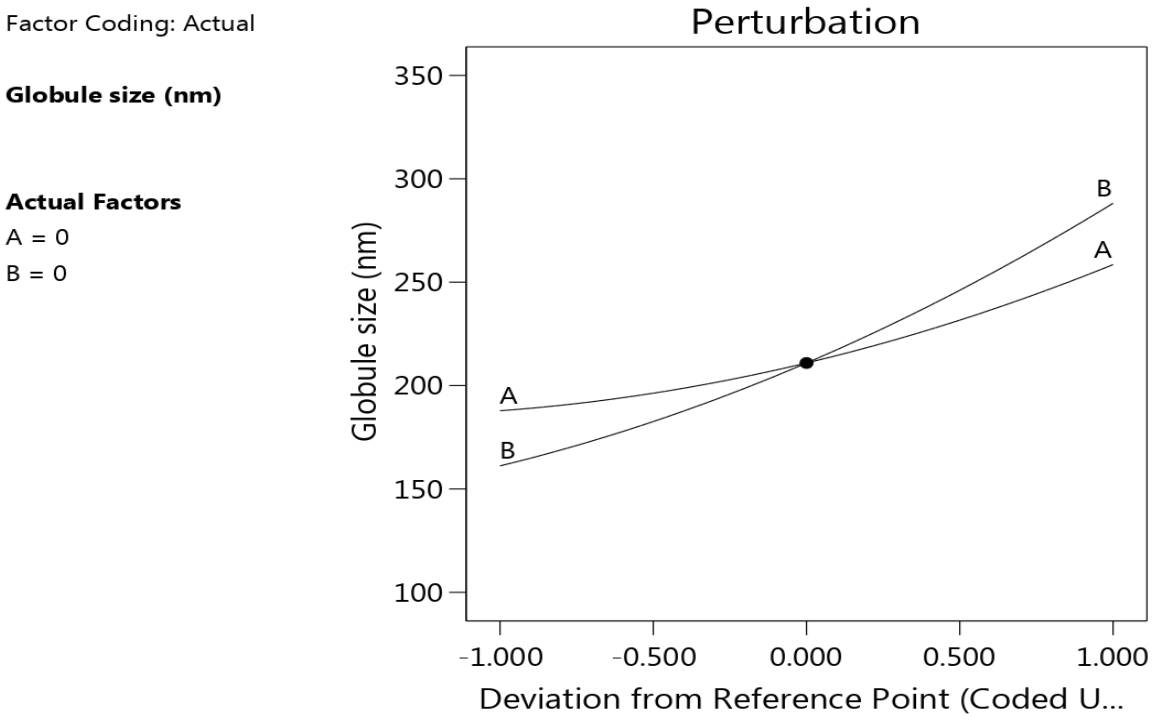

Figure 5.36: Perturbation curve for globule size of nanoemulsion

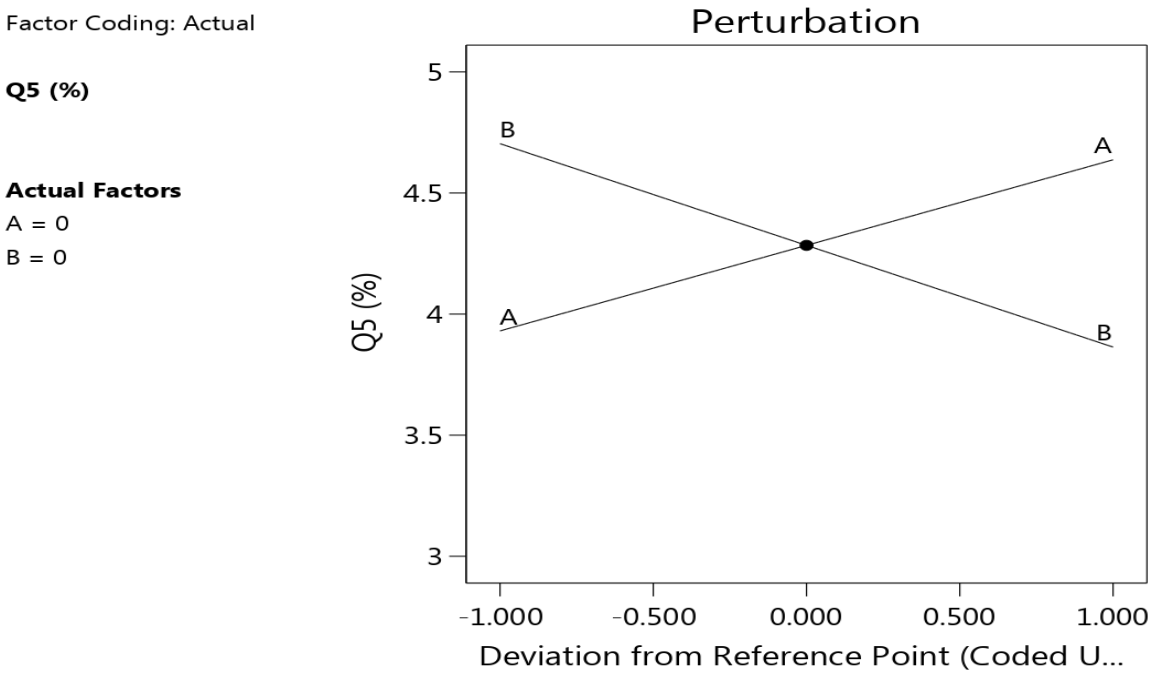

Figure 5.37: Perturbation curve for cumulative drug permeation of nanoemulsion

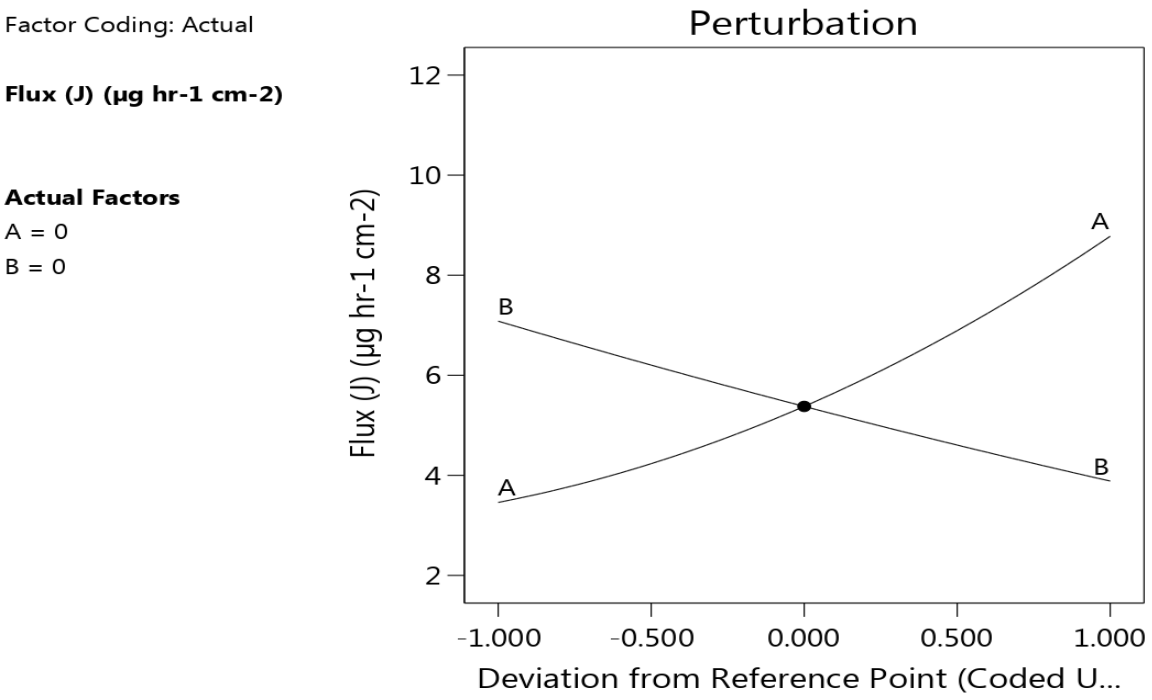

Figure 5.38: Perturbation curve for flux of nanoemulsion

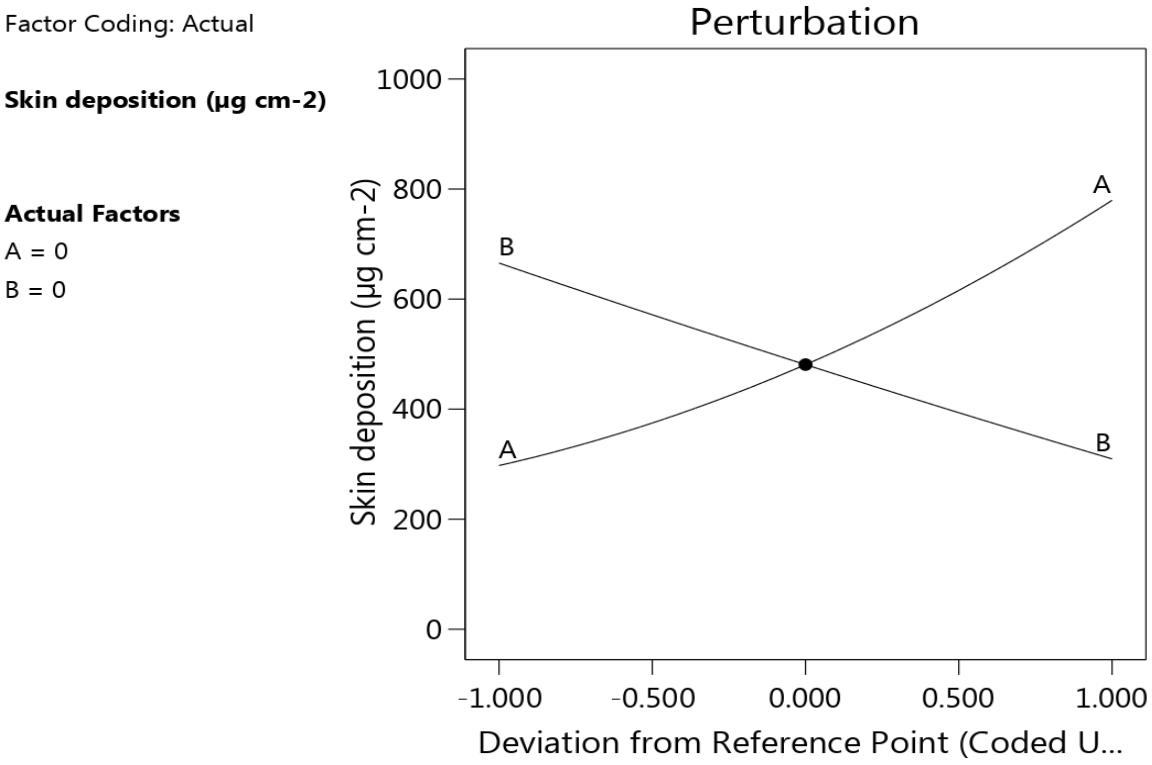

Figure 5.39: Perturbation curve for skin deposition of nanoemulsion

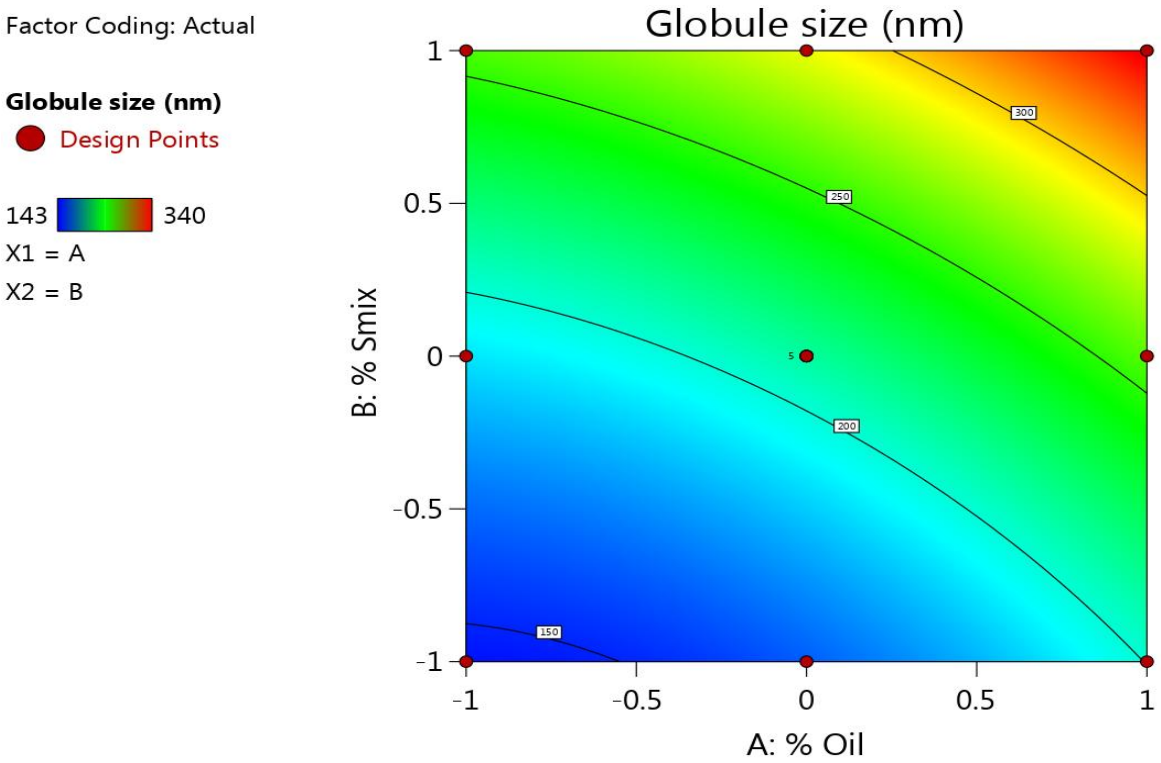

Figure 5.40: 2D Contour plot for globule size of nanoemulsion

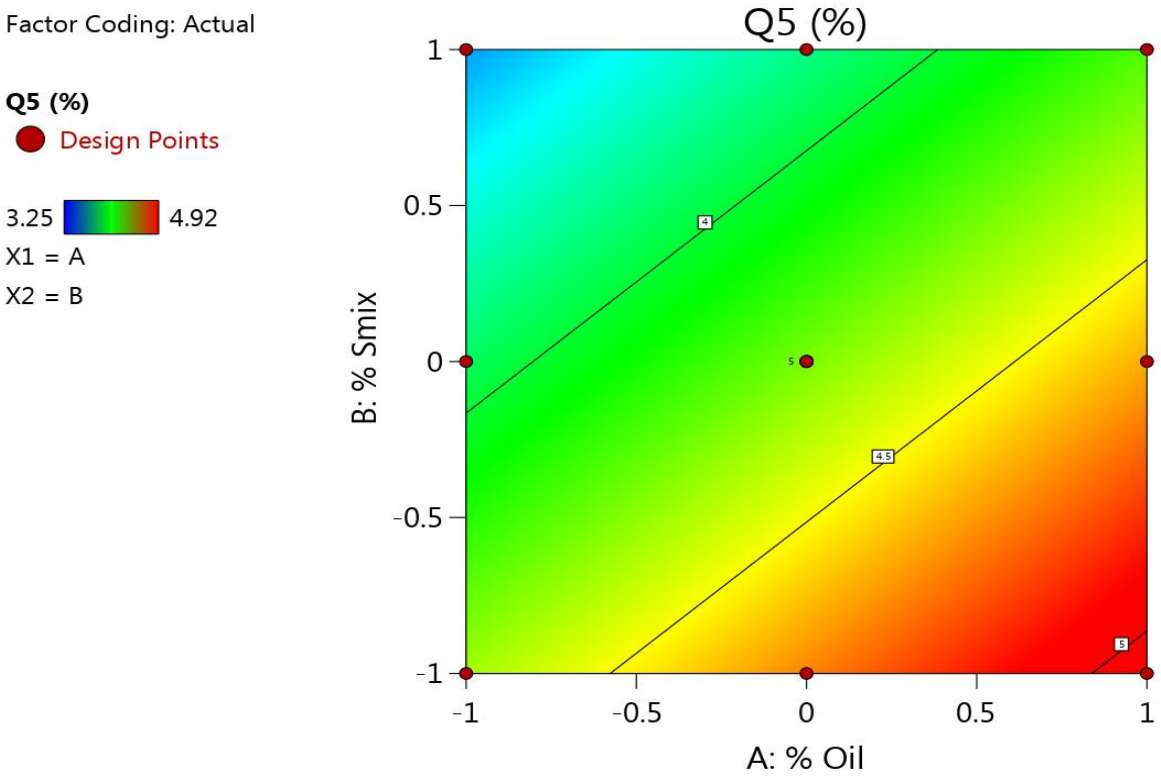

Figure 5.41: 2D Contour plot for cumulative drug permeation of nanoemulsion

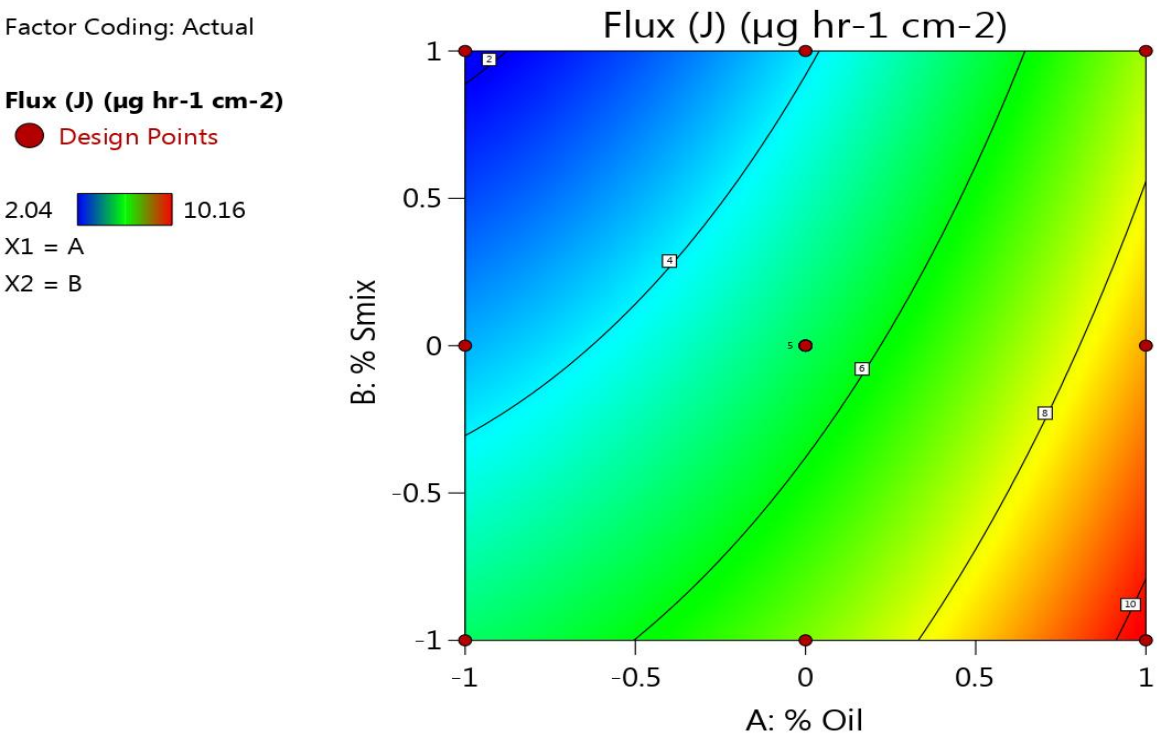

Figure 5.42: 2D Contour plot for flux of nanoemulsion

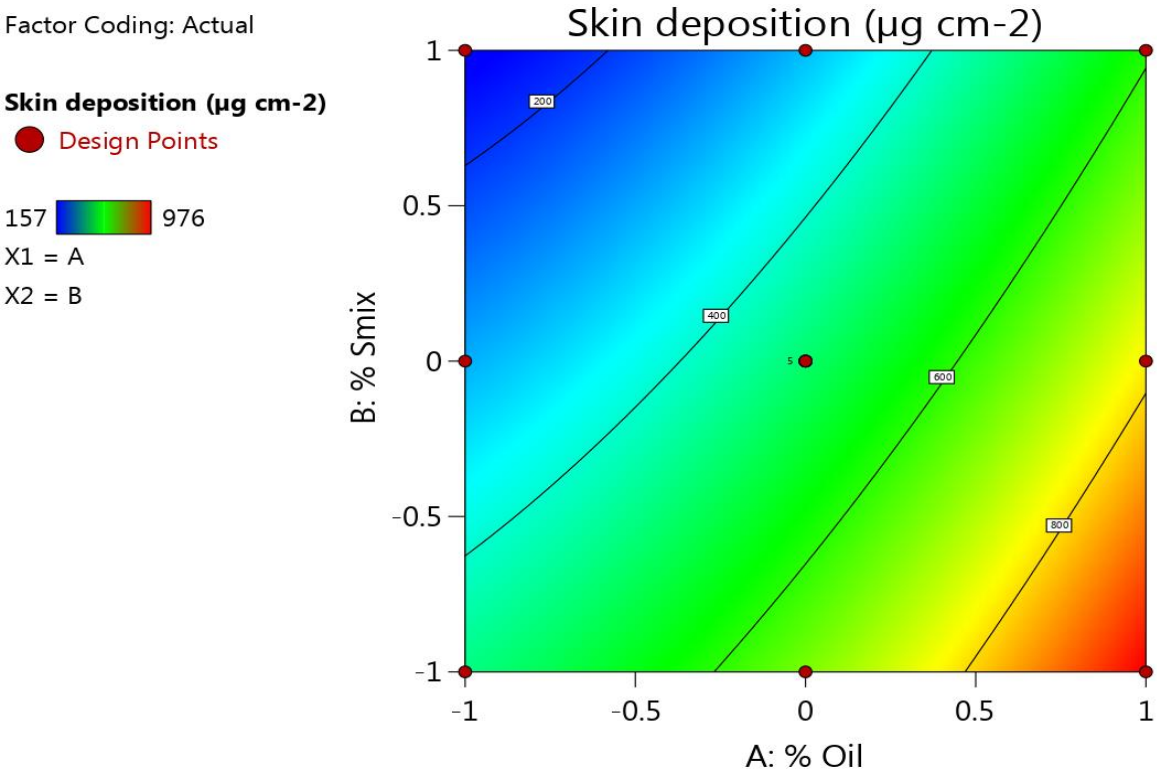

Figure 5.43: 2D Contour plot for skin deposition of nanoemulsion

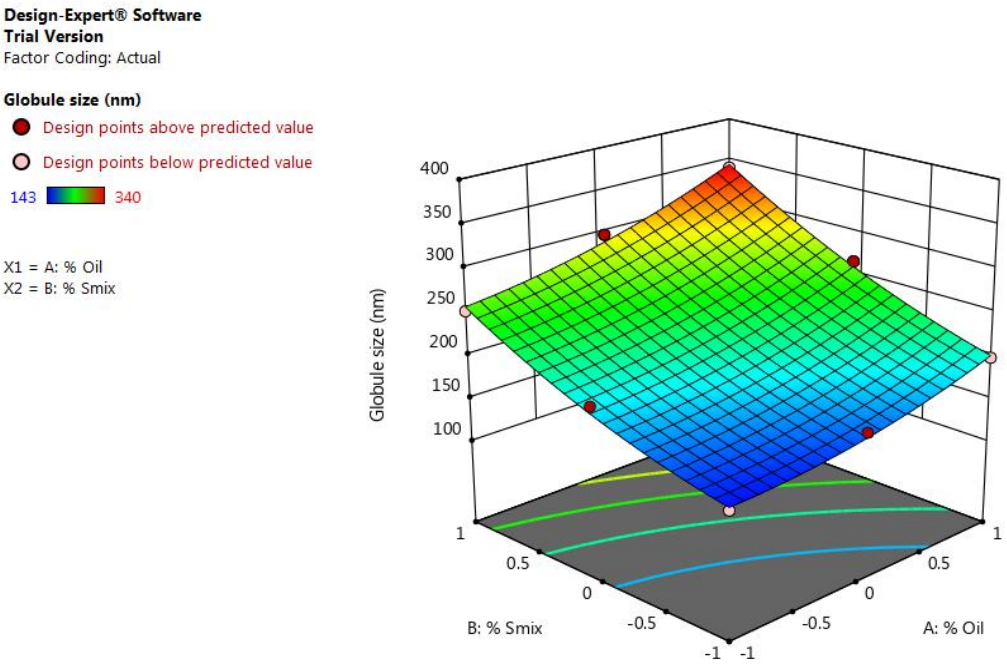

Figure 5.44: 3D Response surface plot for globule size of nanoemulsion

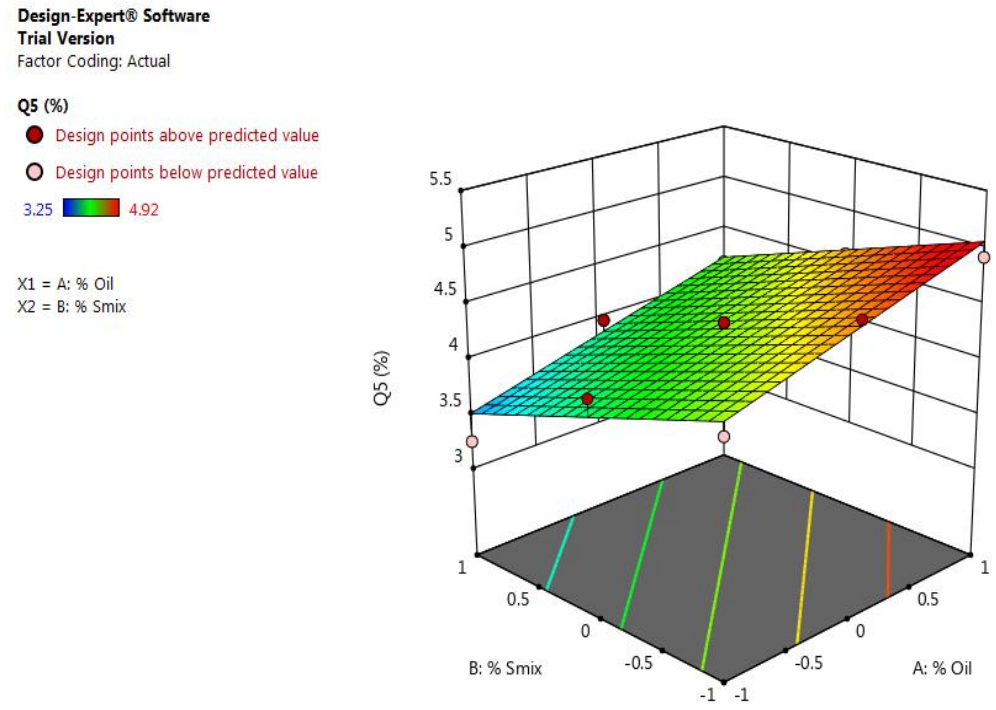

Figure 5.45: 3D Response surface plot for flux of nanoemulsion

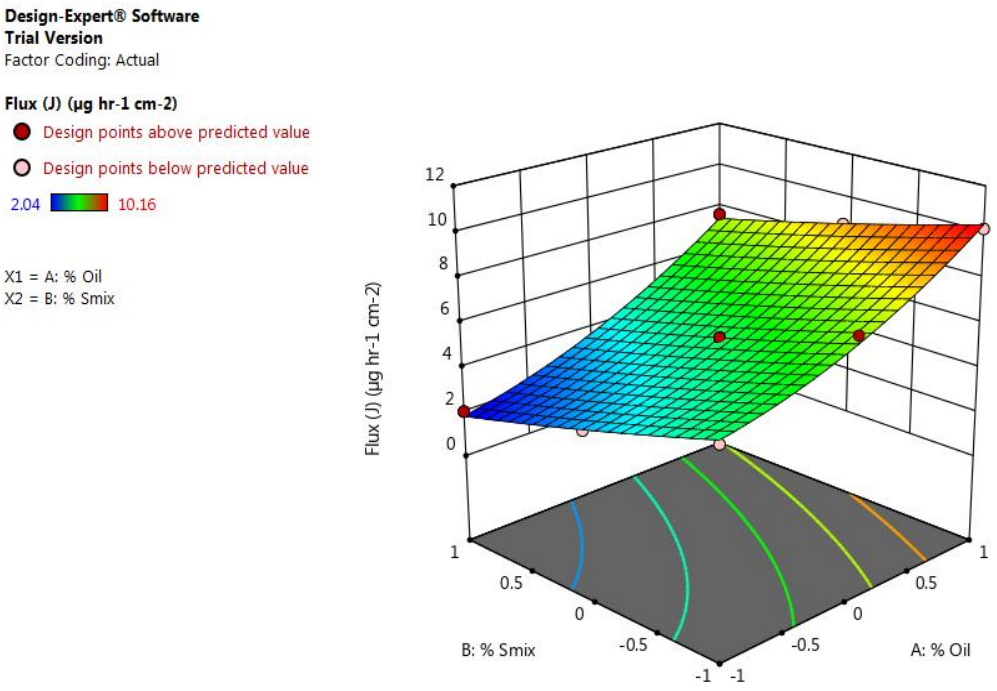

Figure 5.46: 3D Response surface plot for cumulative drug permeation of nanoemulsion

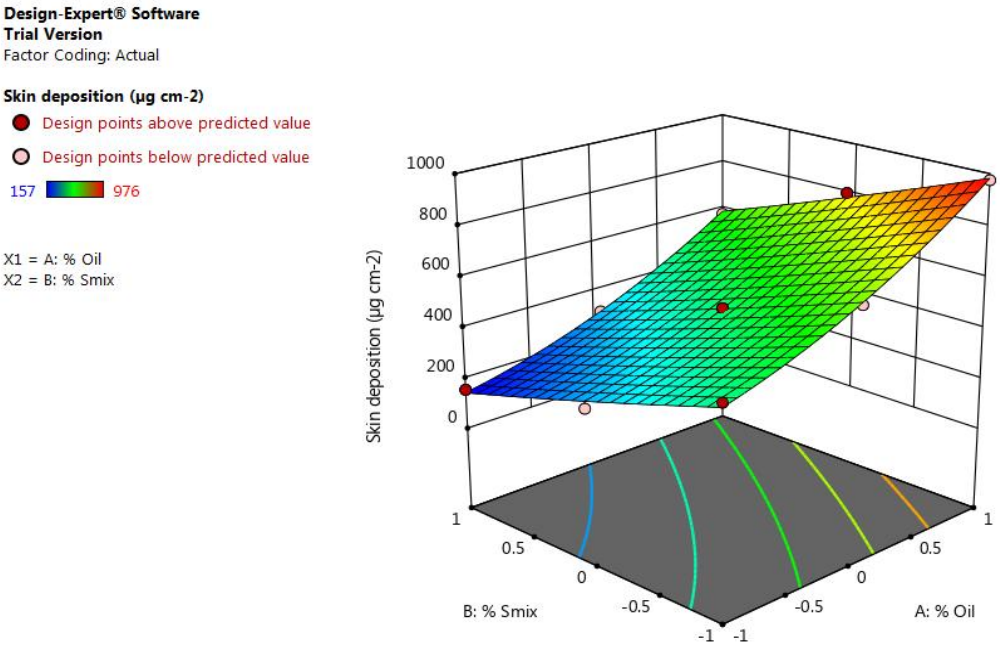

Figure 5.47: 3D Response surface plot for skin deposition of nanoemulsion

5.3.1.7 Optimization using desirability approach and checkpoint analysis

Thus to search the optimum combination of variables to achieve the desired levels of quality attributes, graphical and numerical optimization techniques were employed based on desirability and checkpoint approach (Arora et al. 2016; Arora & Nanda 2019).

Constraints for responses were set as minimal globule size, maximal percent permeation, and skin deposition and flux in the required range as shown in Table 5.18. Predicted values of the responses suggested by the software were found to be as Y1= 160.289 nm, Y2= 4.692 %, Y3 = 7.000 µg hr^{-1} cm^{-2} and Y4 = 657.047 µg cm^{-2}. The optimized combination of formulation variables was obtained at oil concentration (X1) = 9.8% and at a concentration of Smix (X2) = 2.5 % with the corresponding desirability (D) value of 0.784.

The solution obtained after the Post analysis point prediction using the Desirability approach suggested by Design-Expert Software with the predicted values of CQAs along with observed values and percentage prediction error is presented in Table 5.19. Experimental values at this combination checkpoint was found to be as Y1 = 168.3 ± 4.98 nm, Y2 = 4.81 ± 0.65 %, Y3 = 7.62 ± 0.39 µg $hr^{-1}cm^{-2}$ and Y4 = 668.65 ± 11.98 µg cm^{-2}.

The predicted and experimentally observed values were evaluated for calculating percentage prediction error. An acceptable range of percentage prediction error (less than 10 %) as shown in Table 5.19 and desirability value and overlay plot was observed, which indicated a lofty degree of predictive ability and validated the generated design for the evaluation and optimization of nanoemulsion as shown in Figure 5.48 and 5.49 respectively.

Table 5.18: Target constraints set for CMAs and CQAs during numerical optimization of nanoemulsion

Name	Target	Lower Limit	Upper Limit
Concentration of Oil (X1)	Within levels	-1	1
Concentration of Smix (X2)	Within levels	-1	1
Globule size (Y1)	Minimum	143	340
Percent Cumulative Permeation (Y2)	Maximum	3.25	4.92
Permeation flux J (µg hr^{-1} cm^{-2}) (Y3)	Enhanced but in range	5	7
Skin deposition SD (µg cm^{-2}) (Y4)	Maximum	157	976

Table 5.19: Solution obtained after Post analysis point prediction using Desirability approach suggested by Design-Expert Software with the predicted values of CQAs along with observed values and percentage prediction error

Batch No	CMAs		CQAs			
			Globule size (nm)	Cumulative drug permeation Q5 (%)	Permeation flux (J) (µg hr^{-1} cm^{-2})	Skin deposition (sd) (µg cm^{-2})
	X_1 (% Oil)	X_2 (% Smix)	Predicted values			
			160.289	4.692	7.000	657.047
			Observed values			
NE 14	9.8 %	2.5 %	168.3 ± 4.98	4.81 ± 0.65	7.62 ± 0.39	668.65 ± 11.98
Percentage prediction error (%)			4.99	2.51	8.86	1.77

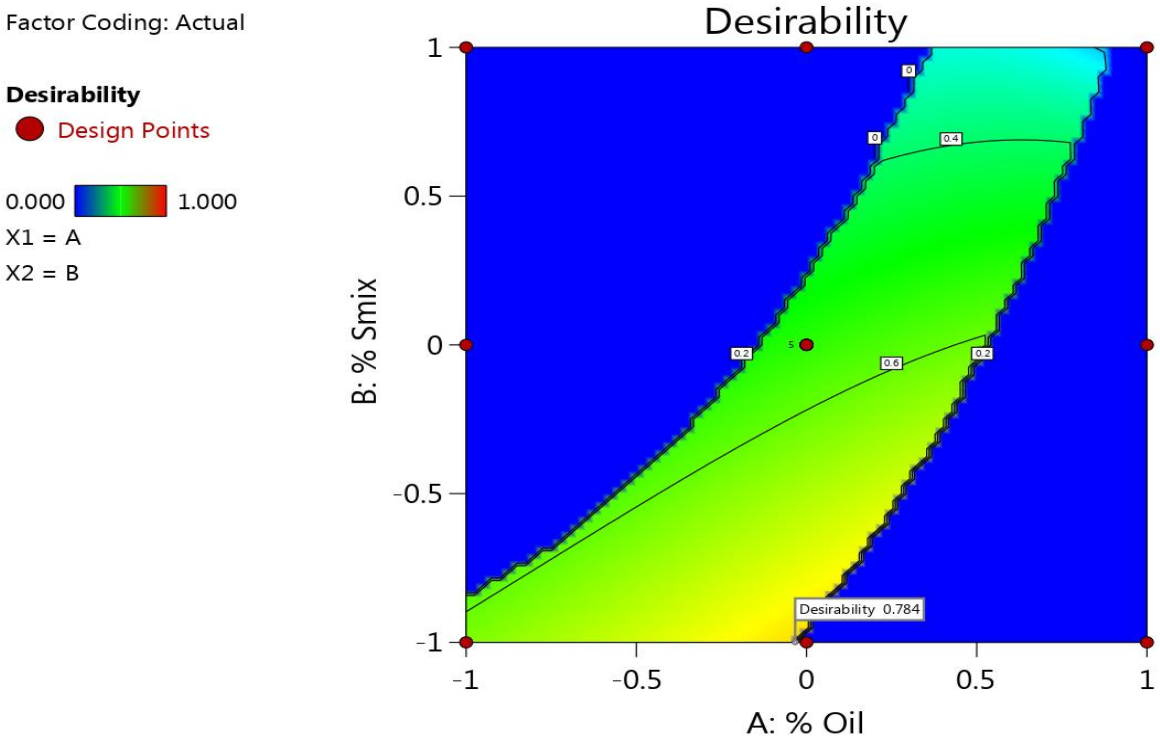

Figure 5.48: Desirability plot for numerically optimized nanoemulsion formulation

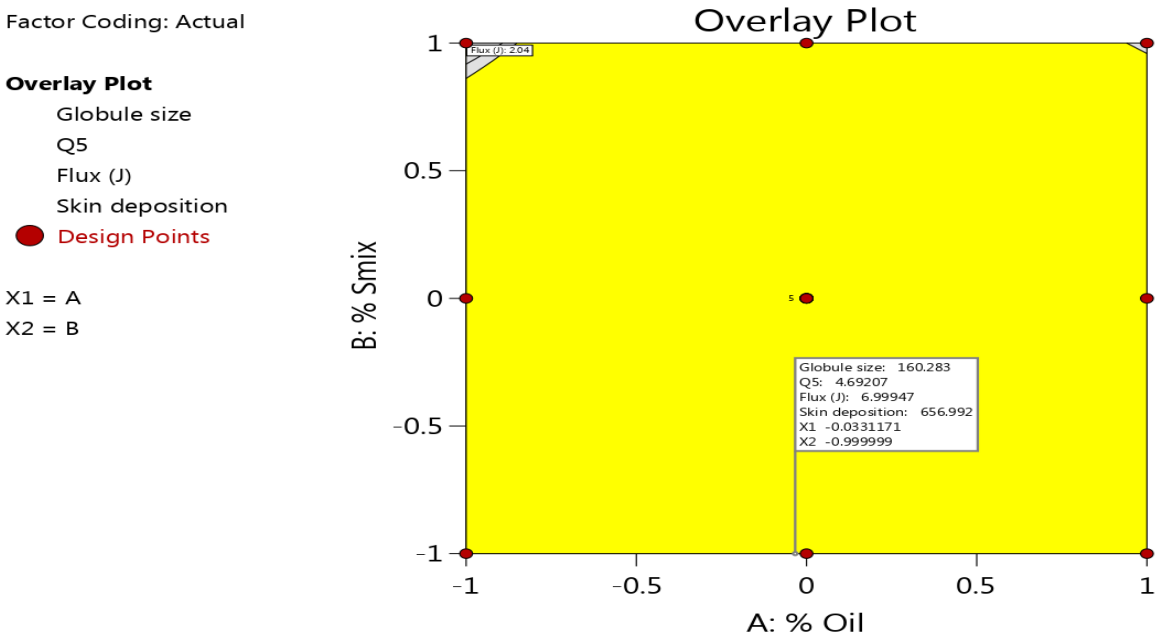

Figure 5.49: Overlay plot showing predicted results during graphical optimization of nanoemulsion formulation

5.3.1.8 Characterization Studies of Developed Resveratrol Loaded Nanoemulsion and Nanoemulgel

5.3.1.8.1 Size, polydispersity index, and zeta potential

The globule size, PDI, and zeta potential of optimized nanoemulsion formulation were found to be 168.3 ± 4.98 nm, 0.181 ± 0.079, and -29.57 ± 3.43 mV respectively. Globule size, PDI, and zeta potential reports are given in Figure 5.50-5.51 respectively.

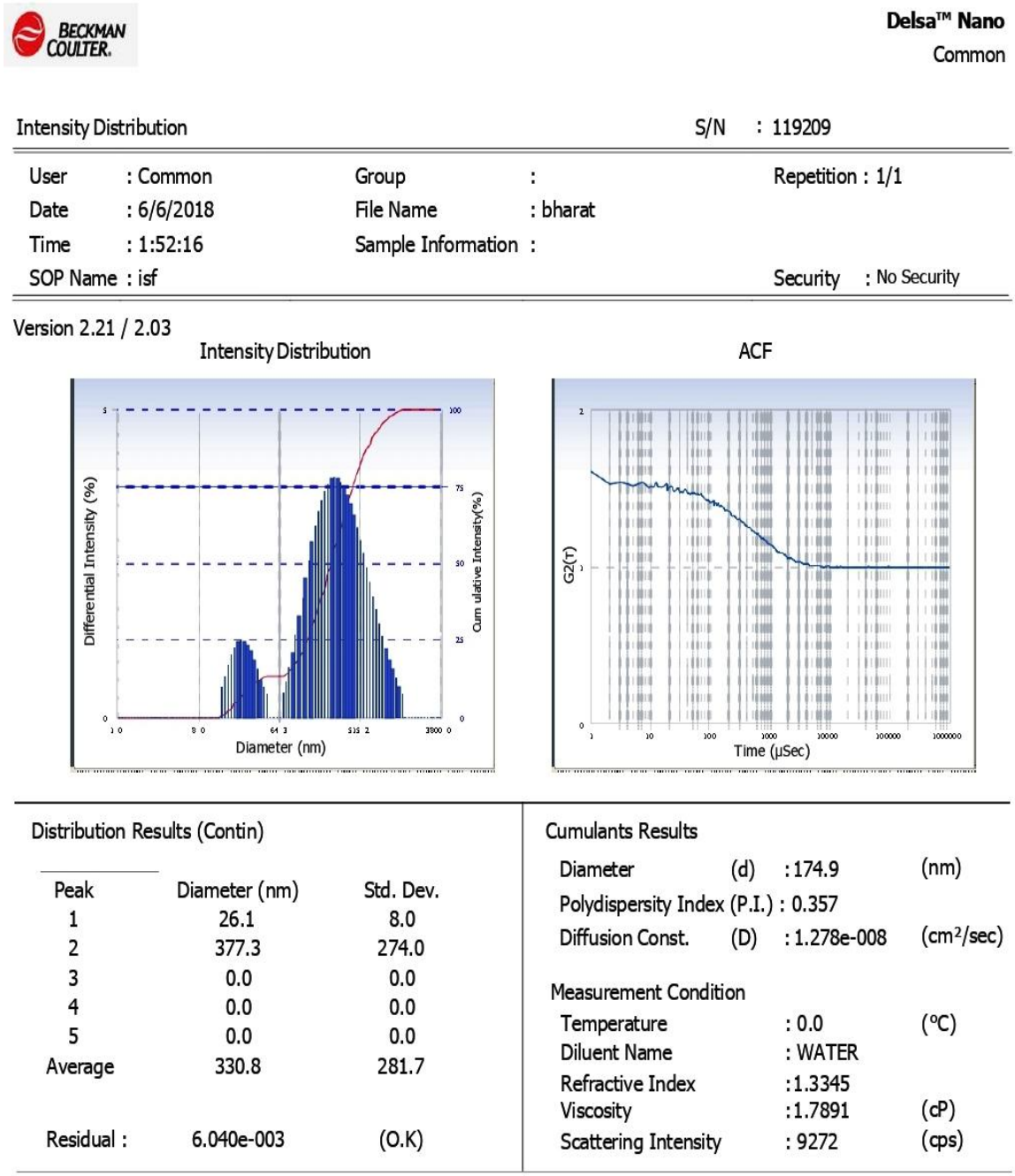

Figure 5.50: Size and PDI report of nanoemulsion

BECKMAN COULTER

Delsa™ Nano
Common

EOS Plot / Distribution Graph S/N :

User	: Common	Group	:	Repetition	: 1/1
Date	: 6/6/2018	File Name	: bharat		
Time	: 11:31:39	Sample Information	:		
SOP Name	: isf			Security	: No Security

Version 2.21 / 2.03

EOS Plot

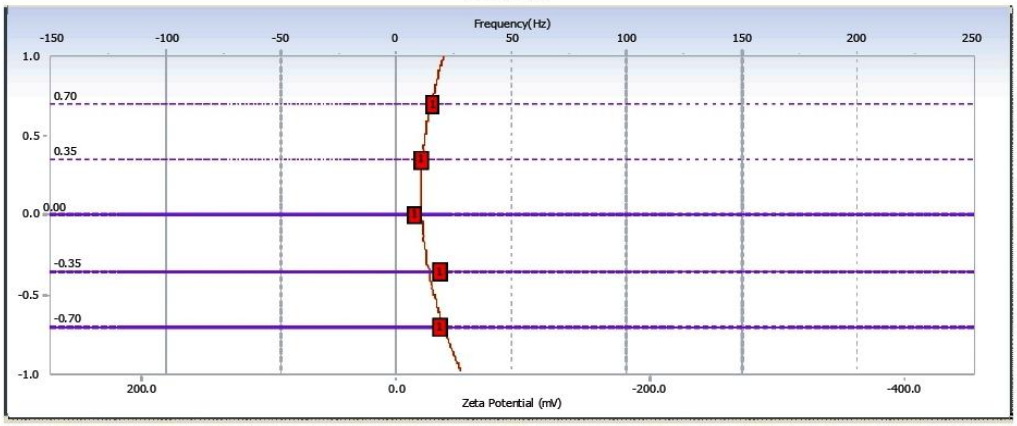

Mobility Distribution

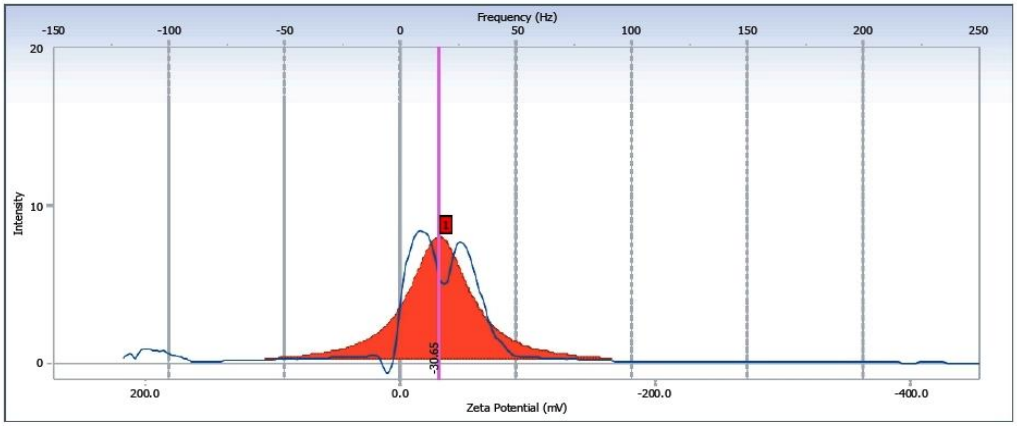

Measurement Results

Zeta Potential	: -30.65	(mV)	Doppler shift	: 16.90	(Hz)
Mobility	: -2.390e-004	(cm²/Vs)	Base Frequency	: 128.4	(Hz)
Conductivity	: 12.2338	(mS/cm)			

Zeta Potential of Cell			Diluent Properties		
Upper Surface	: 7.18	(mV)	Diluent Name	: WATER	
Lower Surface	: 21.62	(mV)	Temperature	: 25.0	(°C)
Cell Condition			Refractive Index	: 1.3328	
Cell Type	: Flow Cell		Viscosity	: 0.8878	(cP)
Avg. Electric Field	: -14.64	(V/cm)	Dielectric Constant	: 78.3	
Avg. Current	: -8.93	(mA)			

Figure 5.51: Zeta potential report of nanoemulsion

5.3.1.8.2 Surface morphology via TEM

Due to poor skin applicability of formulated nanoemulsion formulation, it was incorporated into carbomer based hydrogel (NEG). The globule size of nanoemulsion after incorporating into carbomer gel was also determined at periodic intervals to evaluate the stability of globules in nanoemulgel form. The globule size, PDI, and zeta potential of globules in nanoemulgel were insignificantly affected. A morphological examination of globules in the gel base was also done. The globules were found to be dark spherical droplets with bright surroundings and the absence of any aggregation was confirmed a shown in Figure 5.52.

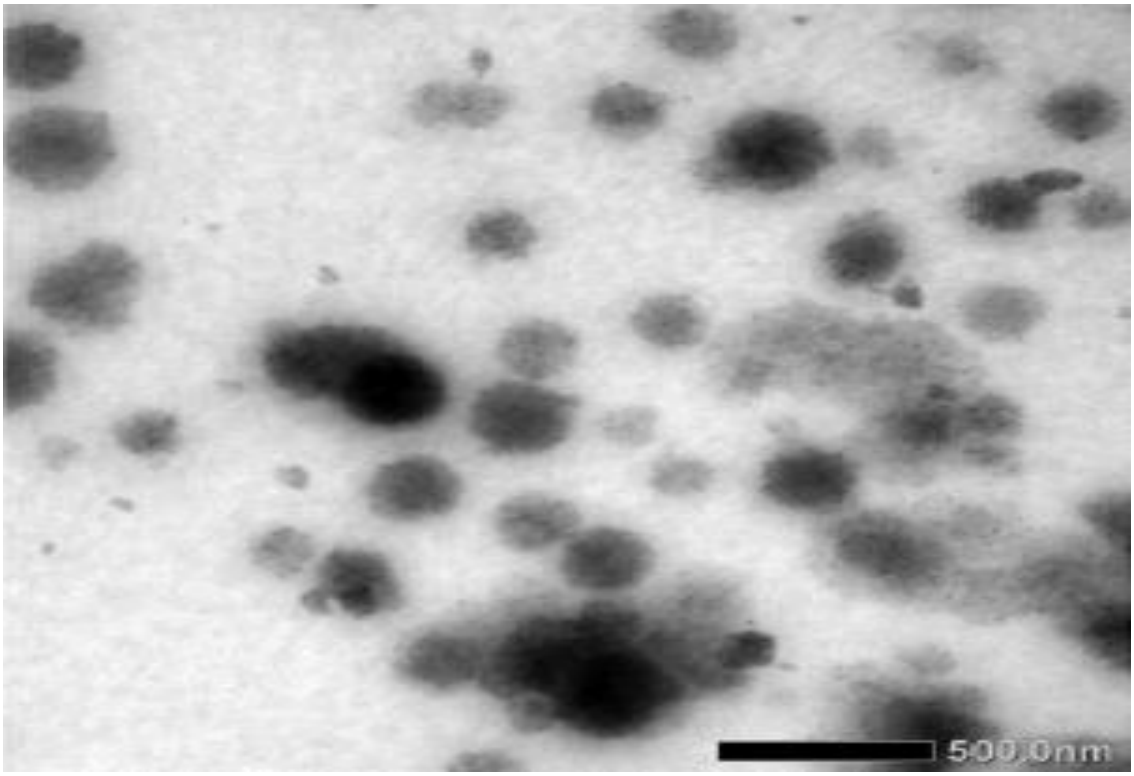

Figure 5.52: Transmission electron microscopic image of Nanoemulsion

5.3.1.8.3 Resveratrol content in NEG

The drug content in nanoemulsion, as well as nanoemulgel, was determined spectrophotometrically. The observed content of resveratrol in nanoemulsion was found to be 0.987 ± 0.008 % w/v. The carbomer-based nanoemulgel was formulated to have strength of 1 % w/w.

The size of both formulations (NE and NEG) was found to be optimum for topical application. It was considered highly critical due to its importance in permeation and retention of the bioactive in the dermal layer. Smaller size facilities movement inside the layers of skin, but beyond a level it leads to systemic absorption. PDI of optimized formulation was also optimum indicating a homogeneous population.

High zeta potential values (negative or positive) are required for better physical stability of nanoformulations because of electrostatic repulsion between each particle. All formulations have adequate surface charges for the physical stability of the colloidal formulation. Further, this zeta potential value does not cause aggregation or flocculation of vesicles.

5.4 Some other important evaluations of formulated micellar hydrogel and nanoemulgel

5.4.1 Determination of pH

To evaluate the risk of irritation upon topical application, the pH of the Micellar hydrogel formulation was evaluated and it was found to be 6.7 ± 0.4 confirming the skin-friendly nature of the topical formulation. The emulgel was also observed as skin-friendly and patient compliant as the pH of the emulgel was 6.9 ± 0.2, similar to biological condition.

5.4.2 Spreadability studies

Spreadability and rheological behavior play an essential role in evaluating the easiness of topical application and the overall efficiency of transdermal/topical formulation. To assess the ease of application on the skin, topical formulations were tested for spreadability analysis using the plate method (Nayak et al. 2018). The plate method was used to assess the spreadability of the hydrogel. The spreadability of the PMG was evaluated and it was found to be 6.98 ± 0.29 cm^2/g. The spreadability of NEG was found to be 5.13 ± 0.87 cm^2/g which was found optimum for topical formulation. While the conventional carbopol hydrogel (CG) has a spreadability of 7.63 ± 0.31 cm^2/g. This minor difference is may be due to increased viscosity of CG.

5.4.3 Rheological behavior and viscosity

The viscosity of NEG and PMG was determined by Brookfield viscometer (Yadav et al. 2016). The flow curve generated from different values of the shear rate *vs* shear rate is represented in Figure 5.53 and 5.54 respectively from which the apparent viscosity was determined. A reduced viscosity at a higher shear rate showed shear-thinning and pseudoplastic flow with a small yield value of both the hydrogels (Yadav et al. 2016). The apparent viscosity of NMG was calculated as 31.47 ± 2.53 Pa.s while the average viscosity of NEG was 28.16 ± 2.98 Pa.s. depicted sufficient firmness of gel structure (Khurana et al. 2013).

The pseudoplastic/shear-thinning property of the gel was indicated by the results. The yield value was found to be less than 1 in both cases, representing less fluidity with more plasticity and rigidity of gel structure.

5.4.4 *In vitro* Resveratrol release

The dialysis bag method was employed to determine the *in vitro* release profile of Resveratrol from formulated hydrogels. The dissolution medium used was 500 mL of 3:7 (v/v) ethanol-pH 7.4 phosphate buffer which was maintained at 32 ± 0.5 °C and 50 rpm.

A controlled release of Resveratrol was observed from PMG. However, complete Resveratrol dissolution was observed in the case of its solution form within the first two hours as shown in Figure 5.55.

Results indicated that conventional gel showed a burst release of Resveratrol of around 80% in the first two hours only. No such burst release was observed in either of the colloidal dispersion or hydrogel. PM and PMG showed a sustained release of up to 12 h, while NE and NEG showed approximately 80 % release in just six hours. This is due to the slow diffusion of Resveratrol from the encapsulating matrix of micelles a shown in Table 5.20.

Mathematical release models (zero-order, first-order, and Higuchi) were then applied to find out the release pattern and release mechanism from the formulated hydrogel. CG and Resveratrol solution both were found to show first-order release kinetics.

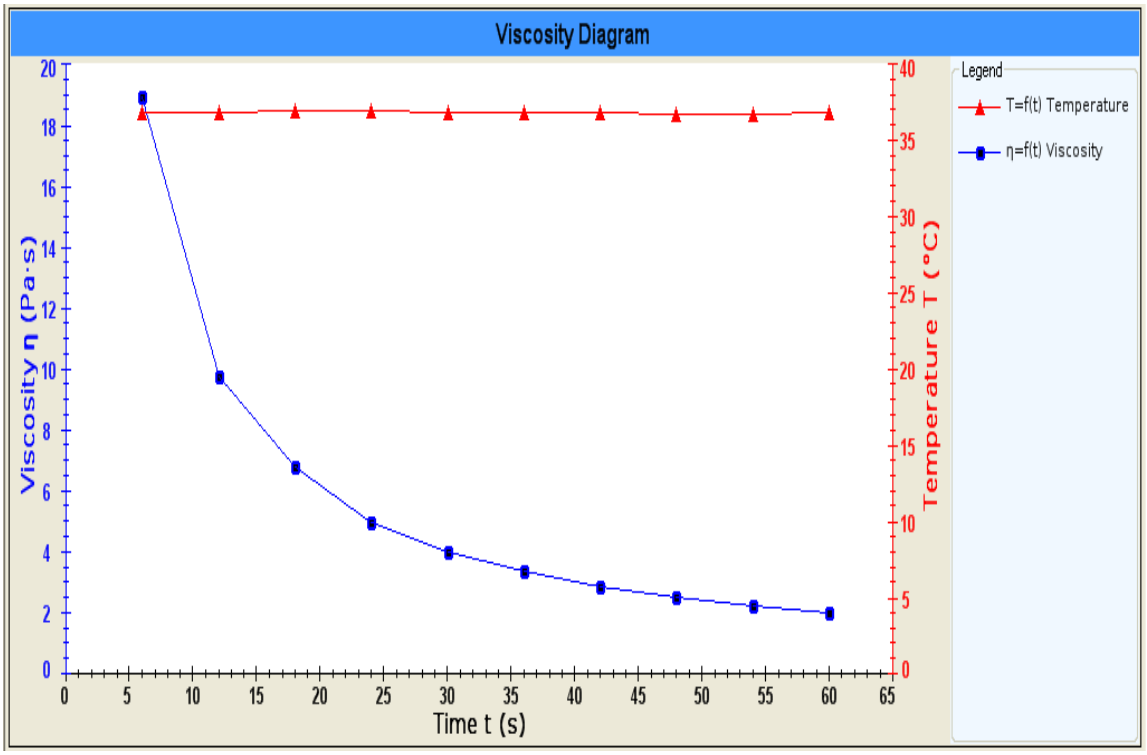

Figure 5.53: Rheogram of NEG

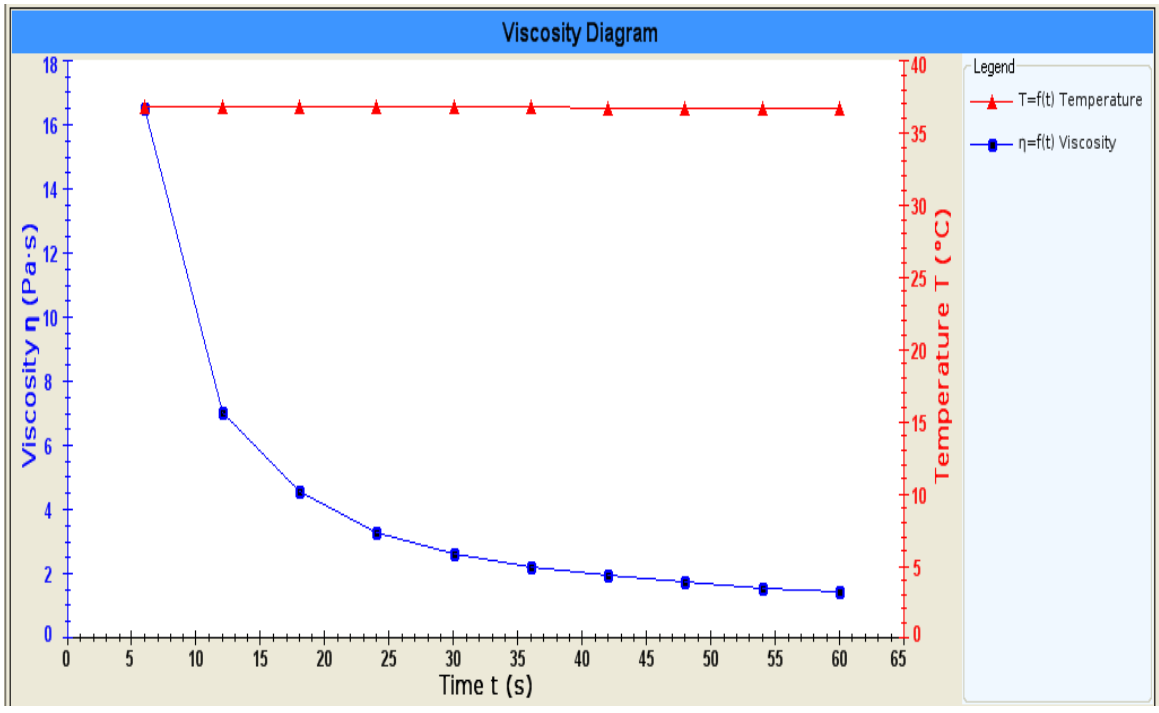

Figure 5.54: Rheogram of PMG

While, both emulsion and micellar colloids as well as corresponding hydrogels showed to follow the Higuchi model which revealed that the release of Resveratrol is occurring in a sustained pattern following the diffusion mechanism. This might be due to the higher diffusion pathway encountered through the entrapment of Resveratrol in PM and PMG.

Further, Korsmeyer- Peppas model was used to assess the type of diffusion mechanism followed by formulated systems. In all colloidal system as and hydrogel value of "n" was found to be greater than 0.45, while lesser than 0.89, indicating Non-Fickian release mechanism as shown in Table 5.21.

Table 5.20: Cumulative % Release of Resveratrol from different formulations

Time (h)	Cumulative % Release of Resveratrol from different formulations					
	PM	**PMG**	**NE**	**NEG**	**CG**	**Res Solution**
0.5	11.54 ± 2.76	10.65 ± 1.9	18.65 ± 1.91	16.76 ± 0.87	21.54 ± 7.98	26.65 ± 3.87
1	21.21 ± 4.13	18.26 ± 1.64	27.73 ± 1.54	26.12 ± 1.76	38.54 ± 6.32	47.87 ± 5.43
1.5	29.87 ± 4.25	33.65 ± 3.81	33.06 ± 2.89	29.77 ± 3.48	53.56 ± 4.87	74.32 ± 7.35
2	35.76 ± 3.66	37.38 ± 2.80	46.81 ± 1.9	41.9 ± 2.9	78.54 ± 2.81	97.23 ± 7.66
4	44.12 ± 2.87	44.62 ± 4.23	65.16 ± 3.53	62.73 ± 5.65	85.32 ± 1.76	98.88 ± 0.87
6	61.12 ± 3.21	55.12 ± 5.22	82.98 ± 7.54	78.17 ± 4.18	97.87 ± 1.12	99.81 ± 0.43
12	96.12 ± 4.88	89.93 ± 3.76	98.54 ± 1.12	98.9 ± 0.49	98.86 ± 0.96	99.76 ± 0.64

[Values are expressed as mean ± S.D., (n = 3)]

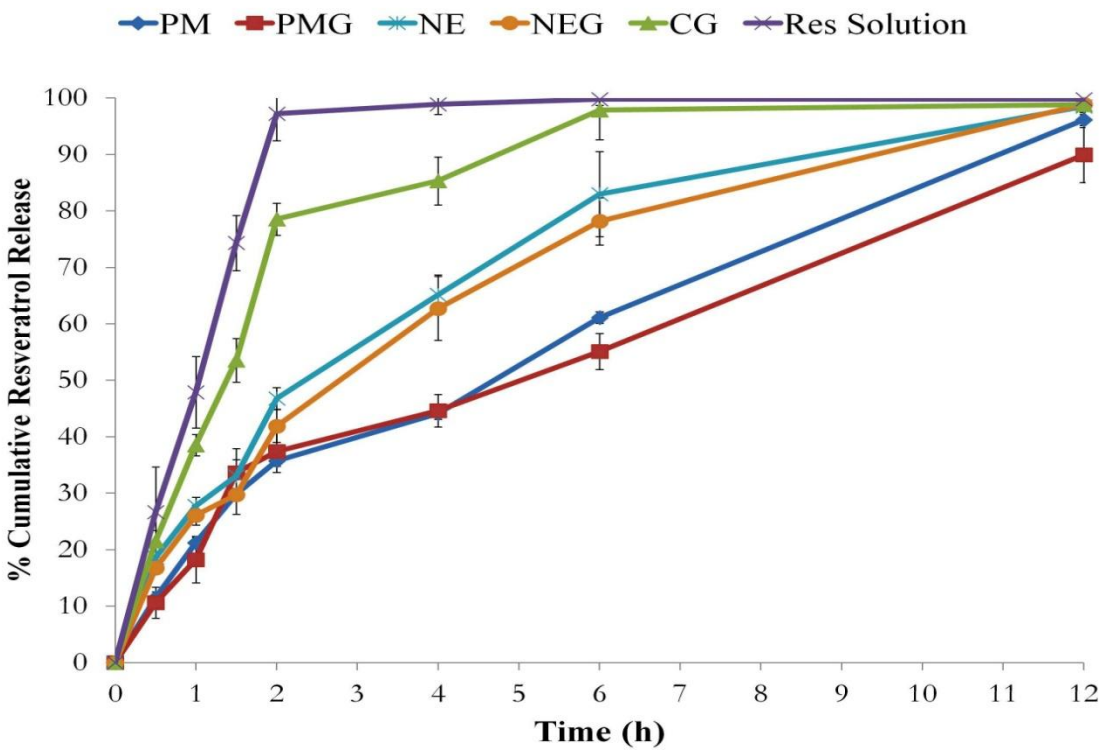

Figure 5.55 Graph showing cumulative % Release of Resveratrol from different formulations

Table 5.21: Mathematical release models of Resveratrol loaded formulation

Model	R^2					
	PM	**PMG**	**NE**	**NEG**	**CG**	**Res. Solution**
Zero order	0.948	0.916	0.843	0.878	0.600	0.436
First order	0.600	0.687	0.697	0.700	0.893	0.938
Higuchi	0.983	0.974	0.976	0.985	0.843	0.709
Korsmeyer- Peppas value of 'n'	0.628	0.627	0.551	0.582	0.478	0.394

5.4.5 Skin permeation studies (*ex vivo)*

The *ex vivo* skin permeation study was performed using the freshly excised skin from pig ear (obtained from the local slaughterhouse) (Nainwal et al. 2019). The histology of Pig-skin is quite analogous to human skin. SC of pig pinna, having a thickness of 21-26 μm with an average 20 hair follicles per centimeter square area, is quite similar to human forehead skin having 14–32 hair follicles per centimeter square area.

Apart from similarity, it's easy availability and wide use in skin permeation studies, make it the most preferable model to be used (Abd et al. 2016). The shaved dorsal fraction of the skin was placed on a static Franz diffusion cell having a cross-sectional area of 3.14 cm^2 and a capacity of 30 mL. The dorsal section was placed between the donor and the receptor compartment with the stratum corneum lining facing towards the donor compartment while the dermal portion facing towards the cell the receptor compartment (Mura et al. 2000; Johnson 2007). The donor compartment was filled with different formulations equivalent to 1.5 mg of Resveratrol (PM, PMG, NE, NEG, and CG). Permeation profiles of all developed formulations were plotted and compared with CG and values of permeation flux, permeability coefficient, enhancement ratio, and skin deposition were calculated as shown in Table 5.22 and Figure 5.56 and 5.57.

PM and PMG successfully enhanced Resveratrol permeation compared to plain carbopol gel, showing the enhancement ratio of 2.934 and 2.741 reflected by a high permeation flux i.e. 7.32 ± 0.54 μg cm^{-2} h^{-1} and 6.83 ± 0.86 μg cm^{-2} h^{-1} respectively as compared to plain carbopol Gel i.e. 2.50 ± 0.65 μg cm^{-2} h^{-1} and the increase was found to be statistically significant ($p < 0.01$). Polymeric micelles induce changes in the SC lipids, thus acting as penetration enhancers is one of the attributed reasons for the obtained results which has been suggested by several scientists lately (Loan Honeywell-Nguyen et al. 2002; Simões et al. 2018). Another possible concerning reason for enhanced skin delivery might be since the small size of micelles provides a higher contact surface with the skin. The proposed mechanism of skin absorption is transappedengeal route as suggested by a few researchers who studies mentioned the presence of polymeric micelles in hair follicles upon topical skin application (Kahraman et al. 2016; Makhmalzade & Chavoshy 2018; Simões et al. 2018).

Though incorporation of carbomer retarded the permeation of micelles the difference between permeation flux of PM and PMG was found to be statistically insignificant ($p > 0.05$). This might be due to attributed to a 3D structural network of hydrogel and the composite nature of the carbomer.

Results indicated that nanoemulsion and nanoemulgel formulations showed a higher rate of skin permeation as compared to conventional gel. The permeation flux of resveratrol from nanoemulsion and nanoemulgel was 7.62 ± 0.39 and 7.18 ± 0.57 µg cm^{-2} h^{-1} respectively which were found to be significantly higher ($p<0.001$) than permeation flux obtained from conventional gel i.e. 2.50 ± 0.65 µg cm^{-2} h^{-1}. The permeability coefficient of both nanoemulsion and nanoemulgel was observed to be three times higher than conventional gel. This may be attributed due to the fact that components present in nanoemulsion led to more solubilization of resveratrol and its partitioning from vehicle to stratum corneum through the lipoidal dermal layer of skin. The smaller droplet size of nanoemulsion is another important explanation of higher permeation as it can easily permeate through skin. Whereas aqueous carbomer based conventional hydrogel (hydrophilic matrix) is associated with poor solubilization and low partitioning properties in the epidermal layer, thus conferred poor permeation properties.

Nanoemulgel has superior ease of application as compared to nanoemulsion dispersion formulation. But carbomer led to a decrease in the flux because of the 3D structural network of hydrogel and composite nature of the material. But this decrease was found to be statistically insignificant ($p > 0.05$), thus associated advantages of nanoemulgel outweighed the drawbacks of incorporating nanoemulsion into the carbomer-based gel.

5.4.6 Skin deposition

Skin deposition values are represented in Table 5.22. The amount of Resveratrol measured in the receptor compartment is the direct marker of transdermal delivery, while dermal delivery is indicated by the amount of Resveratrol retained in the skin layers. Thus, the extent of skin retention of Resveratrol through various developed hydrogels was evaluated. The value of Resveratrol retained in the dermal layer by PM, PMG and CG was quantified as 246.64 ± 9.4 µg cm^{-2} (51.63 ± 1.97 %), 253.90 ± 5.47 µg cm^{-2}

(53.15 ± 3.24), and 49.40 ± 9.62 µg cm^{-2} (10.34 ± 2.01 %) respectively. The skin deposition by PM and PMG is approximately five times higher than CG. The high deposition can be ascribed because micelles are supposed to form a depot in a deeper layer of skin.

In concordance to the above results, significantly higher skin retention ($p<0.001$) was observed in the case of nanoemulsion (44.76 ± 2.14 %) as well as nanoemulgel (47.21 ± 3.87 %) as compared to the conventional hydrogel. Higher contact of nanoformulation with corneocytes, skin occlusion, and a sustained release from the nanoformulations are the apt explanation of the obtained results. These nanoformulations act as depots and provide sustained and controlled delivery of bioactive as well as its high retention at the target dermal layer of skin. The present studies confirmed the superior permeation and skin deposition potential of both PMG and NEG as compared to conventional gel and thus, could be used successfully for topical/dermal delivery of Resveratrol. Thus, found to be highly efficient and appropriate for skin targeting and providing enhanced dermatological benefits.

Table 5.22: Permeation flux and skin deposition of Resveratrol after 24 hours from different colloidal formulations

Formulation Code	Permeation Flux, Jss (µg cm^{-2} h^{-1})	Permeability coefficient, K_p (cm h^{-1}) (*10^{-3})	Enhancement Ratio, Er	Skin retention (%)
PM	7.32 ± 0.54	4.88	2.934	51.63 ± 1.97
PMG	6.83 ± 0.86	4.55	2.741	53.15 ± 3.24
NE	7.62 ± 0.39	5.08	3.048	44.76 ± 2.14
NEG	7.18 ± 0.57	4.78	2.872	47.21 ± 3.87
CG	2.50 ± 0.65	1.66	-	7.05 ± 2.87

[Values are expressed as mean ± S.D., (n = 3)] Significance was tested using one way ANOVA and Tukey–Kramer post-test. Three asterisks represent $p<0.001$ compared to the control CG]

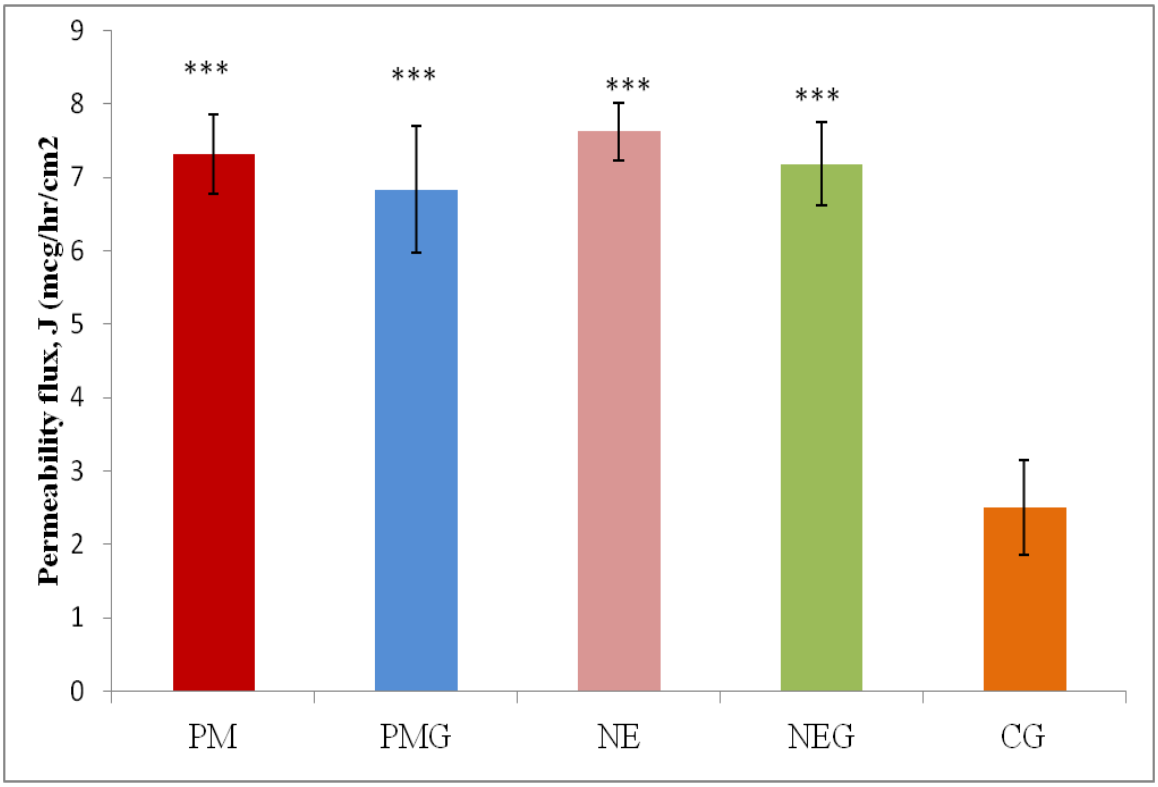

Figure 5.56: Permeability flux of different Resveratrol formulations

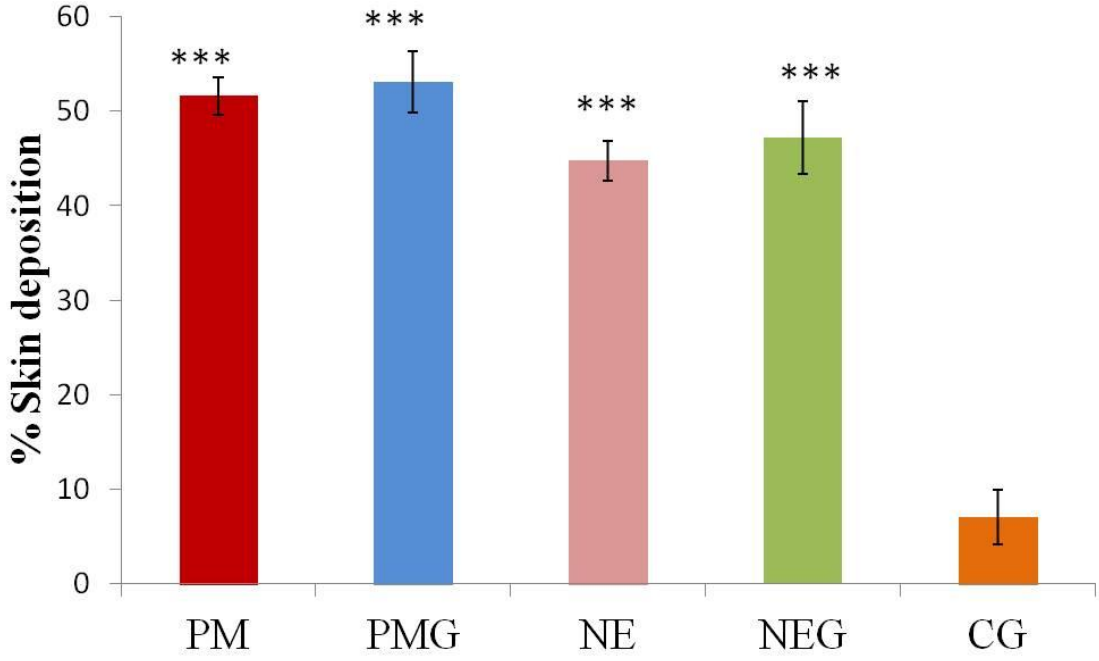

Figure 5.57: Skin deposition values of different Resveratrol formulations

5.4.7 Histopathological studies – skin distribution by CLSM

C6 loaded NEG and PMG were compared with CG for skin targeting properties using CLSM. In the study degree of penetration and mechanistic pathways for skin, permeation was evaluated. CLS images as shown in Figure 5.58 depicted that both NEG and PMG have immensely scattered in the deeper skin layers as a high-intensity fluorescence can be viewed. Whereas, CG unable to show much fluorescence in the deep layer, as it was held and adhered just at the upper layer of stratum cornea as shown in Figure 5.58 A. The enhanced skin permeation and penetration of C6 from nanoemulgel can be attributed to its compositions in which the ingredients such as Tween 80, transcutol, and pluronic act as permeation enhancers, potentially significantly reducing the barrier properties of the SC through the extraction of SC lipids. The above results confirm the efficiency of nanoemulgel for targeting required bioactive into the skin and can act as a potential topical drug delivery system in the treatment of various skin related disorders like psoriasis.

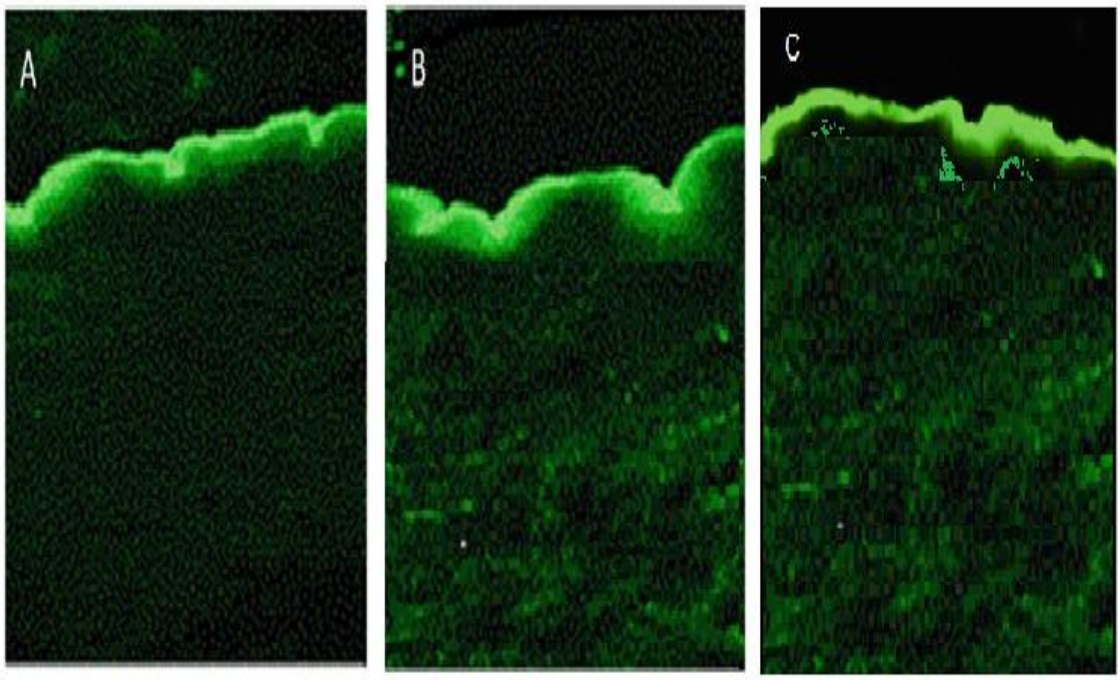

Figure 5.58: CLS micrographs (a) C6 loaded CG (b) C6 loaded PMG (c) C6 loaded NEG

5.4.8 *In vitro* antioxidant activity using DPPH Assay

Resveratrol is a potent antioxidant molecule. After formulating its nano-based formulations, it is a prerequisite to establish and ensure its effectiveness as an antioxidant and to qualify that the components and process parameters adopted in the development of these delivery vehicles have not hampered its properties.

Thus, DPPH assay was employed which is based on the reduction of stable organic free radical i.e. DDPH in the presence of antioxidant molecules (Caddeo et al. 2013). This test is based on the reduction of stable organic free radical i.e. DDPH in the presence of antioxidant molecules. It is an established and well known free radical.

Higher the ability of the formulation to neutralize DPPH, the higher would be its free radical scavenging or antioxidant potential. The stable form is purple, while the radical when it gets reduced by pairing with hydrogen, the solution becomes discolored and the extent of this discoloration can be measured in the terms of absorbance at 517 nm.

The higher the discoloration, the higher is the decrease in absorbance as compared to control, indicating higher free radical scavenging activity (Caddeo et al. 2013). Percent inhibition of free radicals was calculated by taking different concentrations of Resveratrol and ascorbic acid (standard). IC_{50} values were calculated.

Concentration *vs*. % inhibition graph for calculating free radical inhibition activity using DPPH assay in each case is shown in Figure 5.59.

Among all tested formulations, the sequence of antioxidant potential was found to be NEG (IC_{50} = 6.03 µg/mL) Ascorbic Acid (IC_{50} = 8.72 µg/mL) > Res Solution (IC_{50} = 10.62 µg/mL) > PMG (IC_{50} = 11.99 µg/mL) as shown in Table 5.23.

Ascorbic Acid was used as a control for comparison purposes, exhibited comparable DPPH scavenging activity with plain Resveratrol solution. The IC_{50} value of resveratrol in NEG formulation was lesser in comparison with plain resveratrol due to the presence of vitamin E.

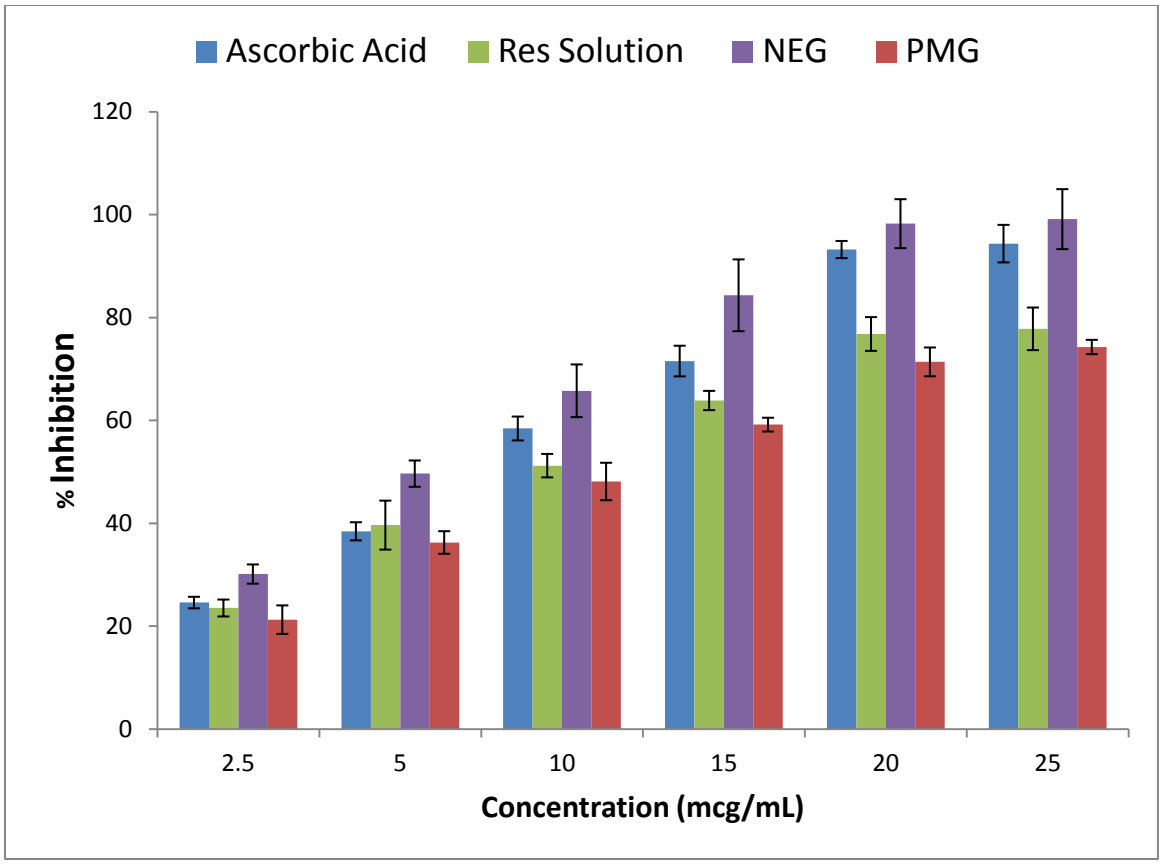

Figure 5.59: Free radical inhibition activity using DPPH assay

The higher IC_{50} value observed with micellar formulation may be due to the slow diffusion of Resveratrol from the gel. Results revealed that Resveratrol retained its potential antioxidant effect in its formulations also and it is indicated that the formulation process and materials attributes have not hampered the activity of Resveratrol, thus considered to be optimum to be used as a topical delivery vehicle.

Table 5.23: IC_{50} values of Resveratrol loaded formulations

Formulation	Ascorbic Acid	NEG	PMG	Res Solution
IC50 (µg/ml)	8.72 ± 0.91	6.03 ± 0.521	11.99 ± 1.34	10.62 ± 0.87

[Values are expressed as mean ± S.D., (n = 3)]

5.5 *In vivo* efficacy studies (antipsoriatic activity) using IMQ-induced psoriatic-like plaque model in Swiss Albino Mice

5.5.1 Psoriasis Area and Severity Index (PASI) score

IMQ is a known immune response activator that acts as a toll-like receptor 7 agonist and produces inflammation on the skin similar to the psoriatic conditions (Gilliet et al. 2004; Avasatthi et al. 2016). Application of IMQ for seven days on shaved skin of the animals prominently showed symptoms of induction of psoriasis such as erythema, scaling, and thickening of the skin. The treatment with developed formulations to animals in different groups as shown in Table 5.24 was started on the 8^{th} day and a clinical average PASI score was assigned to each animal based on the above-mentioned indicators of erythema, scaling, and thickness of the skin.

A decline in PASI scores unswervingly indicates the high therapeutic efficacy of the tested formulations. The severity scoring as mentioned in Table 5.25, clearly revealed that all animals in the disease-induced animals showed a high average score of 3.6 due to increased erythema and scaling of the skin due to IMQ treatment, while the average score recorded in the control group was 0.

Table 5.24: Different animal groups used in antipsoriatic studies

S. No.	Group	Number of animals
I	Control (No disease and no treatment)	6
II	Negative control (Disease induced)	6
III	Disease + Conventional Resveratrol gel formulation (CG)	6
IV	Disease + Test drug (Resveratrol Loaded Polymeric micelles gel) (PMG)	6
V	Disease + Test drug (Resveratrol Loaded Nanoemulsion gel) (NEG)	6

Table 5.25: **Average Psoriasis Area and Severity Index (PASI) score for different groups**

Groups	Erythema		Scaling		Thickness		Average PASI score	
	7^{th} day	15^{th} day	7^{th} day	15^{th} day	7^{th} day	15^{th} day	7^{th} day	15^{th} day
Normal Control	0	0	0	0	0	0	0	0
Disease control	3	3	4	4	4	4	3.6	3.6
CG	3	2	4	2	4	3	3.6	2.3
PMG	3	1	4	1	4	1	3.6	1
NEG	3	1	4	1	4	1	3.6	1

On the 15^{th} day (i.e. after seven days of disease induction and then seven days of treatment), the PASI score of all animals of treated group 3, 4, and 5 (i.e. CG, PMG, and NEG) was found to be statistically lesser ($p < 0.05$, $p < 0.01$ and $p < 0.01$ respectively) as compared to the disease control group. A significant difference in the PASI score in the case of the PMG and NEG treated group was achieved as compared to CG ($p < 0.05$) as depicted by Table 5.25**.** The psoriatic skin is associated with the scaly and inflamed stratum corneum barrier. Both the nanocarriers-based gel has enhanced the efficacy of overcoming this barrier and able to permeate through the skin following all possible mechanisms of skin transport, where CG was unable to penetrate.

Moreover, enhanced Resveratrol availability and deposition in the deeper layer of the skin via NEG and PMG, has resulted in a huge improvement in skin inflammation and psoriatic like conditions. The above results concluded the effectiveness of both micellar based and nanoemulsion based hydrogel formulations containing Resveratrol for better therapeutic and dermatological benefits.

5.5.2 Cytokines level in serum and spleen dimension & weight

Psoriasis, being an autoimmune disorder, is particularly characterized by abnormal proliferation of keratinocytes and increased levels of pro-inflammatory markers and cytokines such as TNF-α, IL-17, and IL-23. Cytokines play an essential role in the pathophysiology of psoriatic like a skin condition. Animals when treated with IMQ for seven days, which is an immunomodulator, leads to enhancement in the particular immune markers as confirmed by the results also. IMQ treated animals were found to have statistically significantly increased ($p < 0.001$) levels of TNF-α, IL-17, and IL-23 as compared to the control group as shown in Table 5.26 and Figure 5.60. This is due to noticeable enhancement in T cells i.e. CD4 and CD8, dendritic cells, and decrease in macrophages thus altering the systemic composition of immune cells. Treating animals with Resveratrol formulations decreased these enhanced levels of cytokines to a different extent. Groups treated with Resveratrol loaded PMG and NEG pronouncedly reduced the levels of TNF-α and IL 23 ($p < 0.001$), as well as IL-17 ($p < 0.01$), while CG was not able to decrease the level of IL-17 much markedly ($p > 0.05$), due to its less permeation and skin deposition ability as compared to the colloidal based hydrogel. Micellar hydrogel has shown a little bit better results as compared to emulgel but the difference was found to be insignificant.

Table 5.26: Concentration of cytokines in serum

Groups	The concentration of cytokines in serum (pg/mL)		
	TNF-α	**IL-17**	**IL-23**
Normal Control	46.12 ± 1.23	290.23 ± 21.76	435.36 ± 43.12
Disease control	94.57 ± 4.67	421.99 ± 45.01	643.61 ± 23.23
CG	64.34 ± 3.2	372.43 ± 23.28	561.67 ± 39.16
PMG	51.31 ± 2.38	325.75 ± 54.11	480.26 ± 54.3
NEG	56.25 ± 2.43	341.56 ± 32.21	494.65 ± 44.32

[Values are expressed as mean ± S.D., (n = 6)]

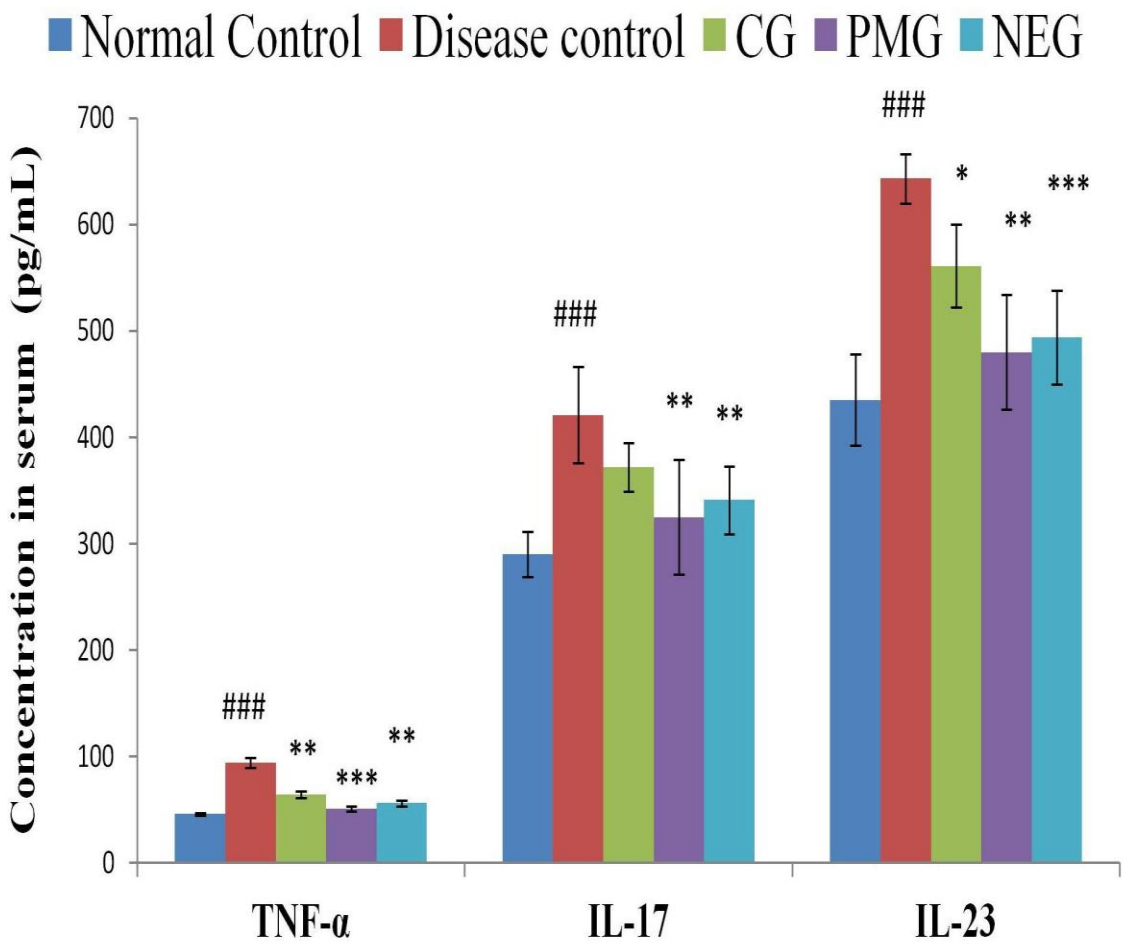

Figure 5.60: Serum cytokines concentration (TNF-α, IL-17 and IL-23) of different groups

Each data represents mean ± S.D. (n=6). Significance was tested using one way ANOVA and Tukey–Kramer post test. $^{###}p < 0.001$ (Normal control *vs*. disease control group), *p < 0.05, **p < 0.01 and ***p < 0.001 (disease control *vs*. treatment groups)

Another important marker of inflammatory diseases such as psoriasis is splenomegaly which leads to enlargement and swelling of the spleen. This is attributed to an increase in levels of pro-inflammatory markers and cytokines. Thus measurement of change in spleen weight and dimension is one of the significant parameters for evaluating the efficiency of tested formulations. A pronounced increment in size and weight of spleen was observed in the animals which were only treated with IMQ and no treatment

was given as compared to the control group which indicated that induction of psoriatic-like condition in animals.

The spleen weight and dimensions are represented in Table 5.27 and Figure 5.61. The weight of the spleen in the control group was found to be 105 ± 12.58 mg, however, a statistically significant difference in spleen weight ($p < 0.001$) was observed in the case of a diseased group which was found to be 189 ± 19.65 mg. While the animals which were given topical treatment with Resveratrol loaded PMG and NEG have shown reduced signs of splenomegaly with a significantly lesser mass of spleen i.e. 127 ± 12.431 mg and 133 ± 8.65 mg which was comparable to the control group animals ($p > 0.5$).

The developed PMG and NEG formulations were able to modulate the immune response considerably thus could be used successfully for the treatment of several topical immune disorders like psoriasis.

Table 5.27: Spleen weight in different animal groups

Group	**Spleen weight (mg)**
Normal Control	105 ± 12.58
Disease control	189 ± 19.65
CG	156 ±14.65
PMG	127 ±12.43
NEG	133 ±8.65

[Values are expressed as mean ± S.D., (n = 3)]

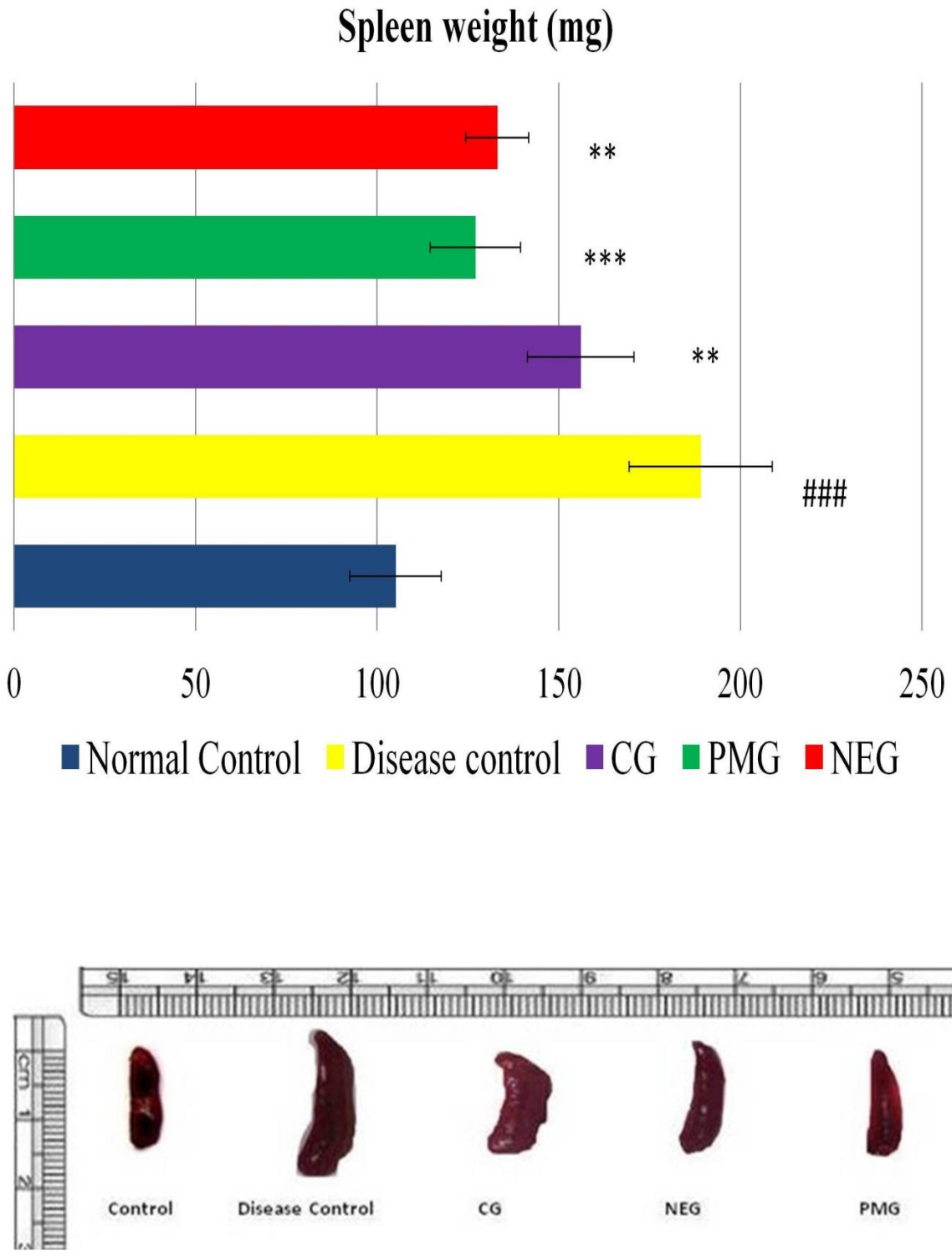

Figure 5.61: Dimension and weight of spleen of animals of different groups

5.5.3 Histology of skin

Histopathological images of H & E stained skin samples of animals of different groups are imaged at 40 X magnification and shown in Figure 5.62. The psoriatic skin of the IMQ treated group showed the expected signs of thickening of epidermis known as hyperkeratosis, abnormal destruction of epidermal cell layer along with parakeratosis, and infiltration of leukocytes into both the dermis and epidermis suggesting induction of psoriatic like skin conditions (Figure 5.62 B).

While the normal control group has not shown any such episodes and has normal histological features of skin excellent (Figure 5.62 A).

However, the application of Resveratrol loaded formulations to the disease-induced animals have shown considerable improvement in skin thickness, as well as alleviation of other signs such as lessened parakeratosis and healing of keratinocytes, was observed.

As compared to disease control and CG group, PMG and NEG formulation has shown significant improvement in skin histology as histological images of animals of PMG and NEG (Figure 5.62 D and 5.62 E) treated group was quite similar to the normal control group (Figure 5.62 C).

Improved signs revealed the enhanced efficacy of the Resveratrol loaded PMG for the treatment of various dermatological benefits such as psoriasis.

5.6 Stability Studies

Stability of the formulation is one of the most important features which is responsible for its superior clinical and therapeutic effects. Also, these are required to maintain the integrity of nanocarrier systems. Changes in physicochemical features of developed formulation could be assessed for exploring its storage stability.

It was assessed by determining mean particle/globule size, zeta potential, pH, and residual drug content after six months of storage at the refrigerated condition (5 ± 3 ºC) and room temperature (25 ± 2 ºC/ 60 ± 5 % RH) (Moghddam et al. 2016).

Insignificant changes in size, zeta potential, residual drug content, and physical appearance ($p>0.05$) were observed at the refrigerated condition in the case of both colloidal hydrogel formulations.

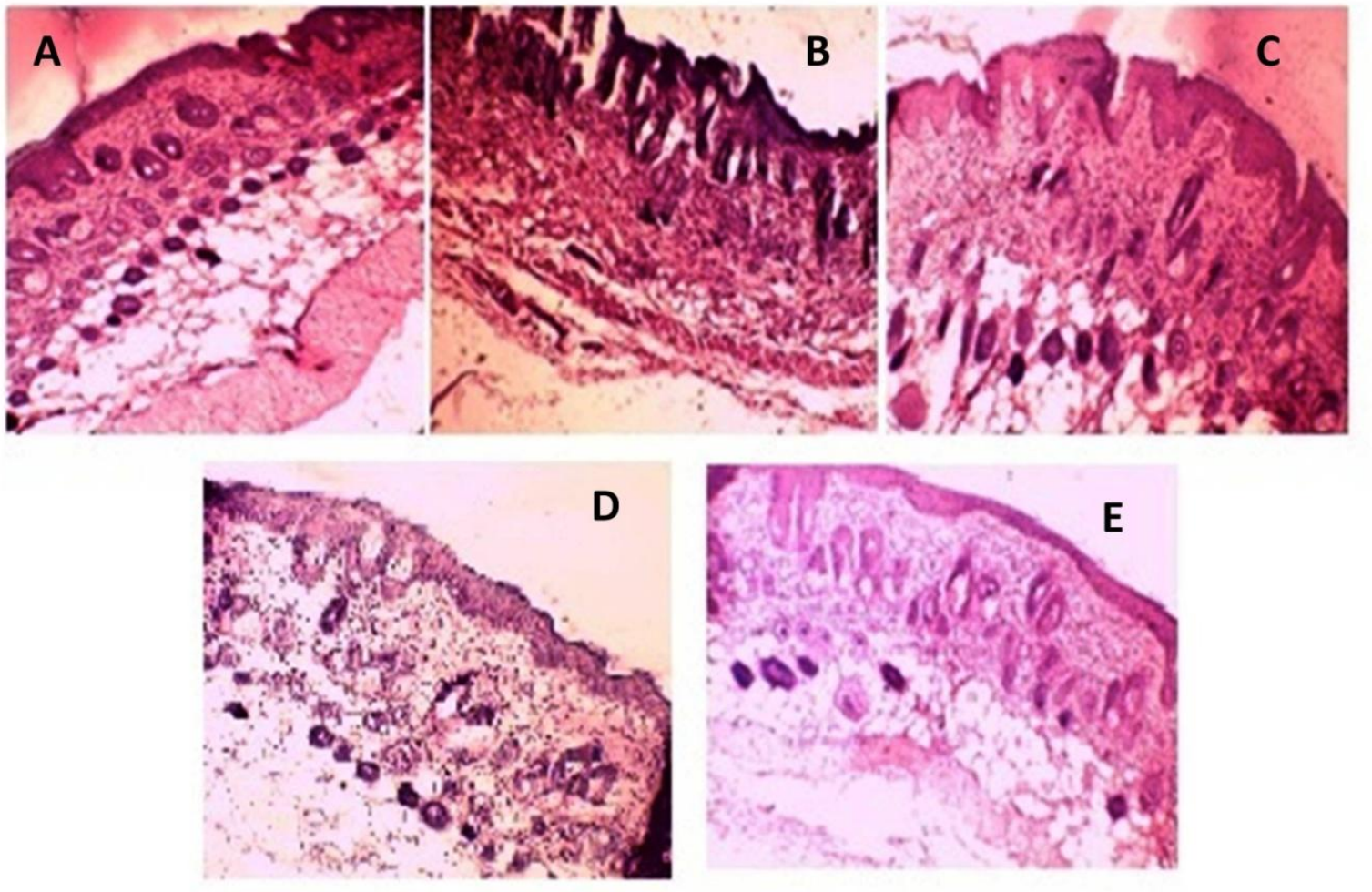

Figure 5.62: Histology of skin of animals of different groups,
Normal control (A), Disease control (B), CG (C), PMG (D) and NEG (E)

In the case of polymeric micelles, particle size, zeta potential, and MIE were found to be 173.98 ± 6.87 nm, -28.86 ± 2.32 mV, and 89.34 ± 1.12 % respectively after six months of storage at refrigerated conditions while initial parameters were 142.67 ± 6.98 nm particle size, -33.65 ± 2.45 mV zeta potential and 93.45 ± 2.34 % MIE as shown in Table 5.28. At refrigerated conditions, no evidence of aggregation or change in physical appearance was observed on visual inspection for 6 months.

However, at temperature conditions equivalent to normal room temperature, significant changes ($p<0.05$) in the stability of micellar formulation was observed. After three months it was found to be 226.43 ± 12.6 nm which was increased significantly up to 291.32 ± 9.17 nm after six months. Similarly, zeta potential value was found to be -27.12 ± 3.02 mV and -24.23 ± 2.45 mV after three and six months of storage respectively. But the physical appearance was homogenous at this temperature also.

A similar kind of stability was observed in the case of nanoemulgel which was found to be highly stable at refrigerated conditions, while at room temperature, significant changes were observed as depicted by Table 5.29. It might be due to fusion, agglomeration, and coalescence of the lipid/polymeric membrane of colloidal hydrogel which is revealed by visible signs of physical instability and loss of consistency (Ahad et al. 2013).

Thus, conclusively, both hydrogels should be stored at lower temperatures for maximum stability and minimum loss of its therapeutic efficacy.

Table 5.28: Stability Studies of Resveratrol loaded PMG

Time	Particle size (nm)		Zeta Potential (mV)		Micellar incorporation efficiency (%)		Physical Appearance of gel	
	5 ± 3 ºC	25 ± 2 ºC/ 60 ± 5 % RH	5 ± 3 ºC	25 ± 2 ºC/ 60 ± 5 % RH	5 ± 3 ºC	25 ± 2 ºC/ 60 ± 5 % RH	5 ± 3 ºC	25 ± 2 ºC/ 60 ± 5 % RH
Initial	142.67 ± 6.98	142.67 ± 6.98	-33.65 ± 2.45	-33.65 ± 2.45	93.45 ± 2.34	93.45 ± 2.34	Homogenous	Homogenous
3 months	158.65 ± 8.16	226.43 ± 12.6	-29.98 ± 1.21	-27.12 ± 3.02	90.78 ± 1.54	87.28 ± 1.08	Homogenous	Homogenous
6 months	173.98 ± 6.87	291.32 ± 9.17	-28.86 ± 2.32	-24.23 ± 2.45	89.34 ± 1.12	85.39 ± 3.84	Homogenous	Homogenous

[Values are expressed as mean ± S.D., (n = 3)]

Table 5.29: Stability Studies of Resveratrol loaded NEG

Time	Globule size (nm)		Zeta Potential (mV)		Residual Resveratrol content (%)		Physical Appearance of gel	
	5 ± 3 ºC	**25 ± 2 ºC/ 60 ± 5 % RH**	**5 ± 3 ºC**	**25 ± 2 ºC/ 60 ± 5 % RH**	**5 ± 3 ºC**	**25 ± 2 ºC/ 60 ± 5 % RH**	**5 ± 3 ºC**	**25 ± 2 ºC/ 60 ± 5 % RH**
Initial	168.3 ± 4.98	168.3 ± 4.98	-29.57 ± 3.43	-29.57 ± 3.43	100	100	Homogenous	Homogenous
3 months	179.12 ± 14.16	281.43 ± 21.45	-25.12 ± 0.87	-21.34 ± 2.08	98.15 ± 0.76	85.14 ± 2.79	Homogenous	Homogenous
6 months	191.23 ± 6.50	415.80 ± 34.87	-21.49 ± 1.32	-16.65 ± 4.12	97.13 ± 1.12	78.32 ± 2.61	Homogenous	Signs of creaming in emulgel

[Values are expressed as mean ± S.D., (n = 3)]